Intrinsic cross-linking of biomimetic glycosaminoglycan-based surface coatings for control of BMP-2 activity towards osteogenesis of cells

Dissertation

zur Erlangung des
Doktorgrades der Naturwissenschaften (Dr. rer. nat.)

der

Naturwissenschaftlichen Fakultät I – Biowissenschaften –

der Martin-Luther-Universität
Halle-Wittenberg,

vorgelegt

von Frau Dipl. Pharm. Reema Anouz

geb. am 01.01.1992 in Qabr Alset, Syrien

Gutachter: Prof. Dr. rer. nat. habil. Thomas Groth

Prof. Dr. Sonja Keßler

Prof. Manuel Salmeron-Sanchez

Halle (Saale), 20.07.2023

Meiner Familie

Table of contents

Abstract

Bone fractures that fail to heal after a prolonged period are known as non-healing unions. Bone morphogenetic protein-2 (BMP-2) is used in the treatment of non-healing bone fractures. However, bolus injections of soluble BMP-2 are rapidly cleared-off from the blood and lose their activity. Hence, high dosages are needed which result in inflammation, increased cancer incidence and ectopic bone formation, in addition to the high costs of the treatment. This study aims to fabricate extracellular matrix-like surface coatings with intrinsic cross-linking property that enables the control and delivery of BMP-2 to the cells in its active matrix-bound state in order to promote osteogenic cell differentiation. Multilayers were fabricated using layer-by-layer (LbL) technique which permits the formation of nanostructured surface coatings with controlled properties and allows the delivery of growth factors (GFs). The use of Glycosaminoglycans (GAGs) as building blocks for multilayers offers a great opportunity to control cell behavior through creating a biomimetic environment that exhibits similar mechanical, chemical and biological cues like the natural extracellular matrix (ECM) and eliminate rejection of the implants due to immunological response. The GAGs heparin (H), chondroitin sulfate (CS) and hyaluronic acid (HA) were combined with either chitosan (Chi) or Collagen I (Col I) to fabricate multilayers on glass substrates. Oxidation of GAGs was used to functionalize them with a reactive aldehyde group which can bind then to the amino groups on Chi or Col I, creating by that a covalent bond (Schiff's base). The latter was used in this study as an intrinsic cross-linking approach of the multilayers to increase their stability, modulate their characteristics and control BMP-2 activity and release compared to the native GAGs (nGAGs) multilayers. The multilayers made using the oxidized GAGs (oGAGs) showed distinguishable physiochemical properties characterized by more polyelectrolytes adsorption during multilayers formation, thicker multilayers, stiffer and rougher multilayers' surface compared to the native ones. Further, oGAGs multilayers supported the natural fibrilization of Col I more than the native ones, as well as, they could preserve its fibrillar structure even at acidic pH. BMP-2 was loaded to the multilayers in 5 and 10 µg mL^{-1} and the adsorption / internalization study showed that higher BMP-2 adsorption and internalization were observed on oGAGs multilayers. BMP-2 from oGAGs multilayers was released in very small amounts over-time, indicating that oGAGs multilayers were keeping the majority of loaded BMP-2 in a matrix-bound state while only little got released to the medium in a soluble state; compared to the nGAGs multilayers that were releasing the highest amounts of BMP-2 over-time. This highlights

the efficiency of the intrinsic cross-linking approach in controlling BMP-2 activity and presentation to cells. Moreover, cell experiments with C2C12 and C3H10T1/2 cells showed a significantly higher cell proliferation on oGAGs multilayers compared to the native ones, indicating no cytotoxicity of oGAGs. In addition, an increasing number of adhering and spread cells were observed on oGAGs multilayers compared to the nGAGs multilayers. The osteogenic differentiation studies concluded that; cells cultured on oGAGs multilayers showed higher expression of mRNA of osteogenic markers as well as higher alkaline phosphatase (ALP) levels and more formation of the mineralized matrix, compared to cells on nGAGs multilayers which did not show any osteogenic differentiation. This points out the difference in efficiency and activity between the matrix-bound BMP-2 presented from oGAGs multilayers compared to the released soluble BMP-2 from nGAGs multilayers. Overall, it can be stated that oGAGs multilayers represent successful efficient candidates to be used as biomimetic surface coatings and GFs delivery systems for tissue regeneration applications.

Zusammenfassung

Knochenbrüche, die nach längerer Zeit nicht heilen, werden als nicht heilende Frakturen bezeichnet. Zur Behandlung nicht heilender Knochenbrüche wird das Knochenmorphogenetisches Protein-2 (BMP-2) eingesetzt. Bolus-Injektionen von löslichem BMP-2 werden jedoch schnell aus dem Blut abgebaut und verlieren ihre Wirkung. Daher sind hohe Dosen erforderlich, die neben hohen Behandlungskosten zu Entzündungen, erhöhter Krebsinzidenz und ektoper Knochenbildung führen. In diesem Projekt sollen extrazelluläre matrixähnliche Oberflächenbeschichtungen mit intrinsischen Vernetzungseigenschaften hergestellt werden, die die Kontrolle und Abgabe von BMP-2 an Zellen in seinem aktiven, matrixgebundenen Zustand ermöglichen, um die osteogene Zelldifferenzierung zu fördern. Die Multilayer wurden mit Hilfe der Layer-by-Layer-Technologie (LbL) hergestellt, die die Bildung von nanostrukturierten Oberflächenbeschichtungen mit kontrollierten Eigenschaften und die Zufuhr von Wachstumsfaktoren (GF) ermöglicht. Die Verwendung von Glykosaminoglykanen (GAGs) als Bausteine für Multischichten bietet eine große Chance, das Zellverhalten zu steuern, indem eine biomimetische Umgebung geschaffen wird, die ähnliche mechanische, chemische und biologische Eigenschaften wie die natürliche extrazelluläre Matrix (ECM) aufweist und eine Abstoßung der Implantate aufgrund immunologischer Reaktionen verhindert. Die GAGs Heparin (H), Chondroitinsulfat (CS) und Hyaluronsäure (HA) wurden entweder mit Chitosan (Chi) oder Kollagen I (Col I) kombiniert, um Multischichten auf Glassubstraten herzustellen. Durch Oxidation der GAGs wurden diese mit einer reaktiven Aldehydgruppe funktionalisiert, die dann an die Aminogruppen von Chi oder Col I binden kann, wodurch eine kovalente Bindung (Schiff'sche Base) entsteht. Letztere wurde in dieser Studie als intrinsischer Vernetzungsansatz der Multischichten verwendet, um ihre Stabilität zu erhöhen, ihre Eigenschaften zu modulieren und die BMP-2-Aktivität und -Freisetzung im Vergleich zu den nativen GAGs (nGAGs) Multischichten zu kontrollieren. Die mit oxidierten GAGs (oGAGs) hergestellten Multischichten wiesen im Vergleich zu den nativen Multischichten andere physikochemische Eigenschaften auf, die durch eine stärkere Adsorption von Polyelektrolyten während der Multischichtbildung, dickere Multischichten sowie eine steifere und rauere Oberfläche der Multischichten gekennzeichnet waren. Darüber hinaus unterstützten die oGAGs-Multischichten die natürliche Fibrillierung von Col I stärker als die nativen Schichten und konnten die fibrilläre Struktur auch bei saurem pH erhalten. Die Multischichten wurden mit 5 und 10 µg mL^{-1} BMP-2 beladen und die

Adsorptions-/Internalisierungsstudie zeigte, dass eine höhere Adsorption und Internalisierung von BMP-2 auf den oGAGs-Multischichten beobachtet wurde. BMP-2 aus oGAGs-Multischichten wurde über die Zeit nur in sehr geringen Mengen freigesetzt, was darauf hindeutet, dass oGAGs-Multischichten den Großteil des beladenen BMP-2 in einem an die Matrix gebundenen Zustand halten, während nur wenig in löslicher Form an das Medium abgegeben wird; im Vergleich zu nGAGs-Multischichten, die über die Zeit die höchsten Mengen an BMP-2 freisetzten. Dies unterstreicht die Effizienz des intrinsischen Vernetzungsansatzes bei der Kontrolle der BMP-2 Aktivität und Präsentation in den Zellen. Darüber hinaus zeigten Zellexperimente mit C2C12 und C3H10T1/2 Zellen eine signifikant höhere Zellproliferation auf oGAGs-Multischichten im Vergleich zu nativen Schichten, was darauf hindeutet, dass die oGAGs keine Zytotoxizität aufweisen. Darüber hinaus wurde auf oGAGs-Multischichten im Vergleich zu nGAGs-Multischichten eine höhere Anzahl adhärierender und proliferierender Zellen beobachtet. Studien zur osteogenen Differenzierung zeigten, dass Zellen, die auf oGAGs-Multischichten kultiviert wurden, eine höhere mRNA-Expression osteogener Marker, höhere Spiegel der alkalischen Phosphatase (ALP) und eine stärkere Bildung der mineralisierten Matrix aufwiesen als Zellen auf nGAGs-Multischichten, die keine osteogene Differenzierung zeigten. Dies deutet auf einen Unterschied in der Effizienz und Aktivität zwischen dem matrixgebundenen BMP-2 aus oGAGs-Multischichten und dem freigesetzten löslichen BMP-2 aus nGAGs-Multischichten hin. Zusammenfassend lässt sich sagen, dass oGAGs-Multischichten erfolgreiche und effiziente Kandidaten für biomimetische Oberflächenbeschichtungen und GFs Delivery-Systeme für Anwendungen in der Geweberegeneration sind.

Chapter 1

Introduction

This cumulative thesis consists of four manuscripts. The first manuscript is a book chapter which is used as an introduction to biomimetic surface modifications of biomaterials using layer-by-layer technique. The remaining three published manuscripts are assembled as chapters 2-4 including a summary at the beginning of each chapter.

CHAPTER 13

Biomimetic Surface Modifications of Biomaterials Using a Layer-by-layer Technique

R. ANOUZ[a] AND T. GROTH*[a,b]

[a] Biomedical Materials Department, Institute of Pharmacy, Martin Luther University Halle Wittenberg, 06120 Halle (Saale), Germany;
[b] Interdisciplinary Center of Materials Research, Martin Luther University Halle Wittenberg, Heinrich-Damerow Strasse 4, 06120 Halle (Saale), Germany
*Email: thomas.groth@pharmazie.uni-halle.de

13.1   Cells and the Extracellular Matrix (ECM)

In multicellular organisms such as mammals, cells reside in a microenvironment which represents a noncellular component filling the interspace between cells, called the extracellular matrix (ECM). The ECM is present in all tissues and organs, playing important roles in tissue morphogenesis, cell growth, differentiation and survival as well as homeostasis through presentation of crucial biochemical and biomechanical cues.[1] Fibrillar and non-fibrillar multi-adhesive proteins, proteoglycans and glycosaminoglycans are the main components of the ECM with great variations in composition, mechanical properties and topography depending on the type of tissue.[2] ECMs can be classified into two major types

Biomimetic Surface Modifications of Biomaterials Using a Layer-by-layer Technique 327

that vary in composition and structure; the interstitial and pericellular ECM (see Figure 13.1).

We will focus here on the pericellular ECM of connective types of tissue that is found in all organs of the body, playing an important role as a structural element of tissues. On the other hand, all epithelial, muscle and neuronal tissues are connected to a specialized type of ECM, the basal lamina, that differs in spatial and molecular organization from connective tissue.[3] The type of connective tissues is related to the composition and organization of the surrounding ECM,[4] with large differences in their mechanical properties.[5] It is also remarkable that in some connective tissues, the matrix dominates like in bone or cartilage with low numbers of cells, whereas in other tissues densely packed cells with relatively low amounts of matrix are found, as seen in adipose tissue.[6]

The ECM is rich in several fibrous proteins such as different types of collagen (Col), elastin and fibronectin (FN) that are important for the mechanical properties of tissues, but also provide topographical cues to cells.[7] Collagen is the most abundant type of protein making up around 30% of all synthesized proteins in the body, providing the ECM with mechanical strength, but also possessing a multitude of other biological functions.
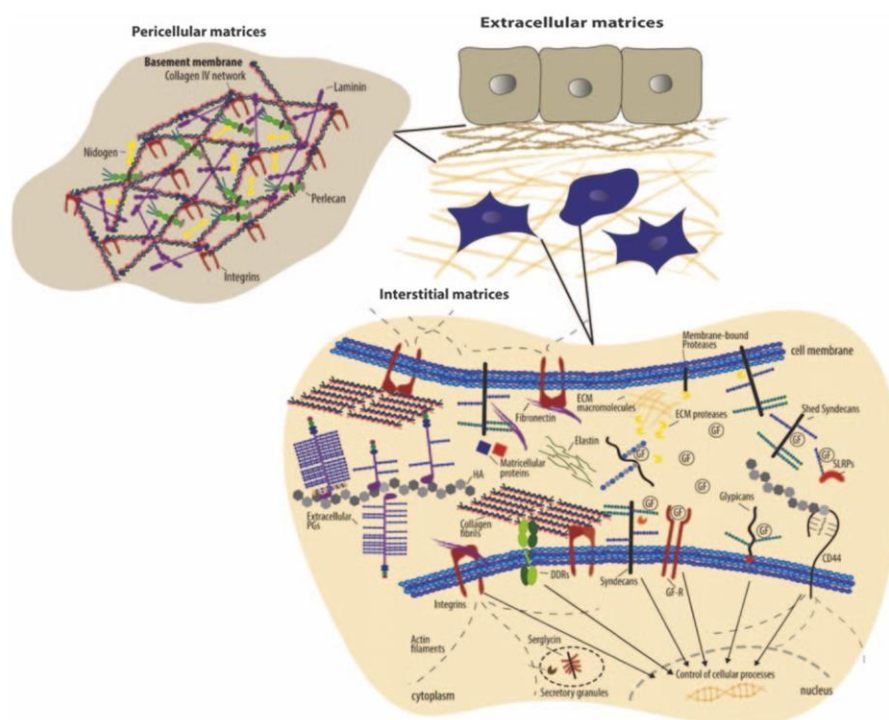

Figure 13.1   Schematic overview of extracellular matrices, their major components and cell surface receptors.
Reproduced from ref. 7 with permission from Elsevier, Copyright 2015.[7]

328   *Chapter 13*

By exerting tension on the developing ECM, fibroblasts organize collagen fibrils, which considerably affect the alignment of collagen fibers into sheets and cables. The collagen superfamily consists of different α chains, which make 28 collagen types from a total of 46 distinct α chains and specific tissue distribution (*e.g.*, collagen I in bone and collagen II in hyaline cartilage).[8] For example, Type I collagen represents a kind of model fibrous protein showing widespread and abundant expression among tissues. It forms heterotrimeric triple helices, which are self-assembled into fibrils through fibrillogenesis, *in vivo,* that requires the activity of cells such as fibroblasts. Type I collagen is a major structural protein in tissues such as bone, dermis and tendons. It should also be noted that not all collagens are fibril-forming, but several like FACIT collagens connecting fibrillar collagens I and II with other matrix components (*e.g.*, proteoglycans and cells) and others are present on cell surfaces or have other functions. Specific collagens are also found in the basal lamina, such as collagen IV.[3] A comprehensive survey on collagens regarding their composition, structure and functions can be found in the literature.[7] Beside their mechanical functions, collagens provide binding sites for cell adhesion receptors and also other types of ECM proteins.[9] In particular, cell surface receptors such as integrins bind to specific collagen sequences like GFOGER (O being hydroxyproline), KGD (in the ectodomain of collagen XVII) and also various bioactive peptides as a result of proteolytic degradation. Collagen I–III also present binding sites for dimeric discoidin receptors, while several collagens also present binding sites for blood platelets and leukocytes.[10] Elastin is produced by several types of cells including smooth muscle cells, endothelial cells and fibroblasts but only perinatally. Elastin fibrillization is guided by microfibrils made of fibulins.[11] It provides tissues that are prone to cyclic stretching, like the dermis, lung tissue and arteries, with the ability to recoil and is responsible for the elasticity of these body structures.[12] Beside their mechanical functions, elastin and elastin peptides possess many biological properties. Elastins regulate terminal arterial and lung airway branching morphogenesis. Elastin receptors on cells regulate skin fibroblast proliferation, chemotaxis of monocytes, fibroblasts and smooth muscle cells and regulate endothelium dependent vasorelaxation to name only a few of the many biological effects of elastin.[11,13]

Fibronectin, a dimeric protein that belongs to the group of multi-adhesive proteins is also able to fibrillize and provides a blueprint for organization of other fibrillar and non-fibrillar matrix components. In particular, collagen and elastin fibrillization are guided by the pre-formed fibronectin matrix that is organized by cells from connective tissue.[14] It fibrillizes driven by cellular activity under mechanical stress, when cryptic self-association sites are being exposed.[14] These self-association sites are responsible for the tension-dependent polymerization, while other binding sites exist for matrix components such as gelatin/collagen, fibrin, heparin and thrombospondin.[15] Beside ECM component binding sites, fibronectin possesses cell binding sites like the RGD sequence and synergy sites that are recognized by

Biomimetic Surface Modifications of Biomaterials Using a Layer-by-layer Technique 329

integrin cell adhesion receptors,[16] and also binding sites for growth factor bone-morphogenic protein 2.[17] Hence, fibronectin provides a very good model for the multi-adhesive nature of this class of proteins to which also belong laminins, vitronectin and others as they provide binding sites for different matrix components (collagens, glycosaminoglycans) and cells. There is a large and heterogeneous family of other matrix (glyco)proteins, which include members such as thrombospondins (TSPs), secreted protein acidic and rich in cysteine (SPARC), tenascins (TNs), fibulins, osteopontin (OPN), cartilage oligomeric matrix protein (COMP), CNN family proteins, periostin and R-spondins. Although they are secreted in the ECM, they can also be found in body fluids and associated with the cell surface. This heterogeneous group of matrix cellular proteins interacts not only with other matrix components and growth factors but also with several cell-surface receptors including integrins, cell surface proteoglycans, toll-like receptors (TLRs), the hyaladherin CD44, growth factor receptors and scavenger receptors.[7]

Proteoglycans (PGs) as another ECM component consist of a core protein to which glycosaminoglycans (GAGs) side chains are covalently bound. PGs are classified into four groups; basement membrane proteoglycans (*e.g.*, Perlecan), hyalectans binding to hyaluronan (*e.g.*, Aggrecan and Versican), small leucine-rich proteoglycans (SLRPs *e.g.*, Decorin) and cell-surface proteoglycans (*e.g.*, syndecans and glycipans).[7] Furthermore, PGs have a specific tissue distribution and play important roles in ECM structure and physical properties, but also in cooperation with other ECM proteins and cell surface receptors. Aggregating PGs bind to hyaluronan (HA), which represents the core to which PGs with many negatively charged GAGs side chains are bound, inducing by that an osmotic pressure which will end up in PG swelling due to the diffusion of ions and water into the matrix. However, collagen limits this swelling to 20% providing rigidity to the matrix tissues, which has the ability to resist compression forces due to presence of PGs.[4] Examples of such PGs are aggrecan which is present in articular cartilage,[18] and versican that is found in many tissues, such as tendons, prone to compressive loading.[19] Decorin and biglycan are among the non-aggregating PGs that do not bind HA and possess only a small number of GAG side chains. Thus, they do not contribute to withstanding pressure but through interacting with collagen they contribute to mechanical stability.[4] Syndecans are another important class of GAGs that represent receptors of the cell surface that are involved in presentation of cytokines to corresponding receptors, cell–matrix and cell–cell adhesions and signal transduction processes.[20]

GAGs represent the carbohydrate part of PGs consisting of repeating disaccharide units containing glucosamine or galactosamine and uronic acid and can be classified into sulfated and non-sulfated GAGs.[21] HA is the only non-sulfated GAG with a large molecular weight of about 1 Mio Da, with a large exclusion volume and an immense capacity to bind water, which is related to compression resistance of tissues like cartilage or fluids like synovial fluid in joints.[22] In addition, HA represents a ligand for

330   *Chapter 13*

hyaladherin cell adhesion receptors which are involved in signal trans-
duction playing important roles in a multitude of processes like inflam-
mation, wound healing and cancer.[22] Sulfated GAGs include heparan
sulfate (HS), heparin (H), chondroitin sulfate (CS), dermatan sulfate (DS)
and keratan sulfate (KS)[22] and also have specific tissue distribution. Beside
their contribution as components of matrix PGs, like aggrecan in binding
ions and water and contributing to compressive resistance of tissues, they
are important components for storage and presentation of growth factors
(GFs) for example by interaction with heparin-binding domains in GFs like
fibroblast growth factors, but also for cell–cell interactions. A survey on the
multitude of functions of heparan sulfate side chains of PGs is shown in
Figure 13.2.

The ECM also represents a reservoir for cytokines including growth factors
(GFs) and other morphogens that control cell fate. The function of GFs
comprises stimulation of cell growth, but also differentiation and survival.
They are also involved in inflammation and tissue repair. Growth factors can
be secreted by neighboring cells of the same or different type (paracrine), but
also in distant tissues (endocrine) or even in the cells themselves (autocrine).
Normal tissue cells need several types of growth factors to proliferate and
stay alive. A comprehensive review on the different classes and functions of
GF can be found in the literature.[23] Briefly, important classes of growth
factors are the fibroblast growth factor family (FGF), the vascular endothelial
cell growth factor family (VEGF), the transforming growth factors family
(TGF), including bone morphogenic proteins (BMPs), and many others.[23]
Different components of the ECM such as proteins like fibronectin and PGs
are able to bind various GFs like FGFs, VEGFs and TGFs controlling their
local bioavailability. The ECM acts as reservoir for GFs by saving them in an
inactive state and thus making them available for cells in a spatially and
timely controlled manner for which matrix PGs with their GAG side chains
play an important role.[1] This represents another important feature of the
ECM to deliver and release GFs on demand by proteolytic activity and other
processes.

The mechanical properties of ECM also play an important role in con-
trolling cell function and fate. Mechanical properties of the ECM control the
tension of cytoskeletal structures transmitted by cellular adhesion receptors,
which affects the mechanical properties of soft tissues to some extent in
response to the compression forces exerted on them from neighboring cells
and the stiffness of the surrounding ECM.[24] Therefore, the applied mech-
anical forces on cells create a certain tension in the cytoskeleton which helps
to maintain the shape of the cells as well as their response to outer forces,
which in turn controls cellular behavior.[25] Control of gene expression is
achieved by transmission of mechanical forces from the surrounding ECM
via integrin or cadherin ligation to the cytoskeletal network and from there
to the nucleus, which is called mechanotransduction.[26] Each tissue has
specific stiffness regulated by its ECM composition and organization, and
this tissue specific stiffness shown in Figure 13.3 regulates cellular

Biomimetic Surface Modifications of Biomaterials Using a Layer-by-layer Technique   331
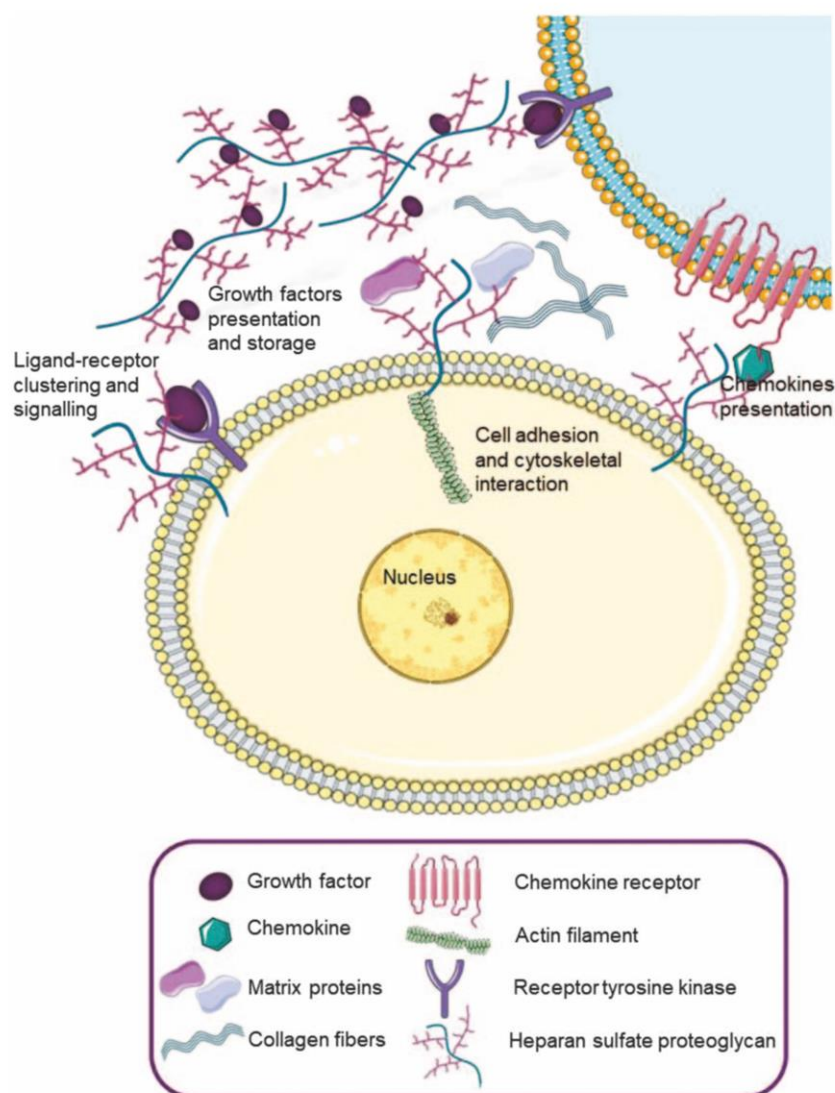

Figure 13.2 Heparan sulfate proteoglycans roles in cell physiology; they act as co-receptors for growth factors and corresponding receptor tyrosine kinases present either on the same or on adjacent cells, transport of chemokines across cells and their presentation at the cell surface, enable cell adhesion to ECM and connect to the cytoskeleton, and store growth factors and morphogens.
Adapted from ref. 160 with permission from Springer Nature, Copyright 2007[160] and from https://smart.servier.com/ under the terms of the CC BY 3.0 license, https://creativecommons.org/licenses/by/3.0/.[161]

behavior.[27] For example, human mesenchymal stem cells tend to undergo tissue-specific cell differentiation to become osteoblasts and start expressing bone-specific transcription factors when they are cultured on ECMs having

332   *Chapter 13*
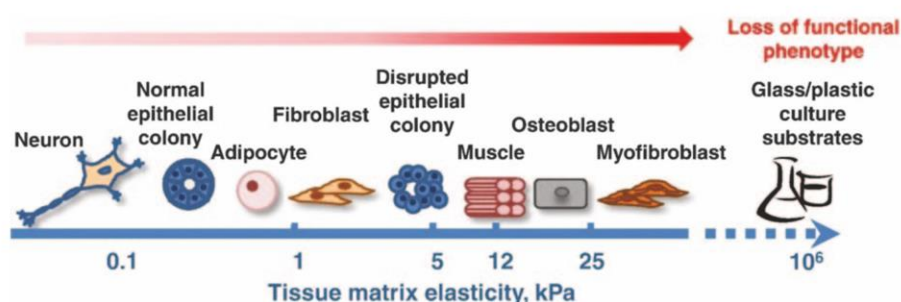

Figure 13.3   Different tissues with their specific elastic modulus in the body are correlated with their functions.
Reproduced from ref. 162 with permission from Elsevier, Copyright 2011.[162]

similar stiffness values that mimic the elastic moduli of bone.[28] On the other hand, the same cell type differentiates into adipocytes and chondrocytes if they are cultured on soft substrata.[29] Thus, this emphasizes the importance of the substrate stiffness in guiding stem cells to the desired lineage, but also in maintaining the gene expression patterns corresponding to the type of tissue.

13.2   Cell–ECM Interactions

Cell adhesion precedes other events such as cell spreading, proliferation and eventually differentiation.[30] It is a complex process that involves specific interactions between cell surface receptors and their appropriate extracellular ligands that are mostly ECM components in connective types of tissue,[31] however, they can also be other cells through cell–cell adhesion receptors like ICAMs, selectins and cadherins, which are important in interaction of epithelial cells and blood-derived cells like platelets, monocytes, macrophages, *etc.*[32] Cells interact with the ECM through adhesion receptors, such as integrins, discoidin domain receptors (DDRs), cell surface PGs and the hyaluronan (HA) receptor CD44 or RHAMMs.[3] In this respect, cells integrate chemical and mechanical signals from ECMs that dictate their functions and behavior (see Figure 13.1). Several types of cell–matrix adhesions named focal complexes, focal adhesions, fibrillar adhesions and 3D-matrix adhesions have been defined.[33] The majority of cell–matrix adhesions are based on ligation of integrins with protein components of the ECM forming these different kinds of adhesions.[34] We will focus here predominantly on integrins and hyaladherins. Integrins are divalent cation-dependent heterodimeric *trans*-membrane glycoproteins consisting of an alpha and beta subunit, with binding to ECM proteins like collagens, fibronectin and others.[35] There are different types of integrins that comprise RGD binding including beta 1 and platelet integrins, collagen-binding, laminin binding and leukocyte integrins.[36] There are

Biomimetic Surface Modifications of Biomaterials Using a Layer-by-layer Technique   333

several integrin-dependent signaling pathways including non-receptor tyrosine kinases, most notably focal adhesion kinase (FAK), integrin-linked kinases and Src kinases, but also other signaling pathways (*e.g.*, phosphatidylinositol signaling pathway). A major and well-studied signaling transduction process is related to mitogen-activated protein kinase pathway (MAPK or ERK) that is involved in regulation of cell growth. It is also remarkable that there is a synergy of integrin-related signaling with growth-factor related pathways that are connected to receptor tyrosine kinases, such as fibroblast growth factor tyrosine kinases with MAPK kinase pathway regulating cell cycle and mitosis.[32,37] This signaling, which integrates numerous proteins like FAK, ERK (extracellularly regulated kinase), bone-specific transcription factor Runx2/Cbfa1, Ras homolog gene family member A(Rho) family, conducts the signal transduction machinery and finally leads to the progression of the cell cycle or various other commitments of cells.[38] In addition, ligation of integrins also provides stop signals for apoptosis of cells due to inhibition of Caspase 9 and increased expression of anti-apoptotic protein Bcl-2, promoting survival of cells.[39] Hence, ligation of integrins provides both stimuli for cell growth and survival (Figure 13.4A).[40]

Cells also express hyaladherins as HA receptors such as CD44, which is not only a HA receptor but also binds to other ECM molecules such as collagens, fibronectin, OPN, MMPs and growth factors. CD44 is a transmembrane receptor undergoing alternative splicing of the extracellular domains, which leads to various isoforms in different types of cells.[7] On the other hand, transmembrane and intracellular domains of CD44 are the same in all variants. The short cytoplasmic tail of CD44 presents several binding motifs that are required for interaction with intracellular proteins and cell signaling as shown in Figure 13.4B.

In summary, cell adhesion with ligation to and sensing of ECM components and corresponding signal transduction processes are important prerequisites for normal cells growth, differentiation and function. Accordingly, to achieve control of cell behavior during use of biomaterials in their medical application as implants and other medical devices, it is imperative to know how materials surface chemistry and topography impact the formation of the adsorbed protein layer, and the bioactive sites exhibited by the same.[41] On the other hand immobilization of ECM components like proteins, derived oligopeptides or PGs or their GAG components may pave the way to bioactive biomaterials for making better implant and scaffold materials.

13.3   Biomaterials, Implants and Tissue Engineering Scaffolds

Damage and degeneration of tissues and organs in the human body can be the result of diseases, trauma and aging. Standard medical treatment methods used for a long time are based on transplantation of autografts

334   *Chapter 13*
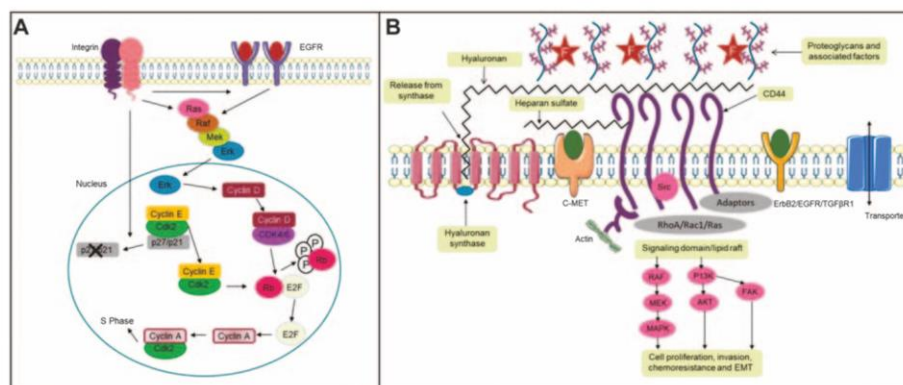

Figure 13.4   (A) Signal transduction pathways from integrins and growth factor receptors showing synergy of the MAPK kinase pathway involved in the control of cell cycle and thus cell growth. Adapted from ref. 40 with permission from Springer Nature, Copyright 2002.[40] Illustration of the phospholipid bilayer is adapted from https://smart.servier.com/ under the terms of the CC BY 3.0 license https://creativecommons.org/licenses/by/3.0/.[161] (B) CD44 acts as a receptor for hyaluronan (HA), though it can also bind to other ECM proteins, such as fibronectin, laminin, heparin-binding growth factors or collagen I, IV and XIV. The extracellular domain of CD44 can be cleaved by MMPs or ADAMs, and the remaining intracellular domain can be released into the cytoplasm by the presenilin-dependent-γ-secretase, where it regulates gene transcription. CD44 interacts with the transforming growth factor β receptor (TGFβR) and the platelet-derived growth factor receptor β (PDGFRβ) and upon HA-activation negatively regulates them. It also associates with epidermal growth factor receptor (EGFR). Versican possibly competes with CD44 to bind HA and with EGF to bind EGFR and therefore blocks CD44 and EGFR signaling. Adapted from ref. 163 https://doi.org/10.3390/biom10081170 under the terms of the CC BY 4.0 license http://creativecommons.org/licenses/by/4.0/.

(from one site to another in the same patient), allografts (from one individual to another) and xenografts (from other species) and conventional synthetic implants. Although transplantation has been relatively successful, limitations and problems are seen as morbidity and pain at the donor site, limited availability and quality of grafts, disease transmission and immunological responses to allogenic or xenogenic transplants leading to rejection.[42,43] Therefore, conventional implants (*e.g.*, total hip or knee prosthesis) and tissue engineering have emerged as alternative approaches.[44] Biomaterials that represent the basis of implants and scaffolds must be biocompatible, having mechanical properties compliant to the type of tissue (soft *vs.* hard) and the ability to support cell attachment, growth and function.[45] Basically, all kinds of material classes are used as biomaterials such as polymers, ceramics, metals and composite materials.[43] However, as we will outline below in more detail, most synthetic biomaterials can be tailored regarding their mechanical and other

Biomimetic Surface Modifications of Biomaterials Using a Layer-by-layer Technique   335

properties, but are less than optimal regarding their interaction with the human body.

The majority of biomaterials approved for medical applications are of synthetic origin.[46] Hence, chemical cues that are normally presented by ECM components to cells are lacking. In addition, when a biomaterial is exposed to the biological environment after implantation, adsorption of proteins takes place before any cell–material interaction occurs. Because of the multitude of proteins that are contained in the surrounding body fluids, their adsorption on the implanted biomaterial is unpredictable regarding the composition of film and the conformation of the adsorbed proteins.[47] Some general rules related to adsorption and conformation of proteins are that hydrophobic biomaterials tend to adsorb larger quantities of proteins due to hydrophobic interaction, which can trigger adsorption of fibrinogen and other proteins promoting adhesion and activation of blood platelets but also inflammation and fibrosis.[48,49] On the other hand, highly wettable biomaterials (*e.g.*, caused by the presence of hydroxyl groups on the surface that are characterized by the presence of bound water) normally reduce the adsorption of proteins, which makes the surfaces repellent, preventing colonization of bone implants and tissue engineering scaffolds with cells.[50] If the hydrophilic surface is highly negatively charged (*e.g.*, due to the presence of carboxylic groups), it can also trigger the activation of the intrinsic system of plasmatic coagulation as another undesired complication.[51,52] On the other hand, moderate wettable materials that are characterized by water contact angles around 60 degree, (*e.g.*, achieved by the presence of amino groups) are known to lead to moderate adsorption of proteins with minor conformational changes promoting attachment of cells.[53]

Because the interaction between the implant material and the host tissue occurs at the biomaterial surface,[54] efforts have been made to tailor the biocompatibility through various physical, chemical and biological surface modification techniques[54] that aim to promote cell adhesion, proliferation, differentiation and function.[55] Generating functional groups or grafting other molecules on surfaces are the main approaches of chemical modification of surfaces, for which several methods have been developed.[56,57] These methods include chemical etching (*e.g.*, with sulfuric acid), plasma treatment and polymerization,[58] ion beam irradiation[59] and surface grafting.[60–62] Physical modifications include surface coatings[63] or entrapment,[64] vapor deposition[65] and surface self-assembly[66,67] methods. Van der Waals forces, hydrogen bonding and electrostatic interactions are among the physical interactions related to these techniques.[68] Even though these physical surface modification techniques are considered simple and relatively inexpensive, limited stability is considered as one of their drawbacks when the interaction force between substrate and immobilized molecules is relatively weak.

Immobilization of biomolecules such as cell receptor ligands, antibodies, enzymes, pharmacological agents, lipids and nucleic acids on biomaterials has been used for various therapeutic and diagnostic purposes and is

336   *Chapter 13*

considered as a biological surface modification approach.[69] Biological surface modification can be achieved by either adsorption or covalent binding of ECM-derived proteins or oligopeptides, cytokines and sugars to address specific adhesion or other receptors on the surface of cells as well as cell–cell-contacts (establishing co-cultures of cells or immobilizing cell–cell-adhesion receptors like Cadherins) in an approach to mimic the native microenvironment of cells.[70,71] Cellular beta 1 integrin adhesion receptors interact with ECM proteins *via* the tripeptide Arg-Gly-Asp.[72] Therefore, the functionalization of the biomaterial surface with RGD sequence has been widely used to improve cell interaction with synthetic biomaterials surfaces. However, some limitations still exist including reduced biological activity or receptor specificity when using synthetic peptides.[73–75] Moreover, many other ECM proteins such as collagen, gelatin, fibrinogen and others have also been used to functionalize biomaterial surfaces by adsorptive or covalent binding as they offer a favorable microenvironment for cells to adhere and differentiate due to ligation of integrins.[76]

Moreover, to better mimic the ECM interaction, introducing other signaling mechanisms is required. For instance, regulating the process of bone regeneration involves the activity of growth factors such as BMPs, VEGF, but also integrin ligation to ECM components like collagens.[77] Furthermore, BMPs interact and bind to ECM *via* PGs with heparan sulfate side chains which provide control over their binding and release and highlight the important role of the ECM as a reservoir of GFs.[78–80] Due to the importance and crucial role of BMPs, namely BMP-2 and BMP-7, in bone healing,[81] several approaches have been developed to functionalize the biomaterial surfaces with BMPs in addition to the presence of cell adhesion cues. However, the short half-life and rapid clearance of BMPs require administration of very high concentrations to obtain the desired therapeutic effect at the site of injury. This in turn can result in severe side effects including ectopic bone formation and cancer risks in addition to the high costs of such treatments.[82,83] Another example is the development of new blood vessels called "angiogenesis" which is a crucial process in wound healing, but also other physiological and pathological processes. In angiogenesis, VEGF plays a key role and is found to always be sequestered to the ECM and not present in a soluble state.[84] Furthermore, FGF-2, which regulates growth, differentiation, migration and survival of many cell types, and also angiogenesis, is also protected from protease cleavage, heat or acidic denaturation by interacting with components of PGs like heparin and heparan sulfate.[85] Therefore, several studies focused on introducing biomaterials that contain specific growth factor-binding sites which allow presentation of GFs in a bound state to overcome the complications associated with their use at high, non-physiological concentration.[78,86] For example, following this strategy, Salmerón–Sánchez and co-workers showed that FN on poly(ethyl acrylate) was self-organized into nanonetworks exposing both the integrin (FNIII9-10) and growth factor (FNIII12-14)-binding sites of the protein which improved cell response compared to the soluble GFs and could efficiently trigger both

Biomimetic Surface Modifications of Biomaterials Using a Layer-by-layer Technique 337

bone formation[17] and vascularization[87] *in vivo* using low GF doses. Furthermore, the matrix-bound VEGF (through an ECM binding domain) in collagen gels exhibited prolonged activation of VEGF receptor which was absent upon exposure to soluble VEGF.[88] Another example is protecting the acidic fibroblast growth factor (aFGF) from proteolytic degradation by conjugating it to heparan sulfate.[89] Pashkuleva and co-workers functionalized their substrate with biomimetic alginate sulfate and could regulate the FGF-2 binding by controlling the degree of sulfation and therefore, a control over FGF-2 loading and subsequent cell growth was obtained.[90] Many other ECM-mimicking GF presentation strategies using different GFs have been explored so far to achieve their local delivery, in a controlled manner while preserving their activity, which underlines the significance of existing clinical problems.

13.4 Brief Introduction to the Layer-by-layer Technique

The layer-by-layer technique is a method to modify surfaces by adsorption of polyelectrolyte macromolecules or other charged entities like particles, liposomes and even cells, as summarized in Figure 13.5, which shows also the multitude of assemblies as 2D and 3D templates.[91] LbL was first introduced by Iler[92] using oppositely charged colloidal particles in the 60s, but gained popularity when it was used by Decher and Hong in 1991 to establish polyelectrolyte multilayers (PEMs).[93] LbL relies traditionally on alternating adsorption of oppositely charged polyelectrolytes or other charged entities to form multilayer film coatings.[94]
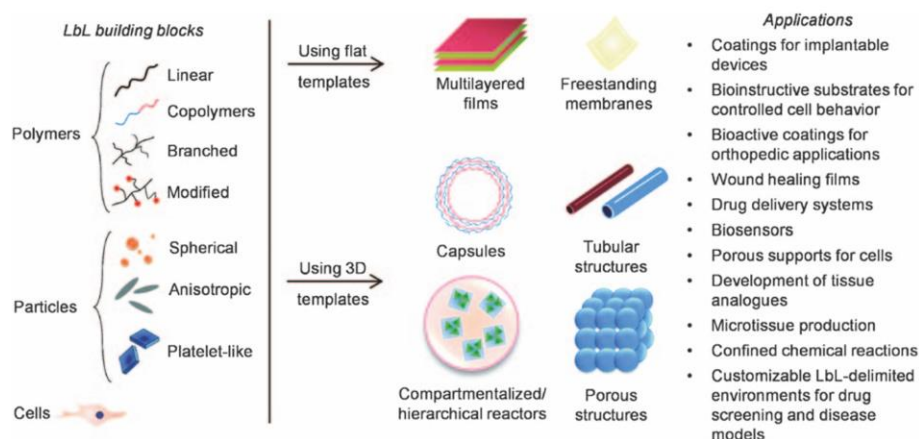

Figure 13.5 Survey on building blocks used in LbL and the various multilayered devices conceived from their assembly onto 2D and 3D templates. Reproduced from ref. 91 with permission from the Royal Society of Chemistry.

338   *Chapter 13*

Meanwhile other kinds of interactions than coulombic attraction and ion pairing have also been employed, to produce multilayers for a variety of applications that have been reviewed recently by Costa and Mano, which are depicted in Figure 13.6 showing the wide range of molecular interactions that can be employed for the formation of multilayers.[91] The LbL technique represents in general a simple, versatile and inexpensive surface modification technique that can be applied to a large variety of materials like ceramics, metals, polymers and even biological objects like cells by dip or spray coating using robots that permits also the coating of 3D objects and inner pores of materials. A major advantage of the LbL technique is that normally no specific pre-treatment or chemical activation of materials is required. In addition, when polyelectrolytes are used with water as the solvent, the technique is not only more environmentally-friendly than others, but it may also permit the inclusion of sensitive biological matter like proteins without harm.[95] It is also important to note that characteristics of multilayer films such as thickness, surface charge, wettability, viscoelasticity and topography can be adjusted by varying the processing conditions (temperature and time of adsorption and washing), medium characteristics (ionic strength and pH value) and the polyelectrolytes used (charge density, molecular weight, weak or strong acids/bases synthetic or biological, macromolecules or particulate matter).[95–97] Overall, LbL represents a technique that may be particularly suitable for biomedical applications.

13.5   Biomedical Applications of the LbL Technique

The LbL technique has been used for a variety of biomedical applications such as drug delivery, the development of tissue analogs and coating of implantable devices using both synthetic and biogenic polyelectrolytes. We will focus on the latter in the subsequent sections.

13.5.1   LbL Technique for Mimicking ECM Properties Using Biomolecules as Polyelectrolytes

The LbL technique has been used to mimic the biological structure and characteristics of ECM using various approaches such as biochemical cues, topography, mechanical properties and storage and presentation capability for GFs and other cytokines. The use of ECM components as building blocks for LbL shall mimic the structure and function of the native matrix and thus provide potentially better control of cell adhesion, growth and differentiation. Thus, it could make surfaces of implant materials more biocompatible and bioactive promoting healing and regeneration of tissues and organs.

Polysaccharides (*e.g.*, GAG) represent important components of ECM in mammals. However, other organisms like Arthropoda, fungus and plants also have them as important structural elements of their exoskeleton, cell wall or other cell components (*e.g.*, chitin, chitosan, cellulose, alginate).
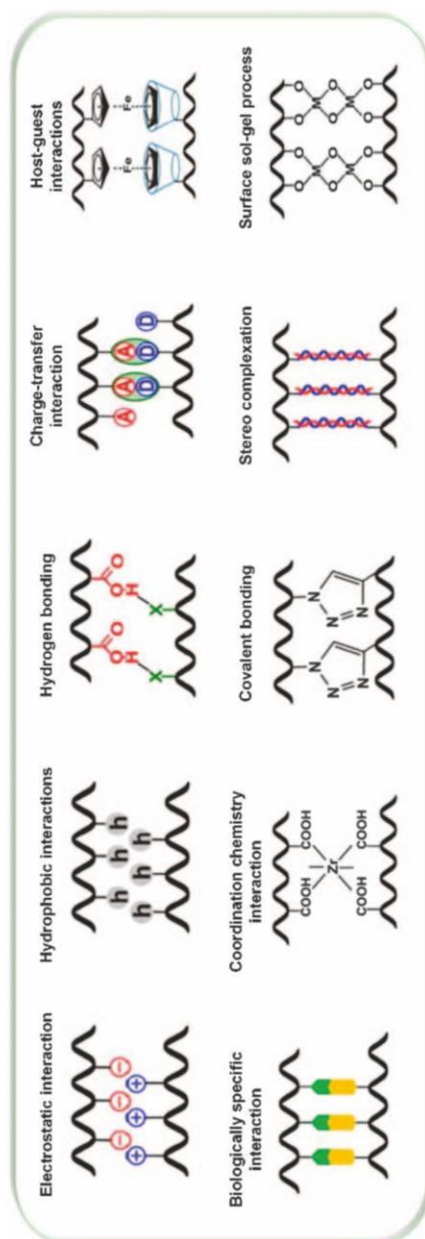
Figure 13.6 Molecular interactions driving the LbL self-assembly of materials. Reproduced from ref. 95 with permission from American Chemical Society, Copyright 2014.

340   *Chapter 13*

GAGs possess a polyelectrolyte character due to the presence of carboxylate and sulfate groups, providing them with their negative charge and polyanion characteristics.[98] Hence, particularly GAGs as LbL building blocks offer a biomimetic environment and a platform to address specific interactions with certain protein ligands of ECM, GFs and cell surface receptors. Other polysaccharides like alginate from sea weeds that consist of alternating blocks of mannuronic acid and guluronic acid with mixed blocks from both also possess polyanionic character, but lack a specific bioactivity in mammals. However, due to their capacity to bind cations, getting cross-linked by calcium and forming hydrogel-like coatings with high capacity to take up water, alginate has also been used frequently as a polyanion in the LbL technique.[99] Chitosan that is composed of repeating units of *N*-acetylglucosamine and glucosamine represents a polycation, when exposed to pH values below its pK_a value around 6. It represents probably one of the most used biogenic polycations that also possesses anti-bacterial and anti-inflammatory properties and excellent biocompatibility.[100,101] The use of GAGs for LbL technique is sometimes hampered by large variations of their chemical composition and bioactivity from batch to batch. Therefore, alternative, semi-synthetic GAG analogs with specific molecular weights and adjustable chemical compositions have been synthesized and used in LbL–ECM mimicking systems. One of the strategies followed to produce these analogs is to introduce sulfate groups to the natural polysaccharide's backbone as reviewed recently.[102] For example, Aggarwal *et al.* used semi-synthetic cellulose sulfate that was combined with chitosan as polycation observing that multilayers of cellulose sulfate had a high bioactivity promoting adhesion and growth of cells.[103] The bioactivity of cellulose sulfates is related to their degree of sulfation that promotes binding and bioactivity of growth factors like FGF-2 and BMP-2 causing high osteogenic activity and moderate mitogenic activity.[104,105] Another example is based on sulfation of alginate and its use as a polyelectrolyte in the studies of Mhanna *et al.* regulating FGF-2 binding, which was increased with the degree of sulfation of alginate sulfate.[90]

ECM proteins like collagens, fibronectin and elastin also represent polyelectrolytes. Though proteins are normally amphoteric or zwitterionic, their net charge depends on their isoelectric point and thus on the pH of the assembly solution.[106] Collagen I represents a soluble polycation at acidic pH values, which was used in studies forming multilayers with GAGs as polyanions promoting adhesion and osteogenic differentiation of mesenchymal stem cells. A further observation was that the use of chondroitin sulfate as a polyanion supported also the fibrillization of collagen I upon adsorption, which represents another topographical feature of ECM in connective tissues.[107] Beside collagens, also gelatin as a collagen degradation product has been used as a polycation for multilayer formation in a multitude of studies due to its bioactivity promoting cell adhesion,[108] but also in combination with fibronectin for coating of cells forming multicellular aggregates, as in the work of Akashi and co-workers.[109] Here, the presence of gelatin-binding domains in FN was used as a prerequisite for the layer formation process

making it a biospecific ligand interaction. FN as a multi-adhesive protein that is another major component of the ECM in connective tissue has also been employed by several other groups for making bioactive, cell-adhesive multilayer coatings.[110] Elastin represents an insoluble fibrous matrix protein that cannot be obtained from mammalian tissues, but soluble bioactive elastin fragments can be expressed in other organisms such as *E. coli*.[111] Such elastin fragments have been used to produce thermoresponsive multilayers that can be used for controlled adhesion of cells.[112] Beside natural proteins and polypeptides, synthetic-like cationic poly-L-lysine (PLL) and anionic polyglutamic acid (PGA) have also been used because of their polyelectrolyte nature and biodegradability, but lack any specific bioactivity. On the other hand, bioactive peptides, such as the tripeptide sequence arginylglycylaspartic acid (RGD) that does exist in ECM proteins like collagen, fibronectin, laminin and others as ligands to various integrins, have been used for grafting to biogenic and synthetic polyelectrolytes to mimic the native ECM structure and function (see Table 13.1). For example, RGD was grafted chemically to PGA on the final layer of the PLL/PGA multilayers improving adhesion and spreading of C2C12 cells.[113]

In addition to biochemical cues, mechanical properties of the matrix are another important parameter that affects cellular function. Hence, introducing mechanical cues *via* various methods was also part of the ECM mimicking strategies in the LbL technique. Schmidt *et al.* incorporated gold nanoparticles (AuNPs) into PLL/HA multilayers to tailor the mechanical properties of the film and observed improved cell adhesion which was due to the increased stiffness and roughness of AuNPs incorporated film.[114] Another method to modulate the stiffness of LbL films is the control of the non-covalent interactions among the building blocks which was well studied by Aggarwal *et al.* They used two different pH values (pH 4 and pH 9) of the heparin solution during assembly of heparin/chitosan multilayers leading to stiffer multilayers at pH 9 controlling adhesion and growth of C2C12 cells.[115] Moreover, chemical cross-linking using cross-linking agents was also used to modulate the mechanical properties of LbL films. Apte *et al.* could increase the elastic modulus of chitosan/alginate free-standing films using Genipin as an extrinsic cross-linker.[99] Other groups used small chemical cross-linkers (*e.g.*, EDC/NHS) for cross-linking that also provides control of mechanical properties of multilayers formed from HA and PLL and with that affects adhesion and differentiation of cells.[116] Others like Zhao *et al.* aimed to control the mechanical properties of HA/Col I and CS/Col I multilayers by intrinsic cross-linking *via* functionalization of HA and CS with aldehyde groups through oxidation forming covalent bonds to amino groups in collagen I. Their results show that intrinsic cross-linked multilayers are more stable and stiffer, compared to non-cross-linked multilayers, therefore enhancing cell adhesion and growth.[117]

Cells residing in native tissues are usually exposed to different porosities and topographies which extend from the macro to the nanoscale depending on the tissue type.[118] Therefore, topographical cues are also used as an

342   *Chapter 13*

Table 13.1   A short summary of the various methods used to achieve LbL systems that mimic properties of the native ECM.

ECM-mimicking approach	Method	References
Biochemical cues	Using natural ECM components such as GAGs (*e.g.*, hyaluronan, heparin and chondroitin sulfate) and proteins (*e.g.*, COL, FN, LM and elastin peptides)	107, 124, 164–167
	Semi-synthetic ECM-mimicking molecules such as cellulose sulfate, sulfated alginate and over-sulfated GAGs (advantageous to native molecules by overcoming batch to batch variations)	90, 102, 103, 168–170
	Grafting of ECM-derived peptides to one of the building blocks, such as RGD, REDV, KRSR and Syndecan targeting peptide derived from laminin-2 (L2synd)	113, 171–175
	Using nature inspired polypeptides having the ability to elicit specific cellular responses such as poly (L-lysine), poly (L-glutamic acid), poly-L-arginine and elastin-like recombinamers	176–181
Topographical cues	Changing pH during assembly, varying layer number, microcontact printing, photolithography, microfluidic techniques and nano/microstructures.	182–193
	Chemical crosslinking, acidic treatment (leading to the formation of microporous and rough topographical features), electric fields, embossing and imprinting	120, 194–200
Mechanical cues	Rigid material incorporation, such as graphene oxide (GO), carbon nanotubes (CNTs), gold nanoparticles (AuNPs), SiO$_2$ particles and montmorillonite (MTM)	114, 201–207
	Modulation of noncovalent interaction among building blocks (ionic cross-linking) by changing assembly parameters such as pH values, ionic strength (by salt concentration or electrochemical induction)	96, 115, 208–210
	Covalent chemical crosslinking using extrinsic crosslinking agents, such as 1-ethyl-3-[3-dimethylamino propyl] carbodiimide (EDC), Genipin (GnP) and glutaraldehyde (GA) Functionalization of building blocks before LbL assembly *via* thiol groups, aldehyde groups, *etc.* (intrinsic).	99, 107, 116, 117, 124, 125, 211–218
	Complex/apparent interfacial stiffness that combines the stiffness of the LbL film and that of the underlying substrate	219, 220
Storage and presentation capability of the matrix	Controlled upload and release of GFs and other morphogens such as BMP-2, transforming growth factor β1 (TGF-β1), FGF-2 and VEGF	121, 122, 124, 141, 221, 222

Biomimetic Surface Modifications of Biomaterials Using a Layer-by-layer Technique   343

ECM-mimicking strategy. Niepel *et al.* presented topographical cues to cells using nanostructured samples modified with multilayers of HA and PLL. A change in human adipose-derived stem cell's adhesion and differentiation was achieved and highly dependent on the distance of anchorage points that were designed by laser interference lithography.[119] Hajicharalambous *et al.* obtained a porosity of LbL films by exposure to acidic solution of pH 2 to obtain nano-porous and of pH 2.3 to get a micro-porous film. The pore diameter in poly(acrylicacid)/poly(allylamine hydrochloride) films was 100 nm and 600 nm for the nano-porous and micro-porous films, respectively. Such porous films exhibiting topographical cues showed enhanced proliferation and migration of corneal epithelial cells on nano-porous films which represent a favorable environment for those kinds of cells.[120]

Since the ECM also represents a reservoir for GFs where they are protected from proteases and may also present them to the corresponding cell receptors; a system that would mimic the *in vivo* situation allowing their local delivery in a bound manner with preservation of their bioactivity and protecting them from degradation has always been an appealing idea in the biomedical field.[121] In this regard, LbL systems have been widely used; as they are fabricated in aqueous solutions that will not expose GFs to harsh conditions, and will also allow for their localized delivery and keeping them bioactive.[122] Crouzier *et al.* used PLL/HA films and loaded them with rhBMP-2 where they proved that loaded BMP-2 remained bioactive for more than 10 days.[121] Furthermore, it was also shown that bound BMP-2 (loaded in the multilayers) could significantly increase cell adhesion and migration of C2C12 cells while soluble BMP-2 added to the medium had no such effect.[123,124] The latter emphasizes and shows that LbL systems can be used to mimic the reservoir role of the ECM as well as the way GFs are presented to cells (in a bound state). There are many other examples on the use of multilayers as reservoirs and delivery tools for other growth factors like FGF, TGF and VEGF (see Table 13.1).

In addition, a combination of more than one approach could be used in LbL technique to mimic the complex properties of native ECM. This can be found in the work of Groth and co-workers where they presented various cues in their LbL system; biochemical cues using GAGs such as HEP and CS, mechanical cues that were achieved using the oxidized versions of GAGs for intrinsic chemical cross-linking affecting mechanical properties of multilayers and mimicking the storage and presentation capability of native ECM by loading BMP-2. The result was an ECM-biomimetic LbL system that offered enhanced stability, stiffness of the substrate and a controlled localized release of BMP-2 that could trigger the differentiation of C2C12 cells into osteoblasts.[124]

13.5.2 Examples of Application of LbL for Coating of Implantable Devices

It has been shown in the previous section that LbL multilayer coatings can mimic properties of ECM. Hence, it can be used to improve the

biorecognition and integration of implantable devices. Because most metals and inorganic materials such as glass, but also most polymers are negatively charged, the adsorption of a polycation and subsequent multilayer formation is possible.[66] Here we provide a brief survey with examples of existing and potential applications of LbL in the field of implantable devices.

13.5.2.1   Use of LbL for Control of Cell Adhesion and Implant Integration

The bio-integration between the implant and the host tissue occurs at the interface of both; hence, the surface of the implant plays a crucial role in determining the initial response which then affects further biological processes.[54] LbL offers the opportunity to modify surfaces for improved cell adhesion and function by varying several factors, such as stiffness or presentation of cell-specific adhesion motifs. To control the mechanical properties of the multilayer coating, Esmaeilzadeh *et al.* used an intrinsic cross-linking approach which was achieved using thiolated chitosan/ thiolated chondroitin sulfate multilayers that were superior to native multilayers in enhancing cell adhesion of human keratinocytes. Such stable coatings could be used for coating scaffolds or implants.[125] Another more selective method of cross-linking was shown in the work done by Phelps *et al.* using carbodiimide to cross-link only the outermost layers of PLL/PGA multilayer coatings. This selective strategy offered a stiff surface that enhanced pre-osteoblast cells adhesion without affecting the interior of films, and thus, still permitting future options to load bioactive molecules without the risk of deactivation of the loaded biomolecules.[126] Here, it is worth mentioning that cross-linking is beneficial in controlling the release of active molecules from the multilayers, which will be highlighted in further paragraphs. The effect of polyelectrolyte multilayer coatings on the osseointegration of titanium alloys was studied by Zankovych *et al.* both *in vitro*[127] and *in vivo*[128] using a rat model. The titanium alloy was coated either with chitosan/gelatine or chitosan/hyaluronic acid multilayer coating and compared to the uncoated titanium alloy where it was found that the multilayer coatings had a positive effect on improving the osseointegration of the implant compared to the uncoated titanium alloy.

13.5.2.2   Control of Tissue Response and Prevention of Bacterial Growth after Implantation

When talking about implantable devices, immune rejection and the formation of biofilms by bacteria represent challenges that might cause implant failure.[91] Therefore, multilayer coatings that have antifouling, but also partly anti-inflammatory properties are a promising solution in that regard. Alkhoury *et al.* showed that heparin/chitosan and hyaluronic

Biomimetic Surface Modifications of Biomaterials Using a Layer-by-layer Technique   345

acid/chitosan multilayers were able to control macrophage activation by the uptake of those molecules through macrophages leading to the suppression of the canonical NF-κB signaling. Such use of multilayers can be used to improve the function of implantable biomedical devices by modulating the inflammatory responses.[129] Moreover, an inclusion of active agents as building blocks of multilayers, permitted Wong *et al.*, to develop a contact-killing approach against bacteria and viruses by using multilayers of *N,N*-dodecylmethyl-polyethylene imine, having antimicrobial activity. The multilayer surfaces were able to kill airborne and waterborne bacteria such as *Escherichia coli* and *Staphylococcus aureus*, as well as, viruses such as influenza virus, strain H1N1.[130] Furthermore, chitosan due to its antimicrobial properties has been used for antimicrobial multilayer coatings, too. Chua *et al.* functionalized titanium substrates, which are extensively used in orthopedic implants, with hyaluronic acid/chitosan multilayers where 80% reduction in bacterial adhesion was observed in comparison to pristine titanium.[131]

13.5.3 Multilayers "Free Standing Films" for Wound Healing Applications

Since the LbL technique offers the opportunity to fabricate not only several layers, but hundreds of layers in addition to the use of aqueous conditions; it became possible to fabricate nanostructured films that are useful for biological applications and exhibiting nanoscale precision. This kind of micrometer thick multilayer is a so-called "freestanding film".[99] Producing films that can be detached from the substrate is challenging. Thus, many strategies have been developed to achieve them. A common approach is using a base layer or substrate that can be dissolved later after the fabrication of the film.[132–134] Some studies focused on preparing cross-linked freestanding films that support and enhance cell adhesion, mostly for bone and cardiac tissue engineering.[135–137] Mano and co-workers were the first to report an adhesive natural-based freestanding film composed of chitosan, alginate and sulfated levan. Their study showed that the cross-linked and non-cross-linked films were both cytocompatible and myoconductive and could be further used for applications in cardiac tissue engineering.[135] Other studies focused on developing non-adhesive films presenting low cell attachment while being able to protect against infection and take up fluids to be used as wound dressings. For that, Groth and co-workers could successfully fabricate detachable free-standing films made of ALG/Chi that were assembled on glass slides, and various cross-linking methods were studied to improve the mechanical properties of the films while maintaining their biocompatibility for use in wound dressings.[99] Furthermore, due to the high capacity of loading offered by those free-standing films and their applicability for wound healing and burns; where large skin areas might be prone to bacterial infections, systemic sepsis or even severe septicemia leading to death,[138,139]
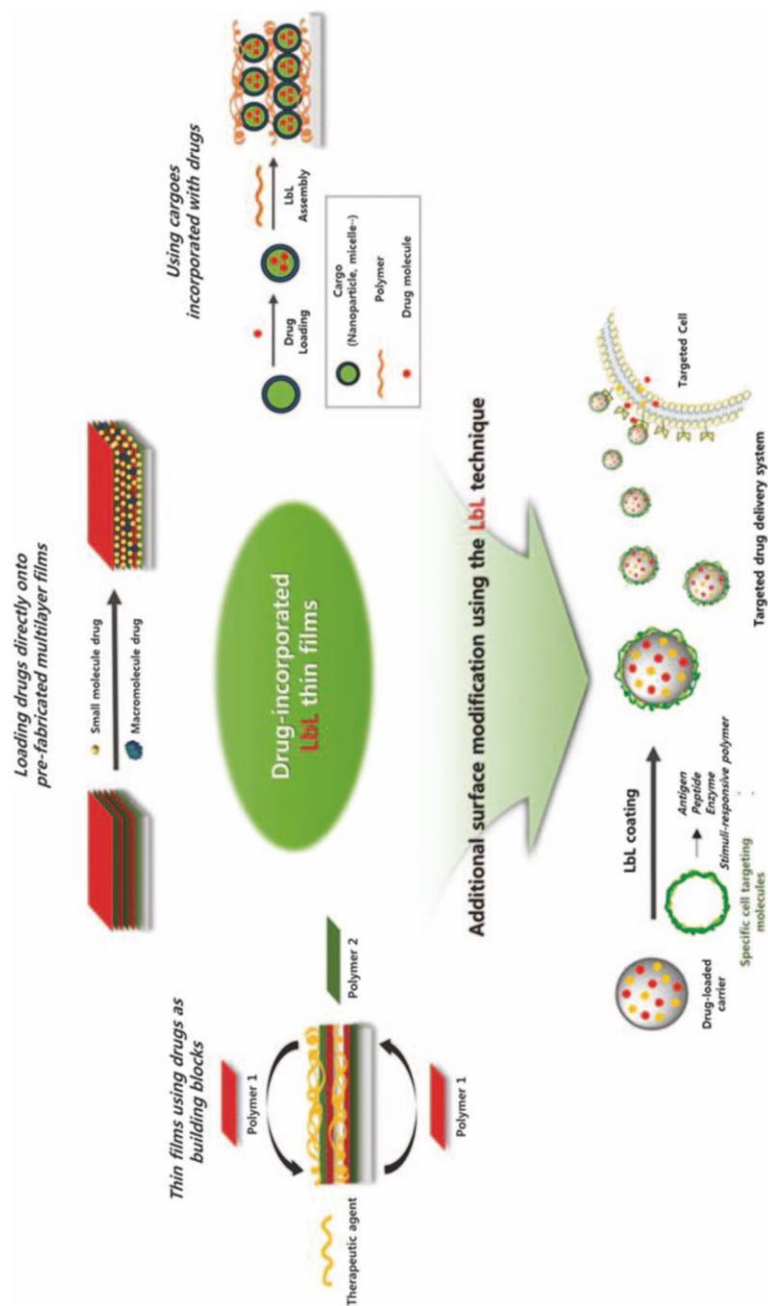
346   *Chapter 13*

Figure 13.7   Illustration showing a drug delivery system using multilayer films assembled by LbL. Reproduced from ref. 267.

Biomimetic Surface Modifications of Biomaterials Using a Layer-by-layer Technique   347

several studies focused on loading the films with antibacterial agents. Shen *et al.* used PLL/HA free-standing films which were then loaded with silver nanoparticles that allowed enhancing the mechanical properties of the film in addition to owning antibacterial properties.[140]

13.5.4 Stabilization and Controlled Release of Biogenic Drugs

Several methods including liposomes, capsules, micelles and polymerosomes were developed due to the need to effectively deliver biogenic drugs while protecting them from degradation (Figure 13.7).[91] This proves the continuous need for effective systems to control the delivery of bioactive molecules and drugs. Macdonald *et al.* used a tetralayer system composed of poly(β-aminoester)/chondroitin sulfate/BMP-2/chondroitin sulfate. This multilayer system proved a capability of microgram-scale release of BMP-2 which was bioactive over several weeks and could direct the host tissue response to create bone from native progenitor cells, both *in vitro* and *in vivo* when intramuscular implants were coated with this film.[141] Preserving the bioactivity of growth factors highlights a very important feature offered by LbL when loading bioactive agents. This proof of concept was extended by Guillot *et al.* for *in vivo* studies in rat models where they used a PLL/HA multilayer system loaded with BMP-2 to coat titanium[142] and tricalcium phosphate/hydroxyapatite macroporous granules.[143] There, the loaded BMP-2 exhibited osteoconductive and osteoinductive properties. Another work was presented by Groth and co-workers using oxidized heparin/CHI and oxidized CS/CHI multilayers loaded with BMP-2 where the released BMP-2 was bioactive to enhance the differentiation of C2C12 myoblasts into osteoblasts.[124] Moreover, the use of multilayers as reservoirs was not restricted to BMP-2 only. Several other growth factors were studied in that regard such as FGF-2 and also VEGF. Hammond and co-workers incorporated FGF-2 in synthetic hydrolytically degradable multilayers, where the GF was kept bioactive and could promote the proliferation of MC3T3 pre-osteoblast cells.[122] Combining two GFs is another interesting strategy that was used by Shah *et al.* to help accelerate joint implant integration and reduce recovery time and failure rates. A combination of rhBMP-2 with rhVEGF was used in degradable [poly(β-amino ester)/polyanion/growth factor/polyanion] multilayers; which were tested both *in vitro* and *in vivo* using an ectopic rat model where the density of formed *de novo* bone was 33% higher than when only rhBMP-2 was introduced to the multilayers.[144] Furthermore, it should be mentioned that LbL coatings have been used to get capsules with tunable permeability[145–147] in order to deliver various drugs to the surrounding environment or even intracellularly,[148,149] which is a promising tool for further applications such as cancer treatments where chemotherapies can be delivered using such drug carriers to the target cells without harming the surrounding cells.

348   *Chapter 13*

13.5.5   Encapsulation of Cells for Cell Therapies and Engineering Tissues

Bioencapsulation strategies have been employed to treat many diseases such as bone and cartilage defects, cancer and diabetes.[150] In this approach, a biocompatible, semi-permeable matrix allowing the exchange of oxygen, nutrients and cell metabolite by-products is used to entrap viable cells. Here, LbL technique has been used in various ways to achieve cell encapsulation either in a direct or indirect way. Taking advantage of the negative charge of cells, fabrication of multilayers on the surface of cells can be used to encapsulate cells or to produce cell aggregates in a direct manner. Whereas multilayer coatings done after cells are encapsulated inside a hydrogel are considered the indirect way.[151] Since immune rejection and other factors might contribute to the failure of allogenic or xenogenic islet transplantation, Wilson *et al.* used ALG and PLL-*g*-PEG multilayers to coat the surface of pancreatic islet cells for *in vivo* studies. The coated islets could maintain viability and function and were able then to convert 47% of the mice receiving the coated islets from a diabetic to normal glycemic state.[152] Furthermore, some limitations are accompanied with indirect cell encapsulation using a solid core matrix. These include low rate of nutrient exchange, reduced cell growth and protein production.[153] Therefore, Mano and co-workers developed a unique concept of liquefied capsules where the core hydrogel used to encapsulate cells is liquefied after LbL deposition, allowing freedom for the encapsulated cells to construct their 3D organization, while permitting the exchange of nutrients. In their work, chitosan/ alginate multilayers were built on the core of alginate hydrogel spheres that were used as cell encapsulation templates for the construction of the LbL. The alginate core was then liquified by chelation of calcium ions using ethylenediaminetetraacetic acid (EDTA).[154] Another study from the same group involved the use of Col I-functionalized PLLA microparticles as solid cell adhesion sites for cells to be encapsulated where poly(L-lysine), alginate and chitosan coatings were built up after which the EDTA was used to liquify the alginate core. Adipose stem cells co-cultured with endothelial cells were immobilized in the liquefied capsules, which could drive self-regulated osteogenesis even in the absence of differentiation factors.[155]

In addition, encapsulation of single cells or making of multicellular aggregates in liquefied capsules may represent the basis to generate complex multicellular tissue-like structures consisting of more than one cell type representing the complexity of human tissues and organs. Akashi and co-workers coated single cells of different types with multilayers from gelatin and fibronectin forming an ECM nanofilm on the cell membrane during the encapsulation. The study involved coating of human induced pluripotent stem cells (hiPSCs) that were co-cultured with cardiomyocyte and used the adhesiveness of the coatings to assemble cells into 3D structures. This ECM nanofilm improved cell–cell interactions by providing matrix components for integrin ligation and cell–cell contact for signal transduction process that

Table 13.2 Summary list of the polyelectrolytes used for functionalizing biomaterials by layer-by-layer assembly. Adapted/reproduced from Gentile *et al.* (2015).[159]

Polyelectrolyte	Properties	Applications	References
Natural polysaccharides			
Heparin	Highest sulfated GAG, binds to GFs, antithrombotic, anticoagulant, anti-inflammatory, anticancer	Implant coating, antimicrobial coating, intravascular stent, ultrafiltration membranes	22, 166, 223–234
Chondroitin sulfate	Major GAG of native cartilage, negatively charged polyelectrolyte, biodegradable, anti-inflammatory	Implant coating, intravascular stent, multilayered capsules, cartilage and bone repair	141, 165, 227, 235–239
Hyaluronic acid	The only non-sulfated GAG, a component of ECM and soft connective tissues	Implant coating, antimicrobial coating, ligament regeneration, freestanding films	22, 140, 240–243
Chitosan	Positively charged polysaccharide, antimicrobial activity, biodegradable	Implant coating, cell encapsulation, intravascular stent, tissue regeneration (ligament, nerve, cartilage), freestanding films, antithrombogenic and antimicrobial coating, nanoparticles	99, 223, 235–237, 240, 244–251
Alginate	Emulsion stabilizer, cross-link in the presence of calcium forming a gel, shear-thinning thickener in absence of calcium	Liquified capsules for cell encapsulation, bioactive coating, nanoparticles, freestanding films	99, 154, 250, 252
Proteins			
Gelatin	Protein produced by partial hydrolysis of collagen	Microcapsules, regeneration of ligament	243, 253, 254
Laminin	A high molecular weight glycoprotein of the ECM and basement membrane	Regeneration of nerves	246, 255
Albumin	The most abundant blood plasma protein	Coating of biomaterial surfaces, reduction of undesirable nonspecific interactions of the surface with blood plasma proteins	232
Elastin-like polymers	Biopolymers having similar structure to elastin	Biomimetic coatings, biomedical applications, drug delivery and tissue engineering	180, 181
Collagen	The main structural protein of the ECM, low antigenicity, biocompatibility	Bone and cartilage regeneration, intravascular stent	165, 225, 228, 229, 235, 241, 251, 256

Table 13.2 (*Continued*)

Polyelectrolyte	Properties	Applications	References
Fibronectin	A high molecular weight glycoprotein of the ECM, cell-adhesion protein	Single cell coating, intravascular stent	156, 166, 257
Silk fibroin	The insoluble protein present in silk, self-assembly biomaterial, biocompatible	Bioactive coating, controlled release application, microcapsules	244, 258, 259
Growth factors			
Vascular endothelial growth factor (VEGF)	Mediator of angiogenesis	Stimulation of vascularization, intravascular stent	222, 223, 260
Bone morphogenetic protein 2 (BMP-2)	Therapeutic protein	Bioactive coating, bone regeneration	124, 141
Fibroblasts growth factor (FGF)	Binds with various ECM polysaccharides	Bioactive coatings, regeneration of bone, cartilage, skin and nerve	122, 261
Transforming growth factor-β (TGF-β)	Soluble extracellular protein	Cartilage and bone regeneration applications, bioactive coatings	221
Polyaminoacids			
Poly-L-glutamine	Negatively charges polyelectrolyte, biodegradable	Tissue regeneration such as, nerves	178, 262
Poly-L-lysine	Biocompatible polyelectrolyte, cell-adhesive properties	Encapsulation of cells, bioactive coating, nanoparticles, nerve regeneration, freestanding films	140, 155, 177, 238, 252, 262–264
Poly-L-arginine	Biocompatible, polyelectrolyte film formation	Microcapsules for drug delivery, bone regeneration, nanoparticles	265, 266

Biomimetic Surface Modifications of Biomaterials Using a Layer-by-layer Technique   351

promote functionality of these bioartificial tissues. The increased cell viability was reflected by the higher beating frequency of the "mini heart issues" formed with ECM-coated cells compared to the non-coated ones.[156]

Since LbL can be used to coat substrates with different geometries, not only implants but also 3D porous scaffolds can be coated with LbL; it provides an alternative for cell growth platforms for tissue engineering applications. Sher *et al.* used a perfusion-assisted LbL strategy to coat paraffin wax particles with CHI–ALG films which were then dissolved by dichloromethane, resulting in a porous and interconnected scaffold that contains the PEM structure only. Human osteoblast-like cells could adhere and proliferate within 7 days on the developed porous scaffold.[157] Another interesting approach in that regard is when using ECM components together with cells as a building block of the multilayers that can be used as transplantable constructs or angiogenesis models. Following this approach, Yoshida *et al.* used layered polyelectrolyte/cell structures as blood vessel analogs.[158] Therefore, such approaches with LbL are promising for the field of tissue engineering where they can be adapted for the production of other tissues such as the heart and pancreas. In conclusion on the above examples, the wide range of polyelectrolytes of synthetic or biological origin, their inherent bioactivity and other properties have opened avenues to a multitude of potential biomedical applications of LbL, which are summarized in Table 13.2.

13.6   Conclusion

Understanding the native extracellular microenvironment of cells, including the cell–ECM interactions can help to design material systems for medical devices like implants that have the capability to guide cell fate in terms of adhesion, proliferation and differentiation, thus, promoting regeneration and replacement of damaged tissues and organs. LbL represents a versatile and flexible tool by which several properties of coatings and 3D systems, such as the kind of biomolecule, mechanical properties and topography can be adjusted to mimic ECM properties to achieve control on interaction of cells with the implant material or to design complex 3D structures made of cells coated with ECM-like multilayers. Although the number of clinical applications of LbL technique, especially using ECM-mimicking approaches, is still limited; we consider it as a promising technique to be used for the development of better conventional implants, tissue engineering and cell-based therapies in the future.

Acknowledgements

352   Chapter 13

References

1. R. O. Hynes, *Science*, 2009, **326**, 1216–1219.
2. C. Frantz, K. M. Stewart and V. M. Weaver, *J. Cell Sci.*, 2010, **123**, 4195–4200.
3. A. D. Theocharis, D. Manou and N. K. Karamanos, *FEBS J.*, 2019, **286**, 2830–2869.
4. E. M. Culav, C. H. Clark and M. J. Merrilees, *Phys. Ther.*, 1999, **79**, 308–319.
5. T. J. McKee, G. Perlman, M. Morris and S. V. Komarova, *Sci. Rep.*, 2019, **9**, 1–15.
6. M. B. Mathews, *Connective Tissue: Macromolecular Structure and Evolution*, Springer Science & Business Media, 2012.
7. A. D. Theocharis, S. S. Skandalis, C. Gialeli and N. K. Karamanos, *Adv. Drug Delivery Rev.*, 2016, **97**, 4–27.
8. T. Rozario and D. W. DeSimone, *Dev. Biol.*, 2010, **341**, 126–140.
9. B. D. Boyan, T. W. Hummert, D. D. Dean and Z. Schwartz, *Biomaterials*, 1996, **17**, 137–146.
10. S. Ricard-Blum, *Cold Spring Harbor Perspect. Biol.*, 2011, **3**, a004978.
11. S. M. Mithieux and A. S. Weiss, *Advances in Protein Chemistry*, Elsevier, 2005, vol. 70, pp. 437–461.
12. S. G. Wise and A. S. Weiss, *Int. J. Biochem. Cell Biol.*, 2009, **41**, 494–497.
13. H. Vindin, S. M. Mithieux and A. S. Weiss, *Matrix Biol.*, 2019, **84**, 4–16.
14. P. Singh, C. Carraher and J. E. Schwarzbauer, *Annu. Rev. Cell Dev. Biol.*, 2010, **26**, 397–419.
15. R. Hynes, *Cell*, 1992, **69**, 11–25.
16. M. L. Smith, D. Gourdon, W. C. Little, K. E. Kubow, R. A. Eguiluz, S. Luna-Morris and V. Vogel, *PLoS Biol.*, 2007, **5**, e268.
17. V. Llopis-Hernández, M. Cantini, C. González-García, Z. A. Cheng, J. Yang, P. M. Tsimbouri, A. J. García, M. J. Dalby and M. Salmerón-Sánchez, *Sci. Adv.*, 2016, **2**, e1600188.
18. T. E. Hardingham and A. J. Fosang, *FASEB J.*, 1992, **6**, 861–870.
19. J. Robbins and K. Vogel, *Eur. J. Cell Biol.*, 1994, **64**, 264–270.
20. Y. Choi, H. Chung, H. Jung, J. R. Couchman and E.-S. Oh, *Matrix Biol.*, 2011, **30**, 93–99.
21. M. Yanagishita, *Pathol. Int.*, 1993, **43**, 283–293.
22. A. Köwitsch, G. Zhou and T. Groth, *J. Tissue Eng. Regener. Med.*, 2018, **12**, e23–e41.
23. A. Bafico and S. Aaronson, in *Holland-Frei Cancer Medicine*, ed. D. W. Kufe, R. E. Pollock, R. R. Weichselbaum, R. C. Bast Jr, T. S. Gansler, J. F. Holland and E. Frei III, 6th edn, 2003.
24. G. Halder, S. Dupont and S. Piccolo, *Nat. Rev. Mol. Cell Biol.*, 2012, **13**, 591–600.
25. F. Gattazzo, A. Urciuolo and P. Bonaldo, *Biochim. Biophys. Acta, Gen. Subj.*, 2014, **1840**, 2506–2519.
26. N. Wang, J. D. Tytell and D. E. Ingber, *Nat. Rev. Mol. Cell Biol.*, 2009, **10**, 75–82.

Biomimetic Surface Modifications of Biomaterials Using a Layer-by-layer Technique   353

27. T. Mammoto and D. E. Ingber, *Development*, 2010, **137**, 1407–1420.
28. A. J. Engler, S. Sen, H. L. Sweeney and D. E. Discher, *Cell*, 2006, **126**, 677–689.
29. J. S. Park, J. S. Chu, A. D. Tsou, R. Diop, Z. Tang, A. Wang and S. Li, *Biomaterials*, 2011, **32**, 3921–3930.
30. C. Alain and L. Valérie, *Surface and Interfacial Aspects of Cell Adhesion*, CRC Press, 2011, pp. 3–18.
31. M. Lotfi, M. Nejib and M. Naceur, in *Advances in Biomaterials Science and Biomedical Applications*, ed. R. Pignatello, INTECH, 2013, pp. 207–240.
32. R. Juliano, *Annu. Rev. Pharmacol. Toxicol.*, 2002, **42**, 283–323.
33. A. L. Berrier and K. M. Yamada, *J. Cell. Physiol.*, 2007, **213**, 565–573.
34. O. Mashinchian, L. A. Turner, M. J. Dalby, S. Laurent, M. A. Shokrgozar, S. Bonakdar, M. Imani and M. Mahmoudi, *Nanomedicine*, 2015, **10**, 829–847.
35. K. Kulangara, Y. Yang, J. Yang and K. W. Leong, *Biomaterials*, 2012, **33**, 4998–5003.
36. R. O. Hynes, *Cell*, 2002, **110**, 673–687.
37. A. Aplin, A. Howe, S. Alahari and R. Juliano, *Pharmacol. Rev.*, 1998, **50**, 197–264.
38. F. G. Giancotti, and E. Ruoslahti, *Science*, 1999, **285**, 1028–1032.
39. J. S. Desgrosellier and D. A. Cheresh, *Nat. Rev. Cancer*, 2010, **10**, 9–22.
40. C. K. Miranti and J. S. Brugge, *Nat. Cell Biol.*, 2002, **4**, E83–E90.
41. J. Robert and A. Latour, *Encycl. Biomater. Biomed. Eng.*, 2005, 1–3.
42. C. T. Laurencin, A. Ambrosio, M. Borden and J. Cooper Jr, *Annu. Rev. Biomed. Eng.*, 1999, **1**, 19–46.
43. F. J. O'brien, *Mater. Today*, 2011, **14**, 88–95.
44. A. Vats, N. Tolley, J. Polak and J. Gough, *Clin. Otolaryngol. Allied Sci.*, 2003, **28**, 165–172.
45. E. Eisenbarth, *Adv. Eng. Mater.*, 2007, **9**, 1051–1060.
46. B. D. Ratner, A. S. Hoffman, F. J. Schoen and J. E. Lemons, *Biomaterials Science: an Introduction to Materials in Medicine*, Elsevier, 2004.
47. T. Groth, G. Altankov, A. Kostadinova, N. Krasteva, W. Albrecht and D. Paul, *J. Biomed. Mater. Res.*, 1999, **44**, 341–351.
48. S. P. Mitra, *J. Surface Sci. Technol.*, 2020, **3**, 7–38.
49. R. Tzoneva, M. Heuchel, T. Groth, G. Altankov, W. Albrecht and D. Paul, *J. Biomater. Sci., Polym. Ed.*, 2002, **13**, 1033–1050.
50. N. Faucheux, R. Schweiss, K. Lützow, C. Werner and T. Groth, *Biomaterials*, 2004, **25**, 2721–2730.
51. T. Groth, J. Synowitz, G. Malsch, K. Richau, W. Albrecht, K.-P. Lange and D. Paul, *J. Biomater. Sci., Polym. Ed.*, 1997, **8**, 797–807.
52. E. A. Vogler and C. A. Siedlecki, *Biomaterials*, 2009, **30**, 1857–1869.
53. N. Faucheux, R. Tzoneva, M.-D. Nagel and T. Groth, *Biomaterials*, 2006, **27**, 234–245.
54. L. Hao and J. Lawrence, *Laser Surface Treatment of Bio-implant Materials*, Wiley, Chichester, UK, 2005.

354   *Chapter 13*

55. Z. Ma, Z. Mao and C. Gao, *Colloids Surf., B*, 2007, **60**, 137–157.
56. R. Williams, *Surface Modification of Biomaterials: Methods Analysis and Applications*, Elsevier, 2010.
57. T. Groth, Z.-M. Liu, M. Niepel, D. Peschel, K. Kirchhof, G. Altankov and N. Faucheux, *Advances in Regenerative Medicine: Role of Nanotechnology, and Engineering Principles*, Springer, 2010, pp. 253–284.
58. P. Hamerli, T. Weigel, T. Groth and D. Paul, *Surf. Coat. Technol.*, 2003, **174**, 574–578.
59. X. Xu, R. W. M. Kwok and W. M. Lau, *Thin Solid Films*, 2006, **514**, 182–187.
60. L. Guo, N. Kawazoe, Y. Fan, Y. Ito, J. Tanaka, T. Tateishi, X. Zhang and G. Chen, *Biomaterials*, 2008, **29**, 23–32.
61. P. Hamerli, T. Weigel, T. Groth and D. Paul, *Biomaterials*, 2003, **24**, 3989–3999.
62. V. Thom, G. Altankov, T. Groth, K. Jankova, G. Jonsson and M. Ulbricht, *Langmuir*, 2000, **16**, 2756–2765.
63. L. Bačáková, K. Walachová, V. Švorčík and V. Hnatowicz, *J. Biomater. Sci., Polym. Ed.*, 2001, **12**, 817–834.
64. A. Vonarbourg, C. Passirani, P. Saulnier and J.-P. Benoit, *Biomaterials*, 2006, **27**, 4356–4373.
65. D. Klee, Z. Ademovic, A. Bosserhoff, H. Hoecker, G. Maziolis and H.-J. Erli, *Biomaterials*, 2003, **24**, 3663–3670.
66. Z. Tang, Y. Wang, P. Podsiadlo and N. A. Kotov, *Adv. Mater.*, 2006, **18**, 3203–3224.
67. M. S. Niepel, B. Fuhrmann, H. S. Leipner and T. Groth, *Langmuir*, 2013, **29**, 13278–13290.
68. S. Zhang, M. Xing and B. Li, *Int. J. Mol. Sci.*, 2018, **19**, 1641.
69. A. J. García, *Found. Regener. Med.: Clin. Ther. Appl.*, 2009, 368–378.
70. C. Mas-Moruno, *Peptides and Proteins as Biomaterials for Tissue Regeneration and Repair*, Elsevier, 2018, pp. 73–100.
71. M. Morra, *Expert Rev. Med. Devices*, 2007, **4**, 361–372.
72. E. Ruoslahti and M. D. Pierschbacher, *Cell*, 1986, **44**, 517–518.
73. T. H. Barker, *Biomaterials*, 2011, **32**, 4211–4214.
74. S. L. Bellis, *Biomaterials*, 2011, **32**, 4205–4210.
75. J. H. Collier and T. Segura, *Biomaterials*, 2011, **32**, 4198–4204.
76. M. Morra, *Eur. Cells Mater.*, 2006, **12**, 15.
77. W. Zhang, C. Zhu, Y. Wu, D. Ye, S. Wang, D. Zou, X. Zhang, D. L. Kaplan and X. Jiang, *Eur. Cells Mater.*, 2014, **27**, 1–11.
78. M. M. Martino, P. S. Briquez, K. Maruyama and J. A. Hubbell, *Adv. Drug Delivery Rev.*, 2015, **94**, 41–52.
79. M. Salmerón-Sánchez and M. J. Dalby, *Chem. Commun.*, 2016, **52**, 13327–13336.
80. Q. Wei, T. L. Pohl, A. Seckinger, J. P. Spatz and E. A. Cavalcanti-Adam, *Beilstein J. Org. Chem.*, 2015, **11**, 773–783.
81. S. N. Lissenberg-Thunnissen, D. J. de Gorter, C. F. Sier and I. B. Schipper, *Int. Orthop.*, 2011, **35**, 1271.

Biomimetic Surface Modifications of Biomaterials Using a Layer-by-layer Technique   355

82. E. J. Carragee, E. L. Hurwitz and B. K. Weiner, *Spine J.*, 2011, **11**, 471–491.

83. E. J. Carragee, G. Chu, R. Rohatgi, E. L. Hurwitz, B. K. Weiner, S. T. Yoon, G. Comer and B. Kopjar, *J. Bone Jt. Surg.*, 2013, **95**, 1537–1545.

84. H. Hutchings, N. Ortega and J. Plouët, *FASEB J.*, 2003, **17**, 1–27.

85. M. A. Nugent and R. V. Iozzo, *Int. J. Biochem. Cell Biol.*, 2000, **32**, 115–120.

86. G. A. Hudalla and W. L. Murphy, *Adv. Funct. Mater.*, 2011, **21**, 1754–1768.

87. V. Moulisová, C. Gonzalez-García, M. Cantini, A. Rodrigo-Navarro, J. Weaver, M. Costell, R. S. I. Serra, M. J. Dalby, A. J. García and M. Salmerón-Sánchez, *Biomaterials*, 2017, **126**, 61–74.

88. T. T. Chen, A. Luque, S. Lee, S. M. Anderson, T. Segura and M. L. Iruela-Arispe, *J. Cell Biol.*, 2010, **188**, 595–609.

89. A. Yoneda, M. Asada, Y. Oda, M. Suzuki and T. Imamura, *Nat. Biotechnol.*, 2000, **18**, 641–644.

90. R. Mhanna, J. Becher, M. Schnabelrauch, R. L. Reis and I. Pashkuleva, *Adv. Biosyst.*, 2017, **1**, 1700043.

91. R. R. Costa and J. F. Mano, *Chem. Soc. Rev.*, 2014, **43**, 3453–3479.

92. R. Iler, *J. Colloid Interface Sci.*, 1966, **21**, 569–594.

93. G. Decher and J. D. Hong, *Macromol. Symp.*, 1991, **46**, 321–327.

94. M. S. Niepel, D. Peschel, X. Sisquella, J. A. Planell and T. Groth, *Biomaterials*, 2009, **30**, 4939–4947.

95. J. Borges and J. F. Mano, *Chem. Rev.*, 2014, **114**, 8883–8942.

96. K. Kirchhof, A. Andar, H. Yin, N. Gadegaard, M. Riehle and T. Groth, *Lab Chip*, 2011, **11**, 3326–3335.

97. K. Ariga, M. McShane, Y. M. Lvov, Q. Ji and J. P. Hill, *Expert Opin. Drug Delivery*, 2011, **8**, 633–644.

98. S. I. Lamberg and A. C. Stoolmiller, *J. Invest. Dermatol.*, 1974, **63**, 433–449.

99. G. Apte, A. Repanas, C. Willems, A. Mujtaba, C. E. Schmelzer, A. Raichur, F. Syrowatka and T. Groth, *Macromol. Biosci.*, 2019, **19**, 1900181.

100. C. H. Jou, L. Yuan, S. M. Lin, M. C. Hwang, W. L. Chou, D. G. Yu and M. C. Yang, *J. Appl. Polym. Sci.*, 2007, **104**, 220–225.

101. M. N. R. Kumar, *React. Funct. Polym.*, 2000, **46**, 1–27.

102. K. Zeng, T. Groth and K. Zhang, *ChemBioChem*, 2019, **20**, 737–746.

103. N. Aggarwal, N. Altgärde, S. Svedhem, K. Zhang, S. Fischer and T. Groth, *Langmuir*, 2013, **29**, 13853–13864.

104. D. Peschel, K. Zhang, S. Fischer and T. Groth, *Acta Biomater.*, 2012, **8**, 183–193.

105. D. Peschel, K. Zhang, N. Aggarwal, E. Brendler, S. Fischer and T. Groth, *Acta Biomater.*, 2010, **6**, 2116–2125.

106. G. Decher, M. Eckle, J. Schmitt and B. Struth, *Curr. Opin. Colloid Interface Sci.*, 1998, **3**, 32–39.

107. M. Zhao, G. Altankov, U. Grabiec, M. Bennett, M. Salmeron-Sanchez, F. Dehghani and T. Groth, *Acta Biomater.*, 2016, **41**, 86–99.

108. Z. M. Liu, Q. Gu, Z. K. Xu and T. Groth, *Macromol. Biosci.*, 2010, **10**, 1043–1054.

356   *Chapter 13*

109. K. Sasaki, T. Akagi, T. Asaoka, H. Eguchi, Y. Fukuda, Y. Iwagami, D. Yamada, T. Noda, H. Wada and K. Gotoh, *Biomaterials*, 2017, **133**, 263–274.

110. C. R. Wittmer, J. A. Phelps, W. M. Saltzman and P. R. Van Tassel, *Biomaterials*, 2007, **28**, 851–860.

111. A. Girotti, J. Reguera, J. C. Rodríguez-Cabello, F. J. Arias, M. Alonso and A. M. Testera, *J. Mater. Sci.: Mater. Med.*, 2004, **15**, 479–484.

112. M. Golonka, M. Bulwan, M. Nowakowska, A. M. Testera, J. C. Rodríguez-Cabello and S. Zapotoczny, *Soft Matter*, 2011, **7**, 9402–9409.

113. V. Gribova, C. Gauthier-Rouvière, C. Albigès-Rizo, R. Auzely-Velty and C. Picart, *Acta Biomater.*, 2013, **9**, 6468–6480.

114. S. Schmidt, N. Madaboosi, K. Uhlig, D. Köhler, A. Skirtach, C. Duschl, H. Möhwald and D. V. Volodkin, *Langmuir*, 2012, **28**, 7249–7257.

115. N. Aggarwal, N. Altgärde, S. Svedhem, G. Michanetzis, Y. Missirlis and T. Groth, *Macromol. Biosci.*, 2013, **13**, 1327–1338.

116. K. Ren, T. Crouzier, C. Roy and C. Picart, *Adv. Funct. Mater.*, 2008, **18**, 1378–1389.

117. M. Zhao, L. Li, C. Zhou, F. Heyroth, B. Fuhrmann, K. Maeder and T. Groth, *Biomacromolecules*, 2014, **15**, 4272–4280.

118. M. M. Stevens and J. H. George, *Science*, 2005, **310**, 1135–1138.

119. M. S. Niepel, B. K. Ekambaram, C. E. Schmelzer and T. Groth, *Nanoscale*, 2019, **11**, 2878–2891.

120. C. S. Hajicharalambous, J. Lichter, W. T. Hix, M. Swierczewska, M. F. Rubner and P. Rajagopalan, *Biomaterials*, 2009, **30**, 4029–4036.

121. T. Crouzier, K. Ren, C. Nicolas, C. Roy and C. Picart, *Small*, 2009, **5**, 598–608.

122. M. L. Macdonald, N. M. Rodriguez, N. J. Shah and P. T. Hammond, *Biomacromolecules*, 2010, **11**, 2053–2059.

123. T. Crouzier, L. Fourel, T. Boudou, C. Albigès-Rizo and C. Picart, *Adv. Mater.*, 2011, **23**, H111–H118.

124. R. Anouz, A. Repanas, E. Schwarz and T. Groth, *Macromol. Biosci.*, 2018, **18**, 1800283.

125. P. Esmaeilzadeh, A. Köwitsch, F. Heyroth, G. Schmidt, S. Fischer, K. Richter and T. Groth, *Carbohydr. Polym.*, 2017, **157**, 1205–1214.

126. J. A. Phelps, S. Morisse, M. Hindié, M.-C. Degat, E. Pauthe and P. R. Van Tassel, *Langmuir*, 2011, **27**, 1123–1130.

127. S. Zankovych, J. Bossert, M. Faucon, U. Finger and K. D. Jandt, *Adv. Eng. Mater.*, 2011, **13**, B454–B461.

128. S. Zankovych, M. Diefenbeck, J. Bossert, T. Mückley, C. Schrader, J. Schmidt, H. Schubert, S. Bischoff, M. Faucon and U. Finger, *Acta Biomater.*, 2013, **9**, 4926–4934.

129. H. Alkhoury, A. Hautmann, B. Fuhrmann, F. Syrowatka, F. Erdmann, G. Zhou, S. Stojanović, S. Najman and T. Groth, *Int. J. Mol. Sci.*, 2020, **21**, 3724.

Biomimetic Surface Modifications of Biomaterials Using a Layer-by-layer Technique   357

130. S. Y. Wong, Q. Li, J. Veselinovic, B.-S. Kim, A. M. Klibanov and P. T. Hammond, *Biomaterials*, 2010, **31**, 4079–4087.
131. P.-H. Chua, K.-G. Neoh, E.-T. Kang and W. Wang, *Biomaterials*, 2008, **29**, 1412–1421.
132. A. A. Mamedov and N. A. Kotov, *Langmuir*, 2000, **16**, 5530–5533.
133. S. Lee, B. Lee, B. J. Kim, J. Park, M. Yoo, W. K. Bae, K. Char, C. J. Hawker, J. Bang and J. Cho, *J. Am. Chem. Soc.*, 2009, **131**, 2579–2587.
134. P. Ott, K. Trenkenschuh, J. Gensel, A. Fery and A. Laschewsky, *Langmuir*, 2010, **26**, 18182–18188.
135. T. D. Gomes, S. G. Caridade, M. P. Sousa, S. Azevedo, M. Y. Kandur, E. T. Öner, N. M. Alves and J. F. Mano, *Acta Biomater.*, 2018, **69**, 183–195.
136. S. G. Caridade, C. Monge, F. Gilde, T. Boudou, J. O. F. Mano and C. Picart, *Biomacromolecules*, 2013, **14**, 1653–1660.
137. S. G. Caridade, C. Monge, J. Almodóvar, R. Guillot, J. Lavaud, V. Josserand, J.-L. Coll, J. F. Mano and C. Picart, *Acta Biomater.*, 2015, **15**, 139–149.
138. S. MacNeil, *Nature*, 2007, **445**, 874–880.
139. G. Revathi, J. Puri and B. Jain, *Burns*, 1998, **24**, 347–349.
140. L. Shen, Y. Jiang, Q. Tang, J. Ji, B. Wang, Y. Huang and Z. Qian, *J. Biomed. Nanotechnol.*, 2017, **13**, 1069–1081.
141. M. L. Macdonald, R. E. Samuel, N. J. Shah, R. F. Padera, Y. M. Beben and P. T. Hammond, *Biomaterials*, 2011, **32**, 1446–1453.
142. R. Guillot, F. Gilde, P. Becquart, F. Sailhan, A. Lapeyrere, D. Logeart-Avramoglou and C. Picart, *Biomaterials*, 2013, **34**, 5737–5746.
143. T. Crouzier, F. Sailhan, P. Becquart, R. Guillot, D. Logeart-Avramoglou and C. Picart, *Biomaterials*, 2011, **32**, 7543–7554.
144. N. J. Shah, M. L. Macdonald, Y. M. Beben, R. F. Padera, R. E. Samuel and P. T. Hammond, *Biomaterials*, 2011, **32**, 6183–6193.
145. R. F. R. da Costa, PhD thesis, Universidade do Minho (Portugal), ProQuest Dissertations Publishing, 2013, 10592575.
146. P. Kainourgios, E. Efthimiadou, L.-A. Tziveleka, G. Pappas, N. Boukos and G. Kordas, *Colloids Surf., B*, 2013, **104**, 91–98.
147. J. Liu, Y. Zhang, C. Wang, R. Xu, Z. Chen and N. Gu, *J. Phys. Chem. C*, 2010, **114**, 7673–7679.
148. A. Szarpak, D. Cui, F. Dubreuil, B. G. De Geest, L. J. De Cock, C. Picart and R. Auzely-Velty, *Biomacromolecules*, 2010, **11**, 713–720.
149. P. Rivera-Gil, S. De Koker, B. G. De Geest and W. J. Parak, *Nano Lett.*, 2009, **9**, 4398–4402.
150. C. R. Correia, M. Ghasemzadeh-Hasankolaei and J. F. Mano, *PLoS One*, 2019, **14**, e0218045.
151. M. B. Oliveira, J. Hatami and J. F. Mano, *Chem. - Asian J.*, 2016, **11**, 1753–1764.
152. J. T. Wilson, W. Cui, V. Kozlovskaya, E. Kharlampieva, D. Pan, Z. Qu, V. R. Krishnamurthy, J. Mets, V. Kumar and J. Wen, *J. Am. Chem. Soc.*, 2011, **133**, 7054–7064.

358   *Chapter 13*

153. R. L. Majewski, W. Zhang, X. Ma, Z. Cui, W. Ren and D. C. Markel, *J. Appl. Biomater. Biomech.*, 2016, **14**, 395–403.

154. C. R. Correia, P. Sher, R. L. Reis and J. F. Mano, *Soft Matter*, 2013, **9**, 2125–2130.

155. C. R. Correia, R. P. Pirraco, M. T. Cerqueira, A. P. Marques, R. L. Reis and J. F. Mano, *Sci. Rep.*, 2016, **6**, 1–12.

156. L. P. Guerzoni, Y. Tsukamoto, D. B. Gehlen, D. Rommel, T. S. Haraszti, M. Akashi and L. De Laporte, *Biomacromolecules*, 2019, **20**, 3746–3754.

157. P. Sher, C. A. Custódio and J. F. Mano, *Small*, 2010, **6**, 2644–2648.

158. H. Yoshida, M. Matsusaki and M. Akashi, *Adv. Funct. Mater.*, 2013, **23**, 1736–1742.

159. P. Gentile, I. Carmagnola, T. Nardo and V. Chiono, *Nanotechnology*, 2015, **26**, 422001.

160. J. R. Bishop, M. Schuksz and J. D. Esko, *Nature*, 2007, **446**, 1030–1037.

161. https://smart.servier.com/, 2020.

162. W. L. K. Chen and C. A. Simmons, *Adv. Drug Delivery Rev.*, 2011, **63**, 269–276.

163. S. Kleiser and A. Nyström, *Biomolecules*, 2020, **10**, 1170.

164. R. F. Mhanna, J. Vörös and M. Zenobi-Wong, *Biomacromolecules*, 2011, **12**, 609–616.

165. X. He, Y. Wang and G. Wu, *Appl. Surf. Sci.*, 2012, **258**, 9918–9925.

166. G. Li, P. Yang and N. Huang, *Phys. Procedia*, 2011, **18**, 112–121.

167. Y. Nakahara, M. Matsusaki and M. Akashi, *J. Biomater. Sci., Polym. Ed.*, 2007, **18**, 1565–1573.

168. N. Aggarwal, N. Altgärde, S. Svedhem, K. Zhang, S. Fischer and T. Groth, *Colloids Surf., B*, 2014, **116**, 93–103.

169. A. van der Smissen, V. Hintze, D. Scharnweber, S. Moeller, M. Schnabelrauch, A. Majok, J. C. Simon and U. Anderegg, *Biomaterials*, 2011, **32**, 8938–8946.

170. M. Schnabelrauch, D. Scharnweber and J. Schiller, *Curr. Med. Chem.*, 2013, **20**, 2501–2523.

171. B. Lanfer, F. P. Seib, U. Freudenberg, D. Stamov, T. Bley, M. Bornhäuser and C. Werner, *Biomaterials*, 2009, **30**, 5950–5958.

172. Q.-K. Lin, Y. Hou, K.-F. Ren and J. Ji, *Thin Solid Films*, 2012, **520**, 4971–4978.

173. T. Wei, W. Zhan, L. Cao, C. Hu, Y. Qu, Q. Yu and H. Chen, *ACS Appl. Mater. Interfaces*, 2016, **8**, 30048–30057.

174. P. Gentile, A. M. Ferreira, J. T. Callaghan, C. A. Miller, J. Atkinson, C. Freeman and P. V. Hatton, *Adv. Healthcare Mater.*, 2017, **6**, 1601182.

175. V. Gribova, I. Pignot-Paintrand, L. Fourel, R. Auzely-Velty, C. Albigès-Rizo, C. C. Gauthier-Rouvière and C. Picart, *ACS Biomater. Sci. Eng.*, 2016, **2**, 415–425.

176. K. Ren, J. Ji and J. Shen, *Bioconjugate Chem.*, 2006, **17**, 77–83.

177. F. Bernsmann, L. Richert, B. Senger, P. Lavalle, J.-C. Voegel, P. Schaaf and V. Ball, *Soft Matter*, 2008, **4**, 1621–1624.

Biomimetic Surface Modifications of Biomaterials Using a Layer-by-layer Technique   359

178. C. Picart, R. Elkaim, L. Richert, F. Audoin, Y. Arntz, M. Da Silva Cardoso, P. Schaaf, J. C. Voegel and B. Frisch, *Adv. Funct. Mater.*, 2005, **15**, 83–94.

179. I. E. Palama, S. D'Amone, A. M. Coluccia and G. Gigli, *Biotechnol. Bioeng.*, 2013, **110**, 586–596.

180. R. R. Costa, C. A. Custódio, F. J. Arias, J. C. Rodríguez-Cabello and J. F. Mano, *Small*, 2011, **7**, 2640–2649.

181. R. R. Costa, C. A. Custódio, A. M. Testera, F. J. Arias, J. C. Rodríguez-Cabello, N. M. Alves and J. F. Mano, *Adv. Funct. Mater.*, 2009, **19**, 3210–3218.

182. J. Fu, J. Ji, L. Shen, A. Küller, A. Rosenhahn, J. Shen and M. Grunze, *Langmuir*, 2009, **25**, 672–675.

183. X.-c. Chen, K.-f. Ren, J.-y. Chen, J. Wang, H. Zhang and J. Ji, *Phys. Chem. Chem. Phys.*, 2016, **18**, 31168–31174.

184. H.-W. Chien, T.-Y. Chang and W.-B. Tsai, *Biomaterials*, 2009, **30**, 2209–2218.

185. M. T. Thompson, M. C. Berg, I. S. Tobias, J. A. Lichter, M. F. Rubner and K. J. Van, Vliet, *Biomacromolecules*, 2006, **7**, 1990–1995.

186. J. Shaikh Mohammed, M. DeCoster and M. McShane, *Biomacromolecules*, 2004, **5**, 1745–1755.

187. M. C. Berg, S. Y. Yang, P. T. Hammond and M. F. Rubner, *Langmuir*, 2004, **20**, 1362–1368.

188. F. Hizal, I. Zhuk, S. Sukhishvili, H. J. Busscher, H. C. van der Mei and C.-H. Choi, *ACS Appl. Mater. Interfaces*, 2015, **7**, 20304–20313.

189. B. Labat, S. Morin-Grognet, F. Gaudière, L. Bertolini-Forno, O. Thoumire, J. P. Vannier, G. Ladam and H. Atmani, *J. Biomed. Mater. Res., Part A*, 2016, **104**, 1988–2000.

190. C. Monge, K. Ren, K. Berton, R. Guillot, D. Peyrade and C. Picart, *Tissue Eng., Part A*, 2012, **18**, 1664–1676.

191. E. Tocce, S. Liliensiek, A. Broderick, Y. Jiang, K. Murphy, C. J. Murphy, D. Lynn and P. Nealey, *Acta Biomater.*, 2013, **9**, 5040–5051.

192. M. S. Niepel, J. O. F. Mano and T. Groth, *ACS Appl. Mater. Interfaces*, 2016, **8**, 25142–25151.

193. K. Chakraborty, N. Kumawat, S. Sultana and M. Varma, *Sens. Actuators, A*, 2016, **244**, 50–55.

194. F. Gaudière, S. Morin-Grognet, L. Bidault, P. Lembrè, E. Pauthe, J.-P. Vannier, H. Atmani, G. Ladam and B. A. Labat, *Biomacromolecules*, 2014, **15**, 1602–1611.

195. A. Mzyk, R. Major, M. Kot, J. Gostek, P. Wilczek and B. Major, *Arch. Civ. Mech. Eng.*, 2014, **14**, 262–268.

196. C. T. McKee, J. A. Wood, I. Ly, P. Russell and C. J. Murphy, *Biophys. J.*, 2012, **102**, 1224–1233.

197. S. Yang, Y. Li, X. Li, Y. Li, X. Zhang and J. Xu, *Thin Solid Films*, 2009, **517**, 3024–3027.

198. C. Cho, J.-W. Jeon, J. Lutkenhaus and N. S. Zacharia, *ACS Appl. Mater. Interfaces*, 2013, **5**, 4930–4936.

360   *Chapter 13*

199. C. Lu, H. Möhwald and A. Fery, *Chem. Mater.*, 2008, **20**, 7052–7059.
200. X. Chen, J. Sun and J. Shen, *Langmuir*, 2009, **25**, 3316–3320.
201. W. Qi, Z. Xue, W. Yuan and H. Wang, *J. Mater. Chem. B*, 2014, **2**, 325–331.
202. L. Feng and Z. Liu, *Nanomedicine*, 2011, **6**, 317–324.
203. Y. Luo, S. Wang, M. Shen, R. Qi, Y. Fang, R. Guo, H. Cai, X. Cao, H. Tomás and M. Zhu, *Carbohydr. Polym.*, 2013, **91**, 419–427.
204. J.-L. Wang, K.-F. Ren, H. Chang, S.-M. Zhang, L.-J. Jin and J. Ji, *Phys. Chem. Chem. Phys.*, 2014, **16**, 2936–2943.
205. M. Delcea, N. Madaboosi, A. M. Yashchenok, P. Subedi, D. V. Volodkin, B. G. De Geest, H. Möhwald and A. G. Skirtach, *Chem. Commun.*, 2011, **47**, 2098–2100.
206. H. B. Yao, Z. H. Tan, H. Y. Fang and S. H. Yu, *Angew. Chem., Int. Ed.*, 2010, **49**, 10127–10131.
207. Z. Tang, N. A. Kotov, S. Magonov and B. Ozturk, *Nat. Mater.*, 2003, **2**, 413–418.
208. J. Blacklock, A. Vetter, A. Lankenau, D. Oupický and H. Möhwald, *Biomaterials*, 2010, **31**, 7167–7174.
209. E. Guzmán, H. Ritacco, J. E. Rubio, R. G. Rubio and F. Ortega, *Soft Matter*, 2009, **5**, 2130–2142.
210. D. J. Schmidt, Y. Min and P. T. Hammond, *Soft Matter*, 2011, **7**, 6637–6647.
211. J. Almodóvar, T. Crouzier, Š. Selimović, T. Boudou, A. Khademhosseini and C. Picart, *Lab Chip*, 2013, **13**, 1562–1570.
212. J. Campbell and A. S. Vikulina, *Polymers*, 2020, **12**, 1949.
213. M. S. Niepel, F. Almouhanna, B. K. Ekambaram, M. Menzel, A. Heilmann and T. Groth, *Int. J. Artif. Organs*, 2018, **41**, 223–235.
214. A. L. Hillberg, C. A. Holmes and M. Tabrizian, *Biomaterials*, 2009, **30**, 4463–4470.
215. A. I. Neto, N. L. Vasconcelos, S. M. Oliveira, D. Ruiz-Molina and J. F. Mano, *Adv. Funct. Mater.*, 2016, **26**, 2745–2755.
216. P. Esmaeilzadeh, M. Menzel and T. Groth, *ACS Appl. Mater. Interfaces*, 2018, **10**, 31168–31177.
217. P. Esmaeilzadeh, A. Köwitsch, A. Liedmann, M. Menzel, B. Fuhrmann, G. Schmidt, J. Klehm and T. Groth, *ACS Appl. Mater. Interfaces*, 2018, **10**, 8507–8518.
218. M. Zhao, R. Anouz and T. Groth, *J. Tissue Eng.*, 2020, **11**, 2041731420940560.
219. P. Cai, M. Layani, W. R. Leow, S. Amini, Z. Liu, D. Qi, B. Hu, Y. L. Wu, A. Miserez and S. Magdassi, *Adv. Mater.*, 2016, **28**, 3102–3110.
220. N. Madaboosi, K. Uhlig, S. Schmidt, A. S. Vikulina, H. Möhwald, C. Duschl and D. Volodkin, *Macromol. Biosci.*, 2018, **18**, 1700319.
221. A. Dierich, E. Le Guen, N. Messaddeq, J. F. Stoltz, P. Netter, P. Schaaf, J. C. Voegel and N. Benkirane-Jessel, *Adv. Mater.*, 2007, **19**, 693–697.
222. S. Müller, G. Koenig, A. Charpiot, C. Debry, J. C. Voegel, P. Lavalle and D. Vautier, *Adv. Funct. Mater.*, 2008, **18**, 1767–1775.

Biomimetic Surface Modifications of Biomaterials Using a Layer-by-layer Technique 361

223. H. Wang, T. Yin, S. Ge, Q. Zhang, Q. Dong, D. Lei, D. Sun and G. Wang, *J. Biomed. Mater. Res., Part A*, 2013, **101**, 413–420.

224. J. Chen, C. Chen, Z. Chen, J. Chen, Q. Li and N. Huang, *J. Biomed. Mater. Res., Part A*, 2010, **95**, 341–349.

225. J. Chen, Q. Li, J. Chen, C. Chen and N. Huang, *Appl. Surf. Sci.*, 2009, **255**, 6894–6900.

226. C.-C. Chou, H.-J. Zeng and C.-H. Yeh, *Thin Solid Films*, 2013, **549**, 117–122.

227. L.-Y. Huang and M.-C. Yang, *Colloids Surf., B*, 2008, **61**, 43–52.

228. Q. Lin, X. Ding, F. Qiu, X. Song, G. Fu and J. Ji, *Biomaterials*, 2010, **31**, 4017–4025.

229. Q. Lin, J. Yan, F. Qiu, X. Song, G. Fu and J. Ji, *J. Biomed. Mater. Res., Part A*, 2011, **96**, 132–141.

230. Y. Mei, C. Yao and X. Li, *Biofouling*, 2014, **30**, 313–322.

231. S. Meng, Z. Liu, L. Shen, Z. Guo, L. L. Chou, W. Zhong, Q. Du and J. Ge, *Biomaterials*, 2009, **30**, 2276–2283.

232. C. Sperling, M. Houska, E. Brynda, U. Streller and C. Werner, *J. Biomed. Mater. Res., Part A*, 2006, **76**, 681–689.

233. Q. Tan, J. Ji, F. Zhao, D.-Z. Fan, F.-Y. Sun and J.-C. Shen, *J. Mater. Sci.: Mater. Med.*, 2005, **16**, 687–692.

234. Y. Tang, Y. Zhao, H. Wang, Y. Gao, X. Liu, X. Wang and T. Lin, *J. Biomed. Mater. Res., Part A*, 2012, **100**, 2071–2078.

235. Y. Gong, Y. Zhu, Y. Liu, Z. Ma, C. Gao and J. Shen, *Acta Biomater.*, 2007, **3**, 677–685.

236. Á. J. Leite, P. Sher and J. F. Mano, *Mater. Lett.*, 2014, **121**, 62–65.

237. H. Xu, Y. Yan and S. Li, *Biomaterials*, 2011, **32**, 4506–4516.

238. Q. Zhao and B. Li, *Nanomedicine*, 2008, **4**, 302–310.

239. J. M. Silva, N. Georgi, R. Costa, P. Sher, R. L. Reis, C. A. Van Blitterswijk, M. Karperien and J. F. Mano, *PLoS One*, 2013, **8**, e55451.

240. H. Li, J. Jiang, Y. Ge, J. Xu, P. Zhang, W. Zhong and S. Chen, *J. Biomater. Sci., Polym. Ed.*, 2013, **24**, 431–446.

241. M. Zhao, L. Li, B. Li and C. Zhou, *eXPRESS Polym. Lett.*, 2014, **8**, 322–335.

242. H. F. Chuang, R. C. Smith and P. T. Hammond, *Biomacromolecules*, 2008, **9**, 1660–1668.

243. H. Li, C. Chen, S. Zhang, J. Jiang, H. Tao, J. Xu, J. Sun, W. Zhong and S. Chen, *Acta Biomater.*, 2012, **8**, 4007–4019.

244. K. Cai, Y. Hu and K. D. Jandt, *J. Biomed. Mater. Res., Part A*, 2007, **82**, 927–935.

245. H. Guo, Q. Guo, T. Chu, X. Zhang, Z. Wu and D. Yu, *J. Mater. Sci.: Mater. Med.*, 2014, **25**, 121–129.

246. L. He, S. Tang, M. P. Prabhakaran, S. Liao, L. Tian, Y. Zhang, W. Xue and S. Ramakrishna, *Macromol. Biosci.*, 2013, **13**, 1601–1609.

247. B.-L. Wang, J.-L. Wang, D.-D. Li, K.-F. Ren and J. Ji, *Appl. Surf. Sci.*, 2012, **258**, 7801–7808.

248. D. G. Yu, W. C. Lin, C. H. Lin, Y. H. Yeh and M. C. Yang, *J. Biomed. Mater. Res., Part B*, 2007, **83**, 105–113.

249. D.-G. Yu, W.-C. Lin and M.-C. Yang, *Bioconjugate Chem.*, 2007, **18**, 1521–1529.

250. J. Zhou, G. Romero, E. Rojas, L. Ma, S. Moya and C. Gao, *J. Colloid Interface Sci.*, 2010, **345**, 241–247.

251. V. Chiono, P. Gentile, F. Boccafoschi, I. Carmagnola, M. Ninov, V. Georgieva, G. Georgiev and G. Ciardelli, *Biomacromolecules*, 2010, **11**, 309–315.

252. S. Kunjukunju, A. Roy, M. Ramanathan, B. Lee, J. E. Candiello and P. N. Kumta, *Acta Biomater.*, 2013, **9**, 8690–8703.

253. Y. Lin and Z. Su, *J. Polym. Sci., Part B: Polym. Phys.*, 2008, **46**, 1252–1257.

254. T. G. Shutava, S. S. Balkundi and Y. M. Lvov, *J. Colloid Interface Sci.*, 2009, **330**, 276–283.

255. H. Ai, H. Meng, I. Ichinose, S. A. Jones, D. K. Mills, Y. M. Lvov and X. Qiao, *J. Neurosci. Methods*, 2003, **128**, 1–8.

256. P. Dong, W. Hao, X. Wang and T. Wang, *Thin Solid Films*, 2008, **516**, 5168–5171.

257. M. Lehnert, C. Rosin, W. Knoll and M. Veith, *Langmuir*, 2013, **29**, 1732–1737.

258. L. Li, S. Puhl, L. Meinel and O. Germershaus, *Biomaterials*, 2014, **35**, 7929–7939.

259. B. B. Mandal, J. K. Mann and S. Kundu, *Eur. J. Pharm. Sci.*, 2009, **37**, 160–171.

260. S. Liu, T. Liu, J. Chen, M. Maitz, C. Chen and N. Huang, *J. Biomed. Mater. Res., Part A*, 2013, **101**, 1144–1157.

261. L. Ma, J. Zhou, C. Gao and J. Shen, *J. Biomed. Mater. Res., Part B*, 2007, **83**, 285–292.

262. I.-C. Lee and Y.-C. Wu, *Colloids Surf., B*, 2014, **121**, 54–65.

263. Z. Poon, D. Chang, X. Zhao and P. T. Hammond, *ACS Nano*, 2011, **5**, 4284–4292.

264. T. Ramasamy, Z. S. Haidar, T. H. Tran, J. Y. Choi, J.-H. Jeong, B. S. Shin, H.-G. Choi, C. S. Yong and J. O. Kim, *Acta Biomater.*, 2014, **10**, 5116–5127.

265. Z. J. Deng, S. W. Morton, E. Ben-Akiva, E. C. Dreaden, K. E. Shopsowitz and P. T. Hammond, *ACS Nano*, 2013, **7**, 9571–9584.

266. L. Szyk-Warszyńska, K. Kilan and R. P. Socha, *J. Colloid Interface Sci.*, 2014, **423**, 76–84.

267. S. Park, U. Han, D. Choi and J. Hong, Layer-by-layer assembled polymeric thinfilms as prospective drug delivery carriers: design and applications, *Biomater. Res.*, 2018, **22**, 29.

Chapter 2

Summary - Novel surface coatings using oxidized glycosaminoglycans as delivery systems of bone morphogenetic protein 2 (BMP-2) for bone regeneration:

The aim of this paper was to study the effect of pH variation *versus* intrinsic cross-linking on the activity and release of BMP-2 towards osteogenesis, as well as, on improving the characteristics of multilayers regarding their stability and cell adhesive properties. The glycosaminoglycans (GAGs) native heparin (H) and chondroitin sulfate (CS) were paired with chitosan to create native multilayers systems. Chitosan was used as polycation due to its biocompatibility, biodegradability, bacteriostatic effect, and low production costs. Multilayers fabricated at pH 4 are thick with higher water content and are expected to store more BMP-2 due to their thickness, while the pH 9 offers thinner layers, less water content and thus, a stiffer surface which supports cell adhesion. Hence, one approach used here; was native GAGs/chitosan multilayers based on pH variation (pH 4+9) at which the first 4 bilayers are deposited at pH 4 while the second 4 bilayers are deposited at pH 9. The other approach was based on the functionalization of the GAGs (H and CS) with an aldehyde group *via* oxidation process to create intrinsically cross-linked multilayers. The aldehyde group can then bind to the amino group on chitosan creating a covalent imine bond (Schiff's base) which results in stiffer, more stable layers and help control the release of the loaded BMP-2 and its presentation to the cells. The multilayers were analyzed by different physical methods such as surface plasmon resonance, ellipsometry, atomic force microscopy and water contact angle. C2C12 myoblasts were used as a cell model not only for osteogenic differentiation studies but also to check if the released BMP-2 has any effect on cell adhesion or not. Further, the cell viability test demonstrated that cell growth was significantly higher on oxidized GAGs multilayers compared to the native pH 4+9 multilayers indicating that the oxidation of GAGs did not cause any cytotoxicity. The multilayers were further loaded with BMP-2 (5 µg mL^{-1}) and the release was quantified using ELISA. The oxidized CS multilayers were releasing the least amounts of BMP-2 i.e. delivering the loaded BMP-2 to cells in its bioactive state as a matrix-bound BMP-2; while the majority of loaded BMP-2 from pH 4+9 multilayers was delivered as released (soluble) BMP-2. Both multilayers' approaches supported cell adhesion. However, a significant increase in cell adhesion and spreading was detected on all multilayers after loading BMP-2 which indicated a synergistic effect of BMP-2 on

cell adhesion. The matrix-bound BMP-2 from oxidized CS multilayers enhanced an osteogenic differentiation of C2C12 cells that was higher than oxidized H multilayers. On the other hand, cells on pH 4+9 multilayers did not show any signs of osteogenic differentiation since the loaded BMP-2 was delivered in a soluble released state. In this study, the oxidation approach was significantly superior to the pH 4+9 approach in term of enhancing the characteristics of multilayers as well as controlling the BMP-2 activity and delivery to cells. Additionally, the results support the further use of oxidized CS multilayers as growth factors reservoirs for tissue regeneration.

Macromolecular
Bioscience
www.mbs-journal.de

Novel Surface Coatings Using Oxidized Glycosaminoglycans as Delivery Systems of Bone Morphogenetic Protein 2 (BMP-2) for Bone Regeneration

Reema Anouz, Alexandros Repanas, Elisabeth Schwarz, and Thomas Groth*

Tissue engineering of bone requires the delivery of growth factors in a localized, sustained manner. Here, chitosan is used as polycation, while heparin and chondroitin sulfate are employed either as native or oxidized polyanions for formation of multilayers by layer-by-layer technique. The use of oxidized heparin and oxidized chondroitin sulfate permits additional stabilization by cross-linking through imine bond formation between amino groups of polycations and aldehydes of oxidized glycosaminoglycans (oGAGs). Since these multilayers are highly hydrophilic, adhesion of C2C12 myoblasts is improved either by the use of a specific 4 + 9 pH regime with native glycosaminoglycans or a terminal collagen I layer in case of oGAGs. Adhesion and proliferation studies with C2C12 myoblasts, seeded either on bone morphogenetic protein (BMP-2) loaded or non-loaded multilayers, show that intrinsic cross-linking in oGAG-based multilayers supports cell adhesion, spreading, proliferation, and subsequent cell differentiation into osteoblasts. This is related to higher thickness and roughness of multilayers made of oGAGs compared to their native counterparts studied by ellipsometry and atomic force microscopy. Taken together, oGAG multilayer systems provide stable surface coatings and are useful as biocompatible reservoirs for sustained release of BMP-2, paving the way for coating implants and scaffolds for repair and regeneration of bone.

1. Introduction

Musculoskeletal disorders are a frequent health problem.[1] Although bone exhibits good recovery and regeneration potential, impaired bone healing after traumata or tumor resections is quite common.[2,3] Therefore, various synthetic or natural-based

R. Anouz, Dr. A. Repanas, Prof. T. Groth
Department of Biomedical Materials
Martin Luther University Halle-Wittenberg
Heinrich-Damerow-Strasse 4 06120, Halle (Saale), Germany
Prof. E. Schwarz
Institute of Pharmacy
Martin Luther University Halle-Wittenberg
Wolfgang-Langenbeck-Strasse 4 06120, Halle (Saale), Germany
Prof. T. Groth
Interdisciplinary Center of Material Research and
Interdisciplinary Center of Applied Research
Martin Luther University Halle-Wittenberg
06099, Halle (Saale), Germany
E-mail: thomas.groth@pharmazie.uni-halle.de

The ORCID identification number(s) for the author(s) of this article can be found under https://doi.org/10.1002/mabi.201800283.

DOI: 10.1002/mabi.201800283

polymers,[4] ceramics, and composites have been used as implant material to replace and regenerate bone tissue.[5] Since the biomaterial's surface plays an important role in determining the initial cell response, surface modification of biomaterials through various techniques has emerged as a strategy to enhance the functionality and bioactivity of bone implants.[6] Additionally, the local application of growth factors (GFs), such as bone morphogenetic protein BMP-2, plays an important role in bone defect repair. However, the delivery of GFs in an effective dosage is needed to induce bone regeneration, although high doses given by bolus injections can also be accompanied by serious adverse clinical side effects.[7]

Cell adhesion, including osteoblasts and mesenchymal stem cells (MSCs), on bone implants is dependent on the presence of extracellular matrix (ECM) molecules that provide a structural support to cells and also on chemical cues to guide cell proliferation and differentiation.[8] Cell adhesion to ECM proteins is mediated by both non-integrin and integrin receptors.[9] Several proteins present in the ECM, such as fibronectin, laminin, and fibrillar collagen (e.g., Col I), mediate the attachment and cell spreading to surfaces, which is related to signal transduction involved in the regulation of gene expression for cell growth and differentiation.[10,11]

Glycosaminoglycans (GAGs) resemble further important components of ECM, such as heparan sulfate, chondroitin sulfate (CS), hyaluronans, and others.[12] GAGs do not only provide structural support related to mechanical properties and hydration of tissues, but also interact specifically with ECM proteins, cytokines, and cell receptors, which impacts cell growth and differentiation.[12] Thus, GAGs can undergo interactions with a plethora of proteins that possess heparin-binding domains, including ECM proteins like fibronectin or laminin, but also interact with GFs such as BMP-2.[13] Another glycan of nonmammalian origin is chitosan (Chi) obtained by partial deacetylation of the acetamido group in chitin, present in the exoskeleton of arthropoda and crustacea.[14,15] Due to its known biocompatibility, biodegradability, bacteriostatic effect, and low production costs, Chi has been widely used for biomedical applications.[16]

ADVANCED SCIENCE NEWS
www.advancedsciencenews.com

Macromolecular Bioscience
www.mbs-journal.de

BMP-2 belongs to the transforming growth factor beta (TGF-β) superfamily and promotes osteogenesis of MSCs, osteoblast progenitor cell lines, as well as other nonosteogenic cell lines such as C3H10T1/2 fibroblasts and C2C12 myoblasts into osteoblasts.[17,18]

A physical technique to modify biomaterial surfaces is the layer-by-layer (LbL) assembly of oppositely charged polyelectrolytes to make multilayer coatings on charged surfaces.[19–21] Intrinsic and surface properties of multilayers, such as thickness, mechanical properties, surface charge, and wettability, can be easily adjusted by varying the type and concentration of polyelectrolytes, pH and ionic strength of solutions, temperature, and other physical parameters.[22] Multilayers can control protein adsorption from surrounding solutions and can be used as reservoirs for controlled release of GFs, that both affect cell fate when used as implant coatings in biomedical applications.[22]

GAGs like heparin (H) and CS can be used as polyanions, while Chi and collagen I (Col I) resemble weak polycations that can be used to generate ECM-like multilayers via LbL. It has been shown that pH changes during complexation of H and Chi lead to significant modifications in the cell adhesive properties. In particular, stepwise changes of pH from an acidic pH 4 to a basic pH 9 (pH 4 + 9) in H/Chi multilayer systems can maintain a certain thickness of multilayers and improved cell adhesion and growth significantly.[23–25] On the other hand, the exchange of polycation Chi by Col I in multilayers with CS resulted in a multilayer system greatly promoting osteogenic differentiation of MSCs. An additional useful invention was the use of oxidized GAGs, forming imine bonds between aldehyde groups of oxidized GAG and amino groups of Col I, achieving intrinsic cross-linking that increased multilayer stiffness and stability.[20] Notably, such multilayers made of different native GAGs with Chi as polycation have also been used as reservoirs for the uptake of BMP-2 to promote osteogenic differentiation of various cell types, including C2C12 myoblasts.[26]

Here, we studied multilayer systems based either on native H or CS as polyanions made more cell adhesive by pH variation (pH 4 + 9) during multilayer formation, as shown previously,[25] while also studying a second set based on oxidized GAGs (oGAGs), using either oH or oCS as polyanions, where cell adhesion was promoted by a terminal Col I layer.[20,27] Chi was used as polycation in all cases. These multilayers were not only compared regarding layer growth, thickness, topography, and wetting properties, but also regarding their ability to support cell adhesion, growth, and subsequent osteogenic differentiation of C2C12 myoblasts through checking their ability to serve as systems for controlled release of BMP-2. Results show that, particularly, multilayers made of oH and oCS with intrinsic cross-linking had superior effects on osteogenic differentiation of cells.

2. Results

2.1. Measurements of Wetting Properties

Static water contact angle (WCA) studies were applied to characterize the change of terminal layer composition and wetting properties during polyelectrolyte multilayer (PEM) assembly, after the deposition of each layer at a predetermined pH value,

for all types of systems. **Figure 1**A shows the WCA values of clean glass, poly(ethylene imine) (PEI) (first bonding layer), polyanions (even number layers), and polycations (odd number layers). In all systems, the polycation-based layers (Chi) had higher WCA than the polyanion-based, revealing an alternating trend. The multilayer CS-based systems exhibited higher WCA with increasing layer number compared to H-based systems. The differences in WCA between GAG and Chi layers were lower in the 4 + 9 pH combination systems after the 10th layer. On the other hand, in the oxidized systems, the WCA differences between GAG and Chi layers showed a different trend for CS-based and H-based PEMs. More specifically, while in the oH4Col system, WCA differences increased with increasing layer number, in the oCS4Col system they did not. In addition, there was no major change in WCA trends when Col I was used as the terminal layer in oxidized multilayer systems.

Multilayer growth with Chi as polycation and native CS or native H as polyanions, as well as their oxidized derivatives (oCS & oH), was investigated by surface plasmon resonance (SPR) (Figure 1B). The measured angle shifts correspond to increasing adsorbed mass. It was observed that both oxidized GAGs led to linear layer growth, which was identical for both oCS and oH as polyanions, while the use of native GAGs showed higher angle shifts with H as polyanion. The pH shift from 4 to 9 led to a decrease of the slope of angle shift for both CS- and H-based multilayers.

2.2. Characterization of PEM Structural Properties

2.2.1. Multilayer Thickness and Swelling Degree

Ellipsometry was used in order to study the thickness of PEMs, both in dry and hydrated states, in three different solutions, namely deionized H_2O, 1 mmol HCl, and phosphate buffer saline (PBS, pH 7.4). **Figure 2**A depicts the calculated layer thickness of the different PEM systems before and after exposure to one of the aforementioned solutions. The overall average thickness significantly increased after immersion in H_2O for all systems ($p \leq 0.001$). The average thickness values remained significantly increased compared to the dry state after subsequent immersion in 1 mmol solution of HCl, while the average thickness values dropped for all systems after final immersion in PBS. The values remained significantly higher compared to dry state films for all systems.

2.2.2. PEM Surface Topography and Roughness

The surface roughness and topography of clean Si wafers (with a terminal layer of SiO_2) and different PEM systems were analyzed by atomic force microscopy (AFM) in dry state and ambient laboratory conditions. Figure 2B shows that the topography of final layers of all systems was highly dependent on the pH conditions during assembly and the terminal layer. All surfaces exhibited granular surface morphology. GAG choice in the oxidized systems did not have a significant effect, neither on the roughness ($p \geq 0.05$) nor on the topography. The main reason is that, in those systems, the final 17th layer was Col
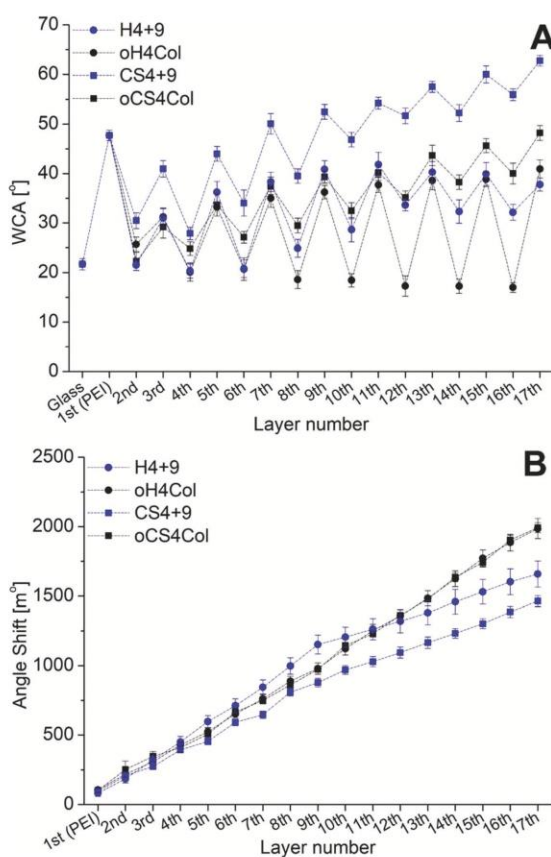
Figure 1. A) Static WCA during multilayer formation up to 17 layers plotted as a function of the layer number; oCS4Col (black square), oH4Col (black circle), H4 + 9 (blue circle). pH value of chitosan (Chi) solution was kept constant at 4.0. For CS4 + 9 and H4 + 9 samples, the pH of GAG solution was 4.0 until 8th layer and 9.0 after 10th layer. Layer 1 was always PEI, even layers: polyanion, odd layers: polycation; 17th layer was Chi (CS4 + 9 and H4 + 9) or Col I (oCS4Col and oH4Col); (mean ± SD). B) Layer growth of PEM systems of oxidized and native polysaccharides measured by surface plasmon resonance angle shifts, plotted as a function of the layer number; oCS4Col (black square), oH4Col (black circle), CS4 + 9 (blue square), H4 + 9 (blue circle). pH value of chitosan (Chi) solution was kept constant at 4.0. For CS4 + 9 and H4 + 9 samples, the pH of GAG solution was 4.0 until 8th layer and 9.0 after 10th layer. Layer 1 was always PEI, even layers: polyanion, odd layers: polycation; 17th layer was Chi (CS4 + 9 and H4 + 9) or Col I (oCS4Col and oH4Col); (mean ± SD).

Figure 2. A) Thickness of PEM systems made of measured by ellipsometry at 70° (light gray columns correspond to dry condition, grey to H_2O immersion, dark gray to HCl immersion, and black to PBS immersion); $n = 9$, (mean ± SD); **($p \leq 0.01$), ***($p \leq 0.001$). B) Surface topography and roughness (Ra = light grey, Rq = dark grey) of type I collagen (Col I) terminated PEMs (oCS4Col and oH4Col) and chitosan (Chi) terminated PEMs (CS4 + 9 and H4 + 9) visualized by atomic force microscopy (AFM); $n = 10$, (mean ± SD); scale bar: 500 nm.

I and not Chi. In the case of PEMs with native GAGs, even though the final layer is Chi in both systems, both roughness ($p \leq 0.001$) and topography differ (Figure 2B).

2.3. Biocompatibility Studies with C2C12 Cells

Measuring cell metabolic activity by QBlue assay (**Figure 3**) indicated that oH4Col and oCS4Col systems significantly supported cell growth more than their native counterparts. Lower fluorescence intensity of about 8500 was found for cells on native multilayer systems (pH 4 + 9) compared to higher fluorescence intensity for cells on oGAGs systems. The highest fluorescence intensity of about 17 000 was measured for cells on multilayers made of oCS. Cells on tissue culture polystyrene (+ control), showed comparable fluorescence intensity (≈16 000) to the oCS4Col system.

2.4. BMP-2 Release Study

Release studies (**Figure 4**) showed that all PEM systems did release BMP-2 over 4 days, but to a different extent. H-based systems released larger quantities than chondroitin-based multilayers. Interestingly, the oCS system released the least amount of BMP-2 over time, making it a good candidate as long-term BMP-2 reservoir.
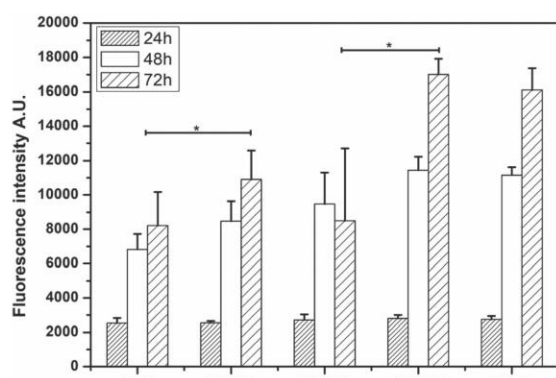
Figure 3. QBlue fluorescence intensity measurements of C2C12 cells cultured in DMEM with 10% FBS, seeded on various LbL systems. Measurements were done after 24, 48, and 72 h of incubation. Fluorescence intensity (FI) was determined at 544 nm excitation and 590 nm emission wavelength. Values represent means ± standard deviations (SD), $n = 8$ replicates of each.

2.5. Cell Adhesion Studies

Immunohistochemical staining of C2C12 cells that was used to study cell adhesion and spreading, through staining of actin filaments, vinculin molecules in focal adhesion (FA), and nuclei, showed more cell spreading on non-BMP-2 loaded CS4 + 9 multilayers compared to the other non-BMP-2 loaded PEM systems (**Figure 5**A, upper row). However, actin filaments were circumferentially distributed. On the other hand, cells on H4 + 9 were almost round and showed neither vinculin expression nor well visible actin organization. Cells seeded directly on glass slides (control) did not possess vinculin-positive FA.
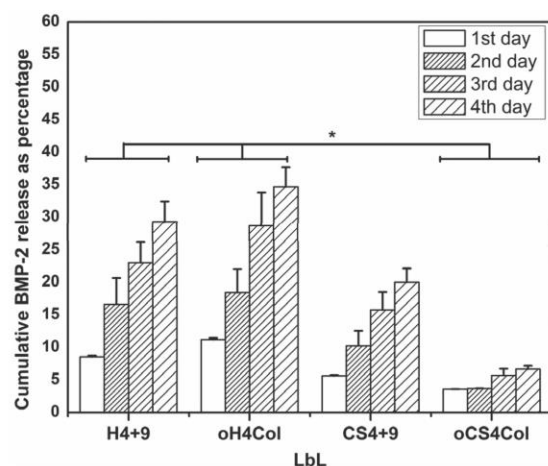
Figure 4. Cumulative BMP-2 release, from the various LbL systems over 4 days, as percentage of the total loaded amount of BMP-2. Release study was done using ELISA. Values represent means ± standard deviations (SD), $n = 10$ replicates of each.

Interestingly, cells on BMP-2 loaded multilayers (Figure 5A, lower row) demonstrated strong organization of actin filaments, which were longitudinally distributed (on all multilayers except for H4 + 9), as well as positioning of vinculin at the end of the actin filaments, which reflected an enhanced interaction of cells with the substratum. The same immunofluorescence images (IF) were used for quantification of cell area (Figure 5B,C), in which a general increase in cell area was found on all BMP-2 loaded multilayers. The latter was significantly larger in case of H4 + 9 and oH4Col multilayers. Interestingly, the positive control (Ctrl) had almost no change in cell area in terms of increased cell spreading when BMP-2 was present in the culture medium.

2.6. Osteogenic Differentiation of C2C12 Cells

C2C12 cells were seeded directly on top of BMP-2 loaded multilayers, and alkaline phosphatase (ALP) assay was performed. C2C12 cells seeded on plain glass with addition of BMP-2 (5 µg mL^{-1}) were used as positive control (Ctrl+BMP-2), whereas as negative control (Ctrl without BMP-2) cells were seeded on plain glass without any BMP-2 (**Figure 6**A). Alizarin red-S staining assay was also performed to check for the formation of mineralized matrix, as another measure of osteogenic differentiation of cells (Figure 6B). The oCS4Col multilayers with Col I as the terminal layer promoted the highest ALP activity in C2C12 cells, which was significantly higher than CS4 + 9 multilayers. oH4Col induced ALP activity comparable to oCS4Col whereas ALP activity of cells induced by H4 + 9 and CS4 + 9 systems was more comparable to the negative control. This was also obvious by alizarin red-S staining as shown in (Figure 6B). The formation of mineralized matrix was well observed on cross-linked multilayers (i.e., on oH4Col and oCS4Col systems), while H4 + 9 and CS4 + 9 systems did not show any mineralized matrix formation. Furthermore, the formation of mineralized matrix was obvious in the positive control (Ctrl+BMP-2).

3. Discussion

The current work demonstrated not only that multilayer coatings made of biogenic polysaccharides can be used as reservoir for release of GF-like BMP-2 that supports osteogenic differentiation of cells, but that particularly multilayers made of oxidized GAGs-like oCS have superior effects on osteogenic differentiation of C2C12 cells.

Physical studies on multilayer surface properties showed that all PEMs exhibited alternating WCA values during formation of multilayers (lower for GAGs layers and higher for Chi layers) as found in previous investigations.[20,27] The use of H, either native or oxidized, as polyanion caused lower WCAs than CS, which is probably due to the higher content of sulfate groups in H.[28] The largest differences in WCA values between alternating layers were also observed in the oH4Col system, highlighting a dominance of either Chi or oH in the outer layers, which also indicates a better separation and lesser intermingling than in the CS-based multilayer systems.[28,29]
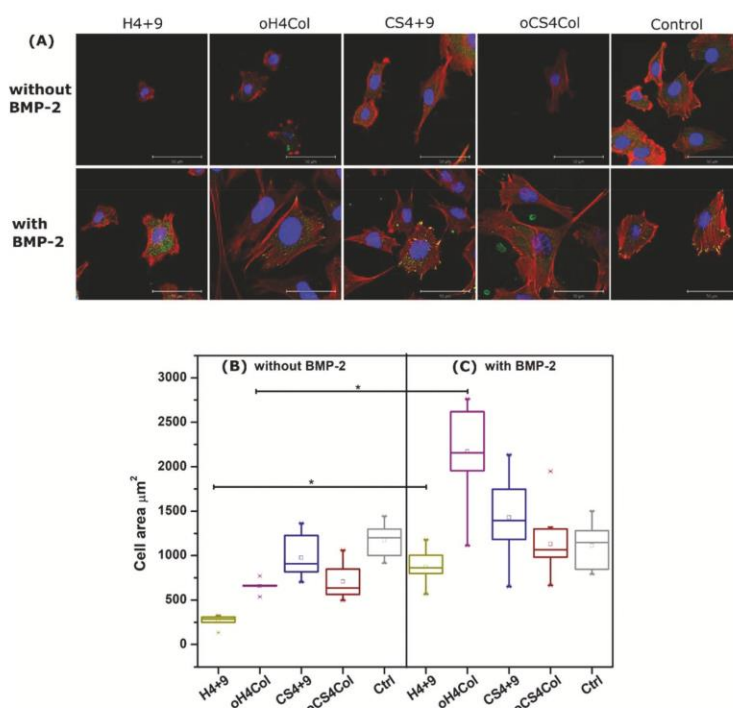
Figure 5. Adhesion of C2C12 cells seeded on native and various cross-linked PEM films, after 24 h of incubation. A) Confocal laser scanning microscopy (CLSM) images show C2C12 cells after 24 h on various native and cross-linked PEM films. The cells were stained for vinculin (green) present in focal adhesions, filamentous actin (red), and nucleus (blue) on multilayers without BMP-2 (upper row) and with BMP-2 loading (lower row). As a control, cells were seeded on plain glass slides either without or with BMP-2 in the medium. Cells were suspended in DMEM 10% FBS and imaged with CLSM 63× oil immersion objective; scale bar: 50 μm. Measurement of cell area done using image analyzing software: B) cells seeded on PEM with no uploading of BMP-2, C) with BMP-2 loaded to the multilayers.

is probably related to the higher charge density of H compared to CS, enabling this system to bind more Chi.[28] PEM thickness, both in dry and hydrated state, was investigated. The type of GAG did not affect the overall PEM thickness in both dry and wet state for the oxidized systems significantly, but H4 + 9 and CS4 + 9 systems exhibited significantly lower overall thickness compared to oCS4Col and oH4Col, which goes along with the results of SPR studies (Figures 1 and 2). Three different solutions were used for exposure of multilayers to investigate how film thickness and stability were affected. The choice of the solutions was based on the different treatments the films underwent during uploading of BMP-2 (1 mmol HCl) or during cell experiments (washing with PBS, culture medium). As expected, the films thickness increased when dry multilayers were immersed in Milli-Q water and 1 mmol HCl solutions (Figure 2A), but no dramatic changes were observed, particularly when HCl solution was used as fluid.[20] One the other hand, after PBS immersion, the average thickness decreased in all cases slightly, which was described previously.[20] Thickness measurements of hydrated PEMs showed that oCS4Col and oH4Col system displayed a significantly higher thickness ($p \leq 0.001$) compared to that of 4 + 9 PEMs. This indicates that the capability of swelling was highest in oxidized systems, although this was not expected due to their intrinsic cross-linking capability, which should have hindered swelling to some extent.

On the other hand, lower WCA value differences were found for both pH 4 + 9 systems after the 10th layer, confirming findings from our previous studies.[30] When studying the CS-based systems, smaller differences in WCA values between CS and Chi were observed, probably because of the lower charge density of CS compared to H, indicating more intermingling of the polyelectrolytes.[28] Indeed, it was observed that CS-based PEM possessed higher WCA angles of their terminal layers compared to H-based PEM, which might affect cell adhesion.[27] Multilayer formation was further studied by SPR through the measurements of angle shifts corresponding to an increase in adsorbed mass, with the obtained results being in accordance with other studies regarding similar systems.[28,29,31] In all PEMs, layer growth was linear; however, in the 4 + 9 systems, it was decreased after switching to pH 9.0 for GAG deposition, as found in our previous investigation, too.[32] The increase in angle shifts was identical for PEM based on oGAGs and higher than their native counterpart, indicating that intrinsic cross-linking capability makes a major contribution to multilayer formation.[25] On the other hand, the increase in angle shift during the pH 4 + 9 condition was higher for H-based PEM, which

AFM studies revealed no major differences in roughness of the terminal multilayers, except that H4 + 9 possessed the smoothest surface of lowest roughness and granularity compared to the other PEMs.

Control of cell differentiation in tissue engineering applications is often based on the use of GF release and dependent on a timely and spatially well-controlled delivery process.[33] On the other hand, also surface-induced effects by presentation of chemical cues to corresponding cell receptors are contributing to cell differentiation.[34,35] We could show previously that such multilayer systems made of oGAGs and collagen I promoted osteogenic differentiation of MSCs greatly, which was also related to a moderate wettability of these surfaces and enhanced cell spreading.[20,36] Such improvement of cell spreading was also achieved by the application of a simple pH 4 + 9 regime that made nonadhesive PEM systems composed of H and Chi highly adhesive, which was also related to an increase in WCA.[25] Here, we extended our previous investigations by the use of PEMs as reservoir for release of BMP-2 as osteogenic inducer of cell differentiation applicable also to C2C12 myoblasts.[17,18]
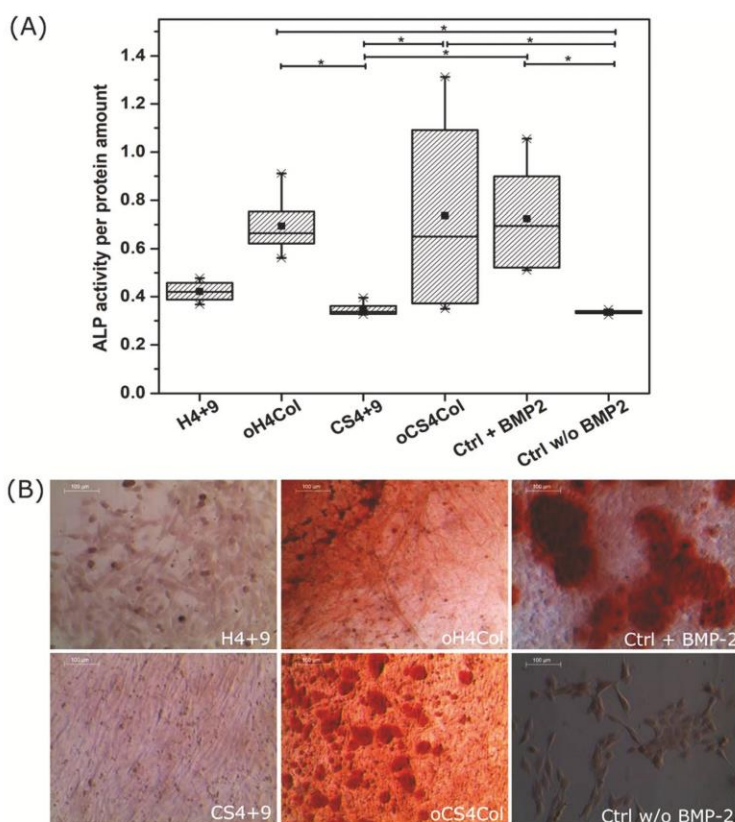
Figure 6. A) Measurements of ALP activity in C2C12 cells seeded directly on top of BMP-2 loaded multilayer systems fabricated in 24-well plate, determined via absorbance measurements at 405 nm after 4 days' incubation time, using plate reader. Measurements are normalized to the total protein amount (BCA values). B) Bright-field images (10×) of C2C12 cells seeded on various native and cross-linked PEM for 14 days and stained with alizarin red-S solution to investigate the formation of mineralized matrix; scale bar: 100 µm.

The BMP-2 release study done here suggested a higher binding affinity between BMP-2 and CS in the fabricated multilayer systems due to the lower release when compared to the H-based systems. In addition, this suggested higher affinity of CS to BMP-2 was more pronounced in oCS4Col multilayers. This was related to an additional method to control BMP-2 release due to the intrinsic cross-linking where we could see the lowest released amounts of BMP-2. Hence such multilayer systems based on oxidized CS seem to have a potential to serve as reservoirs for long-term release of GFs.

Cell adhesion and spreading are strong modulators of gene expression and cell differentiation.[40] Stronger spreading of cells has been found to be related to osteogenic differentiation of stem and other cells,[40] also being important for activation of GFs receptors.[41] Hence, cell adhesion and spreading was studied qualitatively and quantitatively through the immuno-histochemical staining of C2C12 myoblasts for actin cytoskeleton, vinculin in focal adhesions, and cell nuclei. Here, it was found first that CS4 + 9 PEM supported cell adhesion more than other non-BMP-2 loaded systems, which is probably related to its moderate wettability (WCA ≈ 62°) and well in line with our previous studies.[42] This improved adhesion of C2C12 cells on CS4 + 9 multilayers was also evident by the clear formation of the actin filaments and vinculin expression in focal adhesions. On the other hand, cell adhesion was less on multilayer systems with lower WCA and that was evident by round cells accompanied by absence of actin polymerization and vinculin assembly in focal adhesions. Moderate WCA, around 60°, has been related to the promotion of cell adhesion, while more wettable substrata are suppressive.[43] Interestingly, the significant increase in cell adhesion and spreading was pronounced on all multilayer systems loaded with BMP-2, indicating a synergistic effect of BMP-2, surface properties, and composition of PEM on cell adhesion. This increase in cell adhesion was characterized by more cell polarization, expression of logitudinal actin filaments and vinculin molecules in focal adhesion sites. This has been reported and observed previously by others working with different multilayer systems and cross-linking mechanisms.[44] BMP-2, known to induce osteogenesis, has two signaling pathways: canonical signaling through binding of BMP-2 to type I and type II serine/threonine kinase receptors followed by several Smad activation pathways, and non-canonical which involves Smad-independent signaling and cross-talk with other pathways.[45] Further, upon binding of BMP-2 to its receptors, an adhesive phenotype is initiated through β3 integrin clustering and reorganization of the cytoskeleton via filopodia and

Indeed, first studies were carried out culturing C2C12 myoblasts in the presence of 10% serum on the different multilayer systems to learn about their biocompatibility. We found that H-based multilayers either made of native or oxidized H provided support of cell growth to a lesser extent than CS, which is probably related to the higher negative charge density and wettability as indicated by contact angle measurements of this GAG that are known to reduce cell adhesion and growth.[37] On the other hand, longer duration of cell culture showed also that cells grew more on multilayers made of the oxidized forms of GAGs, which might be related to a higher E modulus by intrinsic cross-linking, as shown in a previous work from us and others, and also the adhesion promoting effect of the terminal collagen I layer.[20,38] Overall, these studies provided evidence for the biocompatibility of both systems based on either H or CS.

BMP-2 has a H-binding domain, which consists of positively charged amino acids that can interact with negatively charged sulfated GAGs through electrostatic and other interactions.[39]

stress fibers. The $\beta3$ integrin stimulation via BMP-2 is thought to be necessary for the Smad signaling initiation in addition to the adhesion and migration, and it is the first event of $\beta3$ integrin–BMPR cross-talk that also results in a transient phenotype of cells before converting them from myoblasts to osteoblasts.[46] Another study suggested a possible crosstalk between BMP-2 and integrin-dependent pathways, in which BMP-2 promotes the formation of focal adhesions and stress fibers by increasing $\alpha5$ and $\beta1$ integrin expression.[44] Stronger formation of vinculin-positive focal adhesion plaques containing integrins and formation of actin stress fibers were clearly observed, when multilayers were uploaded with BMP-2 (Figure 5A), which was also supported by quantification of cell area (Figure 5B,C). It is also worth mentioning that the BMP-2 promoting effect on cell adhesion and spreading was noticeably higher in case of bound (loaded) BMP-2 on all multilayers than the BMP-2 added to the solution (dissolved BMP-2) in case of control (plain glass).

The osteogenic differentiation of C2C12 cell was studied to assess the bioactivity and ability of uploaded BMP-2 to differentiate C2C12 cells into osteoblasts. Osteoblasts start synthesizing their ECM which consists mainly of Col I followed by ALP production and later-stage ECM calcification occurs.[47] In our study, ALP activity (Figure 6A) was measured as an early indicator of osteogenesis, while alizarin red-S staining was applied to check the formation of mineralized matrix at later stages of osteogenic differentiation. ALP activity was highest in oCS4Col and oH4Col systems and nearly comparable to the positive control, where BMP-2 was added to cells plated on tissue culture polystyrene (i.e., as dissolved BMP-2), indicating the potential of these multilayer systems to present BMP-2 in an active manner and thus supporting subsequent osteogenesis. This also highlights the important reservoir role of the ECM, in human body, for storing and presenting GFs rather than keeping them in a soluble state.[48] Although, H can stimulate BMP-2 activity through binding it and protecting it from degradation,[39] some studies have shown that H may also inhibit osteogenic activity by sequestering BMP-2 and mediating BMP-2 internalization,[49] which might be the reason behind lesser formation of mineralized matrix on oH4Col compared to oCS4Col. Despite that H4 + 9 and oH4Col possessed a similar release profile, by comparing the oxidized systems (oCS4Col and oH4Col) to their native pH dependent systems (CS4 + 9 and H4 + 9, respectively), more ALP and more formation of mineralized matrix were observed for C2C12 cells cultured on oxidized GAG systems. One reason could be related to the presence of more viable cells on oGAGs systems (as demonstrated from QBlue data, Figure 3) and also to the presence of a terminal Col I layer in the oGAGs systems, creating a better microenvironment for the cells regarding osteogenic differentiation.[36] Furthermore, ligation of $\alpha2\beta1$ and $\beta1$ integrins, that is, collagen receptor signaling, is required for ALP induction as it increases ALP mRNA triggered by BMP-2.[47] Moreover, Col is important in starting and increasing mineralization.[50] However, despite the fact that both oH4Col and oCS4Col have a terminal collagen layer, we could see that oCS4Col, which released less BMP-2, enhanced osteogenic differentiation of cells and formation of mineralized matrix significantly more than oH4Col system, indicating that intrinsic properties of multilayers and not only the terminal collagen layer affected BMP-2 activity and

subsequent osteogenic differentiation of C2C12 cells. All together, these findings underline the efficacy and the successfulness of the multilayers made of oxidized GAGs like chondroitin sulfate and heparin with intrinsic cross-linking to form a biocompatible surface coating that can store and deliver BMP-2 for osteogenic differentiation of cells.

4. Conclusion

The oxidized GAG multilayers with the terminal layer of Col I showed more sustained release of BMP-2 and supported C2C12 cell differentiation more than the native systems, which showed the advantage of intrinsic cross-linking, making these systems more efficient for bioactive presentation of BMP-2 and creating a microenvironment that promotes osteogenic differentiation. To the best of our knowledge, there are currently no published in-depth studies on the combination of multilayer systems made of oxidized GAGs as a tool for achieving in situ cross-linking in multilayers instead of chemical cross-linkers (widely used in the majority of other studies) for bone regeneration. In particular, it should be noted that very low quantities of BMP-2 release, as shown by ELISA, have large effects on cell differentiation, which may also pave the way for safer application of GFs, like BMP-2, in clinical set-ups. Hence, in this study, we tried to address the significance of considering LbL systems as bone tissue engineering candidates, with the potential to apply these systems on 3D scaffolds that may open new pathways in regenerative therapies and could be promising toward finding novel solutions for treating large bone defects.

5. Experimental Section

Materials: Round glass (Ø15 mm), glass object holders, and polystyrene well-plates were obtained from Karl Hecht GmbH & Co (Sondheim, Germany). Chondroitin sulfate, sodium periodate ($NaIO_4$), poly(ethylene imine) (PEI), paraformaldehyde (PFA), and Triton X-100 were purchased from Sigma-Aldrich Chemie GmbH (Steinheim, Germany). Heparin and glutaraldehyde were provided by AppliChem (Darmstadt, Germany). Native Chi was obtained from HMC Heppe Medical Chitosan GmbH (Halle, Germany). Collagen I was from Sichuan Mingrang Bio-Tech (Sichuan, China). The black 96-well plates and cell culture flasks were purchased from Greiner Bio-one GmbH & Co.KG (Frickenhausen, Germany). Dulbecco's Modified Eagle's Medium (DMEM) (phenol red), fetal bovine serum (FBS), and trypsin/EDTA solution were provided by Biochrom (Berlin, Germany). Penicillin/ streptomycin (pen/strep) was from Lonza (Walkersville, MD, USA). Sodium chloride (NaCl), hydrogen peroxide 35% (H_2O_2), bovine serum albumin (BSA), 4-nitrophenylphosphate disodium salt hexahydrate (p-NPP) and alizarin red-S were provided by Carl Roth GmbH & Co. KG (Karlsruhe, Germany). Dialysis bags (Spectra/Por membrane, M_w cutoff = 3500) were purchased from Spectrum Labs (CA, USA). Schiff's reagent was from Merck KGaA (Darmstadt, Germany).

Synthesis of oGAGs: H and CS were used as native glycosaminoglycans (nGAGs) in all experiments. Oxidation of nGAG was done according to our previously published work.[20] Briefly, 1 g of native H (nH $M_w \approx 8$–15 kDa) and native CS (nCS $M_w \approx 75$ kDa) were dissolved in 200 mL of ultrapure water and allowed to react with $NaIO_4$ at a molar ratio of 2:1 and 4:1, at room temperature (RT) under stirring and protection from light for 6 h and 3 h, respectively. Purification of the reacted GAGs was done using dialysis membrane against distilled water for 3 days at RT. The final products were obtained by freeze-drying

(ALPHA 1–2 LDplus, Christ, Osterode am Harz, Germany) and stored at 4 °C. The quantity of aldehyde groups present in oGAGs was determined photometrically using Schiff's test and has been described previously.[51] Oxidation degrees of 5.71% and 6.33% were obtained for oH and oCS, respectively.

Preparation of Substrata: For ellipsometry and AFM, as well as WCA and several cell experiments, Si wafers (Silicon Materials, Kaufering, Germany) and round glass cover slips, respectively, were prepared following the "RCA-1" cleaning protocol.[52] For SPR studies, fresh Au-coated glass sensors (glass squares, 16 × 16 × 1 mm, 50 nm Au, Ssens BV, Enschede, The Netherlands) were prepared as previously described.[22]

Formation of Polyelectrolyte Multilayers (PEM): When appropriate, silicon wafers, Au-coated glass sensors, polystyrene well-plates, or glass cover slips (ø15 mm) were used as substrata. All polyelectrolytes were dissolved in deionized water containing 0.15 mol L^{-1} NaCl at a concentration of 2 mg mL^{-1}. Chi solution containing 0.05 mol L^{-1} acetic acid was solubilized at 50 °C for 3 h. Col I was prepared in deionized water containing 0.15 mol L^{-1} NaCl and 0.2 mol L^{-1} acetic acid at a concentration of 2 mg mL^{-1}, centrifuged for 10 min to remove insoluble precipitates, and a working solution of 0.5 mg mL^{-1} was prepared by diluting the stock solution in 0.2 mol L^{-1} acetic acid supplied with 0.15 mol L^{-1} NaCl.[20] All polyelectrolyte and washing solutions were filtered through a 0.2 μm pore size membrane (Whatman). All multilayer formation procedures were carried out at RT under gentle shaking (Heidolph, Polymax 1040, at 30 rpm). PEI and polycations (Chi, Col I) were prepared at pH 4 while polyanions (nH and nCS) were prepared at pH 4 and pH 9 for the different LbL systems. oH and oCS were prepared at pH 4 only.

First, PEI was adsorbed on the substrates as the primary layer for 30 and 7 min for glass and well-plates, respectively. Thereafter, for systems relying on pH variation (H4 + 9 and CS4 + 9), alternating layers of H pH 4 (H4) or CS pH 4 (CS4) and Chi were used in the first eight layers. Then H9 or CS9 were used for the following eight layers, each deposited for 15 and 4 min on glass and well-plates, respectively. For oGAGs systems, alternative layers of oH or oCS and Chi were used, and Chi was replaced by Col I only in the terminating layer. The deposition step was repeated until reaching total number of 17 layers. Each step was followed by three washing steps, each for 2.5 min. The washing solution was 0.15 mol L^{-1} NaCl pH 4 or pH 9 with respect to the different LbL systems.

Measurement of Multilayer Growth: The layer growth and multilayer formation were investigated via SPR (IBIS Technologies B.V., Enschede, The Netherlands) as previously described.[29] Chi and CS, oCS, H, or oH (each at a concentration of 2 mg mL^{-1} in 0.15 mol L^{-1} NaCl) were injected in turns into the flow cell for 15 min. Interval washing steps (2 × 2.5 min cycles) after adsorption of each layer were employed using NaCl (0.15 mol L^{-1}, at appropriate pH) to remove any unbound molecules. The average of the 10 angle shift values (m°) at the end of each washing step was used for plotting the layer growth.

Water Contact Angle Measurements: In order to determine the wettability of the multilayer surfaces, static Water Contact Angle Measurements (WCA) measurements were conducted using an OCA15+ device (DataPhysics, Filderstadt, Germany) as previously described.[53] The experiments were conducted in duplicates with five droplets per sample using a flow rate of 0.5 μL s^{-1}. The software of OCA15+ device for each droplet recorded at least 10 independent measurements.

Characterization of PEM Thickness and Swelling: Spectroscopic ellipsometry was used to determine the average thickness of the samples (M–2000 V, J.A. Woollam Company, Lincoln, NE, USA). Cleaned Si wafers were used as reference substrate with SiO$_2$ layer thickness at 2.5 nm. In order to extract the optical constants of the PEMs, a Cauchy model was used as previously described.[34,54,55] In order to study the thickness of the samples under wet conditions, a special cell was used. The latter was filled with Milli-Q H$_2$O, 1 mmol HCl, or PBS in order to sufficiently wet the surface of the samples, and both the optical constants and the thickness were measured as before.

Measurement of PEM Surface Roughness: PEM surface topography and roughness were investigated using AFM (Nano-R, Pacific Nanotechnology, Santa Clara, CA). Si wafers (10 × 10 mm^2), either cleaned or PEM coated, were probed under ambient (air) laboratory conditions of temperature and humidity in close contact mode, as previously described.[27] For topography pictures, scans of 5 × 5 μm^2 were recorded at 512 × 512 pixel resolution. For the determination of the average roughness Ra and the mean square root roughness Rq (RMS), scans of 3 × 3 μm^2 were recorded at 512 × 512 pixel resolution. Two different Si-coated wafers were used for each condition, and pictures were taken in five individual locations in every sample. Ra and Rq were determined using the topography analysis software "Gwyddion 2.49 64-bit".

Uploading of Recombinant Human Bone Morphogenetic Protein 2 (rhBMP-2) to Multilayers for Cell and Release Studies: rhBMP-2 which was recombinantly produced in *Escherichia coli* (*E. coli*) cells[56] was loaded to the layers one day prior to cell seeding overnight at 4 °C. For all experiments, a concentration of 5 μg mL^{-1} in 1 mmol HCl was prepared from the stock solution (50 μg mL^{-1}) and loaded to the multilayers. After incubation, BMP-2 was aspirated and the samples were washed quickly with 0.15 mol L^{-1} NaCl at pH 7.4 for further cell experiments.

BMP-2 Release Studies via ELISA: PEMs were fabricated in 96-well plates, and BMP-2 was adsorbed at 5 μg mL^{-1} in 1 mmol HCl (50 μL each well) overnight at 4 °C. Samples were collected over 4 days, each time followed by a washing step with PBS and adding new PBS. Using an ELISA kit from PeproTech (Hamburg, Germany), the released amounts of BMP-2 were calculated.

Culture of C2C12 (Mouse Myoblast Cell Line) Cells: Cryopreserved C2C12 cells were thawed and grown in DMEM medium supplemented with 10% v/v FBS and 1% pen/strep at 37 °C in a humidified 5% CO$_2$/95% air atmosphere using a NuAire DH Autoflow incubator (NuAire Corp., Plymouth, Minnesota, USA). At ≈80% confluency, the cells were washed with PBS at pH 7.4 and detached from the flask using 0.05% trypsin/0.02% EDTA solution for 3–5 min at 37 °C. Thereafter, trypsinization was stopped using DMEM (10% FBS). Cells were collected in a 12-mL tube and centrifuged at 250 g for 5 min. The supernatant was aspirated and the cells pellet was re-suspended in 1 mL of DMEM 10% FBS. A dilution of 1:100 was prepared, and cells were counted manually using a Neubauer counting chamber.

Studies on Viability and Adhesion of C2C12 Cells: QBlue cell viability assay kit was employed according to the manufacturer's instructions (BioChain, Newark, USA). PEMs were prepared in 96-well plates (no BMP-2 loaded) and cells were seeded on top (200 000 cell mL^{-1}) in DMEM 10% FBS and incubated at 37 °C/5% CO$_2$. QBlue assay was performed after 24, 48, and 72 h of incubation for the first, second, and third well plate, respectively. Fluorescence measurements were taken in a black 96-well plate at 544 nm excitation and 590 nm emission wavelength using a plate reader (FLUOstar Optima, BMG LabTech, Offenburg, Germany). QBlue solution (10%) without cells represented the blank value. Statistical analysis of all quantitative cell data was performed using OriginPRO 8G (OriginLab Corporation, Northampton, USA). For the adhesion study, glass cover slips were used for LbL coating, placed in 24-well plates. Afterward, 1 mL of DMEM (10% FBS)–C2C12 cell suspension (50 000 cells mL^{-1}) was added to each sample and incubated at 37 °C for 24 h. Plain glass slides supplied with and without 5 μg mL^{-1} BMP-2 were used as cell-adhesive surface and served as positive and negative control, respectively. After 24 h of incubation, the cells were fixed with 4% w/v paraformaldehyde for 15 min, then rinsed twice with PBS. Cells were permeabilized with 0.1% Triton X-100 in PBS v/v for another 10 min. After further washing with PBS, the nonspecific binding sites were blocked by incubation of samples in 1% w/v BSA in PBS for 1 h. Cells were stained for vinculin in focal adhesion plaques using a primary mouse antibody vinculin (7F9) (1:50, Santa Cruz Biotechnology) and a secondary CY2-conjugated goat anti-mouse antibody (1:100, Dianova); for actin cytoskeleton and cell nuclei using BODIPY-Phalloidin (1:50, Invitrogen) and TO-PRO-3 (1:400, Invitrogen), respectively, for 30 min each. All reagents were diluted in 1% w/v BSA in PBS. The samples were then washed with PBS twice, briefly dipped

into ultrapure water, mounted with Mowiol (Calbiochem, Darmstadt, Germany), and examined using a confocal laser scanning microscope (CLSM, LSM 710, Carl Zeiss, Oberkochen, Germany) with 10×, 20×, and 63× oil immersion objective lenses. Images were processed with the ZEN 2011 software (Carl Zeiss). Later, images were analyzed by ImageJ.

Differentiation Studies (ALP Assay and Alizarin red-S Staining): For ALP assay, PEM were prepared in 24-well plates, loaded with BMP-2, and cells (125 000 cell mL^{-1}) in DMEM (2% FBS) were seeded on top and incubated for 4 days at 37 °C/5% CO_2. The cells were washed once with PBS, and cell lysis was done using 1% Triton X-100 for 30 min under slow shaking. Then 100 µL of cell lysate was incubated with 1 mg mL^{-1} *p*-NPP in a 96-well plate and incubated for 30, 60, and 90 min at 37 °C for ALP assay, and measurements were done using a plate reader (FLUOstar OPTIMA, BMG LABTECH) at 405 nm wavelength. Pierce BCA Protein Assay Kit from Thermo scientific (Rockford, IL, USA) was employed according to manufacturer's instructions in order to normalize the obtained ALP values to the total protein amounts. For alizarin red-S staining, cells were seeded on BMP-2 loaded multilayers made on glass substrates, at a density of 50 000 cell mL^{-1} in DMEM 10% FBS+1% pen/strep and incubated for 14 days at 37 °C/5% CO2. Alizarin red-S staining was performed as reported previously.[57] Bright-field images were taken using 10× lens via Leica DM IL microscope (Germany).

Statistical Analysis: All statistical computations were performed with Origin 8G software. Mean, standard deviation, and analysis of significance (ANOVA) (indicated as *) were calculated and indicated in the respective figures. A value of $p < 0.05$ was considered as significantly different. Further, box-whisker diagrams are shown where appropriate. The box indicates the 25th and 75th percentiles, the median (dash), and mean value (black square), respectively, whereas the 95–5% confidence interval is represented by the whiskers.

[1] R. C. Lawrence, C. G. Helmick, F. C. Arnett, R. A. Deyo, D. T. Felson, E. H. Giannini, S. P. Heyse, R. Hirsch, M. C. Hochberg, G. G. Hunder, *Arthritis Rheum.* **1998**, *41*, 778.

[2] O. P. Gautschi, S. P. Frey, R. Zellweger, *Aust. N. Z. J. Surg.* **2007**, *77*, 626.

[3] E. Gómez-Barrena, P. Rosset, D. Lozano, J. Stanovici, C. Ermthaller, F. Gerbhard, *Bone* **2015**, *70*, 93.

[4] M. Kellomäki, H. Niiranen, K. Puumanen, N. Ashammakhi, T. Waris, P. Törmälä, *Biomaterials* **2000**, *21*, 2495.

[5] L. Roseti, V. Parisi, M. Petretta, C. Cavallo, G. Desando, I. Bartolotti, B. Grigolo, *Mater. Sci. Eng., C* **2017**, *78*, 1246.

[6] L. Hao, J. Lawrence, *Laser Surface Treatment of Bio-Implant Materials*, John Wiley & Sons, Chichester **2005**.

[7] N. J. Shah, M. L. Macdonald, Y. M. Beben, R. F. Padera, R. E. Samuel, P. T. Hammond, *Biomaterials* **2011**, *32*, 6183.

[8] R. O. Hynes, *Science* **2009**, *326*, 1216.

[9] F. Rosso, A. Giordano, M. Barbarisi, A. Barbarisi, *J. Cell. Physiol.* **2004**, *199*, 174.

[10] M. Mrksich, G. M. Whitesides, *Annu. Rev. Biophys. Biomol. Struct.* **1996**, *25*, 55.

[11] B. D. Boyan, T. W. Hummert, D. D. Dean, Z. Schwartz, *Biomaterials* **1996**, *17*, 137.

[12] A. Köwitsch, G. Zhou, T. Groth, *J. Tissue Eng. Regen. Med.* **2017**, *12*, e23.

[13] I. Capila, R. J. Linhardt, *Angew. Chem., Int. Ed.* **2002**, *41*, 390.

[14] I. A. Sogias, A. C. Williams, V. V. Khutoryanskiy, *Biomacromolecules* **2008**, *9*, 1837.

[15] J.-K. F. Suh, H. W. Matthew, *Biomaterials* **2000**, *21*, 2589.

[16] J. Berger, M. Reist, J. M. Mayer, O. Felt, N. Peppas, R. Gurny, *Eur. J. Pharm. Biopharm.* **2004**, *57*, 19.

[17] T. Sakou, *Bone* **1998**, *22*, 591.

[18] A. Yamaguchi, T. Ishizuya, N. Kintou, Y. Wada, T. Katagiri, J. M. Wozney, V. Rosen, S. Yoshiki, *Biochem. Biophys. Res. Commun.* **1996**, *220*, 366.

[19] A. J. García, in *Foundations of Regenerative Medicine: Clinical and Therapeutic Applications*, Elsevier, UK **2009**, p. 368.

[20] M. Zhao, L. Li, C. Zhou, F. Heyroth, B. Fuhrmann, K. Maeder, T. Groth, *Biomacromolecules* **2014**, *15*, 4272.

[21] M. S. Niepel, D. Peschel, X. Sisquella, J. A. Planell, T. Groth, *Biomaterials* **2009**, *30*, 4939.

[22] M. S. Niepel, K. Kirchhof, M. Menzel, A. Heilmann, T. Groth, in *Layer-by-Layer Films for Biomedical Applications* (Eds: C. Picart, F. Caruso, J. Voegel), Wiley-VCH, Weinheim **2015**, p. 1.

[23] K. Kirchhof, A. Andar, H. Yin, N. Gadegaard, M. Riehle, T. Groth, *Lab Chip* **2011**, *11*, 3326.

[24] O. Guillame-Gentil, O. Semenov, A. S. Roca, T. Groth, R. Zahn, J. Vörös, M. Zenobi-Wong, *Adv. Mater.* **2010**, *22*, 5443.

[25] N. Aggarwal, N. Altgärde, S. Svedhem, G. Michanetzis, Y. Missirlis, T. Groth, *Macromol. Biosci.* **2013**, *13*, 1327.

[26] J. M. Silva, R. L. Reis, J. F. Mano, *Small* **2016**, *12*, 4308.

[27] M. Zhao, G. Altankov, U. Grabiec, M. Bennett, M. Salmeron-Sanchez, F. Dehghani, T. Groth, *Acta Biomater.* **2016**, *41*, 86.

[28] N. Aggarwal, N. Altgarde, S. Svedhem, K. Zhang, S. Fischer, T. Groth, *Langmuir* **2013**, *29*, 13853.

[29] N. Aggarwal, N. Altgarde, S. Svedhem, G. Michanetzis, Y. Missirlis, T. Groth, *Macromol. Biosci.* **2013**, *13*, 1327.

[30] P. Dong, W. Hao, Y. Xia, G. Da, T. Wang, *J. Mater. Sci. Technol.* **2010**, *26*, 1027.

[31] T. Crouzier, C. Ren, C. Nicolas, C. Roy, C. Picart, *Small* **2009**, *5*, 598.

[32] T. Crouzier, C. Picart, *Biomacromolecules* **2009**, *10*, 433.

[33] T. N. Vo, F. K. Kasper, A. G. Mikos, *Adv. Drug Delivery Rev.* **2012**, *64*, 1292.

[34] A. Köwitsch, M. J. Abreu, A. Chhalotre, M. Hielscher, S. Fischer, K. Mäder, T. Groth, *Carbohydr. Polym.* **2014**, *114*, 344.

[35] C. Picart, F. Caruso, J.-C. Voegel (Eds), *Layer-by-Layer Films for Biomedical Applications*, Wiley-VCH, Weinheim **2015**.

[36] M. Zhao, G. Altankov, U. Grabiec, M. Bennett, M. Salmeron-Sanchez, F. Dehghani, T. Groth, *Acta Biomater.* **2016**, *41*, 86.

[37] G. Altankov, K. Richau, T. Groth, *Materialwiss. Werkstofftech.* **2003**, *34*, 1120.

[38] Á. J. Leite, B. Sarker, T. Zehnder, R. Silva, J. F. Mano, A. R. Boccaccini, *Biofabrication* **2016**, *8*, 035005.

[39] M. Kisiel, A. S. Klar, M. Ventura, J. Buijs, M.-K. Mafina, S. M. Cool, J. Hilborn, *PLoS One* **2013**, *8*, e78551.

[40] R. McBeath, D. M. Pirone, C. M. Nelson, K. Bhadriraju, C. S. Chen, *Dev. Cell* **2004**, *6*, 483.

[41] M. Salmerón-Sánchez, M. J. Dalby, *Chem. Commun.* **2016**, *52*, 13327.

[42] N. Aggarwal, N. Altgärde, S. Svedhem, G. Michanetzis, Y. Missirlis, T. Groth, *Macromol. Biosci.* **2013**, *13*, 1327.

[43] J. H. Lee, G. Khang, J. W. Lee, H. B. Lee, *J. Colloid Interface Sci.* **1998**, *205*, 323.

[44] E. Migliorini, A. Valat, C. Picart, E. A. Cavalcanti-Adam, *Cytokine Growth Factor Rev.* **2016**, *27*, 43.

[45] R. N. Wang, J. Green, Z. Wang, Y. Deng, M. Qiao, M. Peabody, Q. Zhang, J. Ye, Z. Yan, S. Denduluri, *Genes Dis.* **2014**, *1*, 87.

[46] L. Fourel, A. Valat, E. Faurobert, R. Guillot, I. Bourrin-Reynard, K. Ren, L. Lafanechère, E. Planus, C. Picart, C. Albiges-Rizo, *J. Cell Biol.* **2016**, *212*, 693.

[47] A. Jikko, S. E. Harris, D. Chen, D. L. Mendrick, C. H. Damsky, *J. Bone Miner. Res.* **1999**, *14*, 1075.

[48] J. D. Mott, Z. Werb, *Curr. Opin. Cell Biol.* **2004**, *16*, 558.

[49] X. Jiao, P. C. Billings, M. P. O'Connell, F. S. Kaplan, E. M. Shore, D. L. Glaser, *J. Biol. Chem.* **2007**, *282*, 1080.

[50] A. M. Ferreira, P. Gentile, V. Chiono, G. Ciardelli, *Acta Biomater.* **2012**, *8*, 3191.

[51] V. Korzhikov, S. Roeker, E. Vlakh, C. Kasper, T. Tennikova, *Bioconjugate Chem.* **2008**, *19*, 617.

[52] A. Köwitsch, M. Jurado Abreu, A. Chhalotre, M. Hielscher, S. Fischer, K. Mader, T. Groth, *Carbohydr. Polym.* **2014**, *114*, 344.

[53] A. Köwitsch, Y. Yang, N. Ma, J. Kuntsche, K. Mader, T. Groth, *Biotechnol. Appl. Biochem.* **2011**, *58*, 376.

[54] J. Almodovar, L. W. Place, J. Gogolski, K. Erickson, M. J. Kipper, *Biomacromolecules* **2011**, *12*, 2755.

[55] P. Esmaeilzadeh, A. Köwitsch, F. Heyroth, G. Schmidt, S. Fischer, K. Richter, T. Groth, *Carbohydr. Polym.* **2017**, *157*, 1205.

[56] F. Hillger, G. Herr, R. Rudolph, E. Schwarz, *J. Biol. Chem.* **2005**, *280*, 14974.

[57] M. S. Niepel, F. Almouhanna, B. K. Ekambaram, M. Menzel, A. Heilmann, T. Groth, *Int. J. Artif. Organs* **2018**, *41*, 223.

Chapter 3

Summary - Intrinsically cross-linked ECM-like multilayers for BMP-2 delivery promote osteogenic differentiation of cells:

In the previous publication; oxidized chondroitin sulfate (oCS)/chitosan multilayers exhibited the most promising results in terms of BMP-2 delivery, cell adhesion and osteogenesis. Therefore, the aim of this paper was to further investigate the effect of intrinsically cross-linked oCS-based multilayers, with varying molecular composition, on BMP-2 activity. Collagen I (Col I) was used as polycation instead of chitosan due to its importance in promoting cell adhesion as well as being a major protein in bone tissue, thus, creating a biomimetic microenvironment. BMP-2 loading concentration was increased (10 µg mL^{-1}) to check if there would be any increase in the osteogenic differentiation rate. The multilayers used were composed of either; oxidized chondroitin sulfate (oCS100), native chondroitin sulfate (nCS) or a 50:50 mixture of both oxidized and native (oCS50), together with Col I as polycation. The 50:50 mixture was introduced to check the effect of varying the molecular composition on multilayers' characteristics, cellular behavior and BMP-2 activity. Studies of physiochemical characteristics of the multilayers demonstrated that; oCS50 multilayers had the softest layers, highest water content and the thickest layers in term of swelling, while oCS100 had the stiffest surface and highest roughness with intermediate wetting properties. Both oCS100 and oCS50 multilayers supported the natural fibrilization of Col I, had the thickest Col I fibers and could preserve them even at acidic conditions compared to nCS multilayers. Moreover, oCS100 multilayers adsorbed the highest amount of BMP-2 during loading and it released the least amount over time, indicating its capability of storing BMP-2 for longer periods and presenting it to the cells in a matrix-bound manner rather than as soluble released BMP-2. On the contrary, nCS multilayers released the highest amount of BMP-2 while oCS50 multilayers showed an intermediate release profile. Cell adhesion studies, performed using C2C12 myoblasts, showed an enhanced cell adhesion and spreading on both BMP-2 loaded and non-loaded oCS100 multilayers while oCS50 multilayers, due to their high water content were not supportive in that regard. Further, BMP-2 internalization was the highest on oCS100 multilayers and the cells cultured on oCS100 multilayers expressed more osteogenic markers, showed higher ALP levels and staining and more staining of mineralized matrix compared to nCS and oCS50 multilayers.

It has been found that osteogenesis is not only about how much BMP-2 is getting released but rather how much BMP-2 the multilayers can store to present it to the cell in its active state as matrix-bound. Here, the intrinsic cross-linking of multilayers proved its efficiency in enhancing multilayers' characteristics, preserving the natural fibrilization of Col I and controlling the delivery of BMP-2 to cells and hence, guiding cell differentiation. Overall, these multilayers with intrinsic cross-linking can be further used as biomimetic coatings for implants to deliver bioactive growth factors to the site of defects for various tissue regeneration applications.
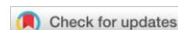
RESEARCH ARTICLE

ADVANCED
MATERIALS
INTERFACES
www.advmatinterfaces.de

Intrinsically Cross-Linked ECM-Like Multilayers for BMP-2 Delivery Promote Osteogenic Differentiation of Cells

Reema Anouz, Tamaradobra Selekere, Adrian Hautmann, Catharina Husteden, Matthias Menzel, Christian Woelk, Christian E. H. Schmelzer, and Thomas Groth*

Dedicated to the pure soul of my little brother who passed away in 2021 during the Corona pandemic

Surface coatings prepared by layer-by-layer technique permit loading of growth factors (GFs) and their spatially controlled release. Here, native chondroitin sulfate (nCS), oxidized CS (oCS100), or mixture of both (oCS50) are combined with collagen I (Col I) to fabricate polyelectrolyte multilayers (PEMs) that exhibit structural, mechanical, and biochemical cues like the natural extracellular-matrix. The use of oCS enables intrinsic cross-linking of PEM that offers higher stability, stiffness, and better control of bone morphogenetic protein-2 (BMP-2) release compared to nCS. oCS100 PEMs have enhanced stiffness, promote Col I fibrillization, and present BMP-2 in a matrix-bound manner. oCS50 PEMs show intermediate effects on osteogenesis, soft surface, high water content but also moderately slow BMP-2 release profile. C2C12 myoblasts used for osteogenesis studies show that oCS PEMs are more stable and superior to nCS PEMs in supporting cell adhesion and spreading as well as in presenting BMP-2 to the cells. oCS PEMs are triggering more osteogenesis as proved by the quantitative real-time polymerase chain reaction, immune and histochemical staining. These findings show that intrinsic cross-linking in oCS/Col I multilayers provides a successful tool to control GFs delivery and subsequent cell differentiation which opens new opportunities in regenerative therapies of bone and other tissues.

1. Introduction

Unlike the usual nature of bone tissue, which is capable to regenerate by itself, large bone defects are one of the most faced challenges in orthopedic surgeries. Such defects, which occur after fractures or tumor resections, do not heal on their own and often require surgical intervention.[1] Since the gold standard method using bone autografts or allografts to regenerate bone still has its drawbacks and limitations, tissue engineering has emerged as an alternative approach.[2] Further, biomaterials used for tissue engineering approaches are mostly of synthetic origin.[3] Therefore, lacking biochemical cues that are usually present in the extracellular matrix (ECM). In native tissues, cells reside in the ECM which is a microenvironment filling the space among cells and varies from one tissue type to another providing each tissue with unique characteristics and plays many important key roles in cell adhesion, migration, proliferation, and differentiation through presentation of crucial biochemical and biomechanical cues.[4] Glycosaminoglycans (GAGs) and fibrous proteins (e.g., collagen I) are major components of the ECM.[5] Collagen I (Col I) does not only provide topographical cues and mechanical strength for tissues but also exhibits many biological functions such as mediating cell attachment and spreading.[6] GAGs such as chondroitin sulfate

R. Anouz, T. Selekere, A. Hautmann, T. Groth
Department of Biomedical Materials
Institute of Pharmacy
Martin Luther University Halle-Wittenberg
Heinrich-Damerow-Strasse 4, 06120 Halle Saale, Germany
E-mail: thomas.groth@pharmazie.uni-halle.de

C. Husteden
Biochemical Pharmacy
Institute of Pharmacy
Martin Luther University Halle-Wittenberg
Wolfgang-Langenbeck-Straße 4, 06120 Halle Saale, Germany

M. Menzel, C. E. H. Schmelzer
Fraunhofer Institute for Microstructure of Materials and Systems IMWS
Walter-Hülse-Straße 1, 06120 Halle Saale, Germany

C. Woelk
Pharmaceutical Technology
Medical Faculty
University Leipzig
Eilenburger Straße 15a, 31, 04317 Leipzig, Germany

T. Groth
Interdisciplinary Center of Material Research and Interdisciplinary Center of Applied Research
Martin Luther University Halle-Wittenberg, Halle
06099 Saale, Germany

(CS) and hyaluronic acid (HA) play many important roles in cell growth and differentiation when interacting with cytokines, proteins, and cell receptors.[7] Hence, the ECM plays a role as a reservoir for storage and release of growth factors (GFs) such as bone morphogenetic protein-2 (BMP-2),[1,8] which induces the differentiation of mesenchymal stem cells (MSCs) and nonosteogenic cell lines such as C2C12 myoblasts into osteoblasts.[9] Therefore, scaffolds and biomaterials that mimic the ECM constitute a very promising strategy to induce tissue regeneration due to the unique properties of the ECM. Efforts to tailor the biocompatibility and to introduce biochemical cues to synthetic biomaterials have been made through physical, chemical, and biological surface modification techniques that were employed to modify biomaterials' surfaces due to their importance in creating the very first response when implanted in the body.[10] Layer-by-layer (LbL) is a physical modification technique that relies on alternative adsorption of oppositely charged polyelectrolytes to produce thin polyelectrolytes multilayers (PEMs)[11] that vary in their thickness, surface charge, wettability, viscoelasticity, and topography by varying the assembly conditions, medium characteristics, and the polyelectrolytes used.[12,13] In bone repair field, metals, ceramics, and polymers are used as implant materials. Since, multilayers can be deposited by LbL on any kind of substrate, it is an attractive surface modification technique for implantable devices; particularly when bioactive coatings mimicking composition of bone matrix and delivery of bioactive molecules are desired.[14] Due to its versatility, simplicity, low cost, and the use of water as a solvent, LbL enables the insertion of sensitive biomolecules like proteins and GFs and release them in a sustained manner over-time while preserving their bioactivity.[13] Using ECM biomolecules as polyelectrolytes in LbL is one of the strategies used to mimic the ECM properties for tissue regeneration. In that regard, GAGs and Col I are suitable candidates representing polyanion and polycation, respectively, which permits their use as building blocks for PEMs to create a biomimetic environment offering specific interactions with cell receptors and GFs.[10] Moreover, chemical cross-linking has been widely used to improve the stability of multilayers.[15–17] However, it causes changes in the physiochemical properties of the multilayers[18] and leads to cytotoxicity.[19] In a previous work, it was found that functionalization of GAGs with aldehyde groups through oxidation allows their immobilization on amino functionalized surface at which the bioactivity of the oxidized GAGs was not altered.[20] This functionalization method made the oxidized GAGs useful candidates to be used for generation of bioactive surface coatings. Further, Zhao et al. employed the latter functionalization method to fabricate multilayers with intrinsic cross-linking (covalent bond) between the aldehyde groups on the oxidized GAGs and the amino groups of Col I. An enhanced stability, Col I fibrillization, and cell adhesion were the characteristics of the intrinsically cross-linked multilayers compared to native GAGs multilayers.[21] Hence, we thought of using the same cross-linking method not only to enhance the multilayers properties but also to study it as a tool to control BMP-2 release and presentation to cells in order to achieve osteogenic differentiation of cells using multilayers exhibiting both physical and biochemical cues like the natural ECM. It is also worth mentioning that the cytotoxicity of this intrinsic cross-linking

method of PEM using different cell types was already studied previously and revealed no toxic effect.[8,21,22] Thus, cytotoxicity measurements will not be performed again in this study.

Since Col I is a major protein in bone tissue[23] that has a significant impact on osteogenesis, it was used in this study as a polycation. Here, we studied multilayers composed of either oxidized chondroitin sulfate (oCS100), native chondroitin sulfate (nCS), or a 50:50 mixture of both (oCS50) together with Col I as polycation. The 50:50 mixture was introduced in this study to see the effect of the molecular composition on multilayers' characteristics and cellular behavior. The efficiency of the intrinsic cross-linking in controlling BMP-2 release and presentation was studied, in addition to physiochemical properties of the multilayers as well as the biological studies using C2C12 cells. C2C12 cells were chosen due to their potency to differentiate into either myotubes or osteoblasts. They have been used previously by other groups for studying BMP-2 signaling because of the presence of BMP receptor on C2C12 cells.[24] Therefore, C2C12 cells are responsive to both soluble[9] and matrix-bound BMP-2[25] with alkaline phosphatase (ALP) and Osterix expression being measurable after 3 days, while MSCs need at least 1 week to have detectable expression.[26] Results show that oCS/Col I multilayers are superior in many aspects, particularly in controlling BMP-2 release, presentation, and osteogenic differentiation of C2C12, compared to nCS/Col I multilayers. **Figure 1** illustrates the various multilayers used in this study and the occurring molecular interactions.

2. Results

2.1. Characterization of PEMs Properties

2.1.1. Multilayers Formation and Thickness

The multilayers formation of the various systems was controlled in a real-time measurement via quartz crystal microbalance with dissipation monitoring (QCM-D) as shown in **Figure 2**A–D. In general, it was shown that the frequency was decreasing after each layer for all PEMs, indicating that mass is added during deposition. However, the oCS50 PEMs exhibited higher decrease in frequency compared to the nCS and oCS100 PEMs. A rapid decrease in frequency from the base line was observed after the adsorption of the cationic poly(ethylene imine) (PEI). This also corresponded to a rapid increase in the energy dissipation in the layer, as shown in Figure 2B. It was possible to obtain information about the viscoelastic properties of the PEMs in term of change in dissipation. The increase in the energy dissipated through the multilayers formation was the highest for oCS50 PEMs followed by oCS100 and the lowest energy dissipation was observed for nCS, indicating that oCS50 PEMs have the softest layers. The PEM thickness was calculated using two types of equations: Sauerbrey equation, which is usually used with rigid, evenly distributed layers, and the Voigt model, which takes into consideration the contribution of the viscoelasticity to the sensed mass.[27] The latter is most probably more reliable to calculate the thickness in our study, since the change in energy dissipation is quite high and the analyzed PEMs are assumed to be viscoelastic layers.
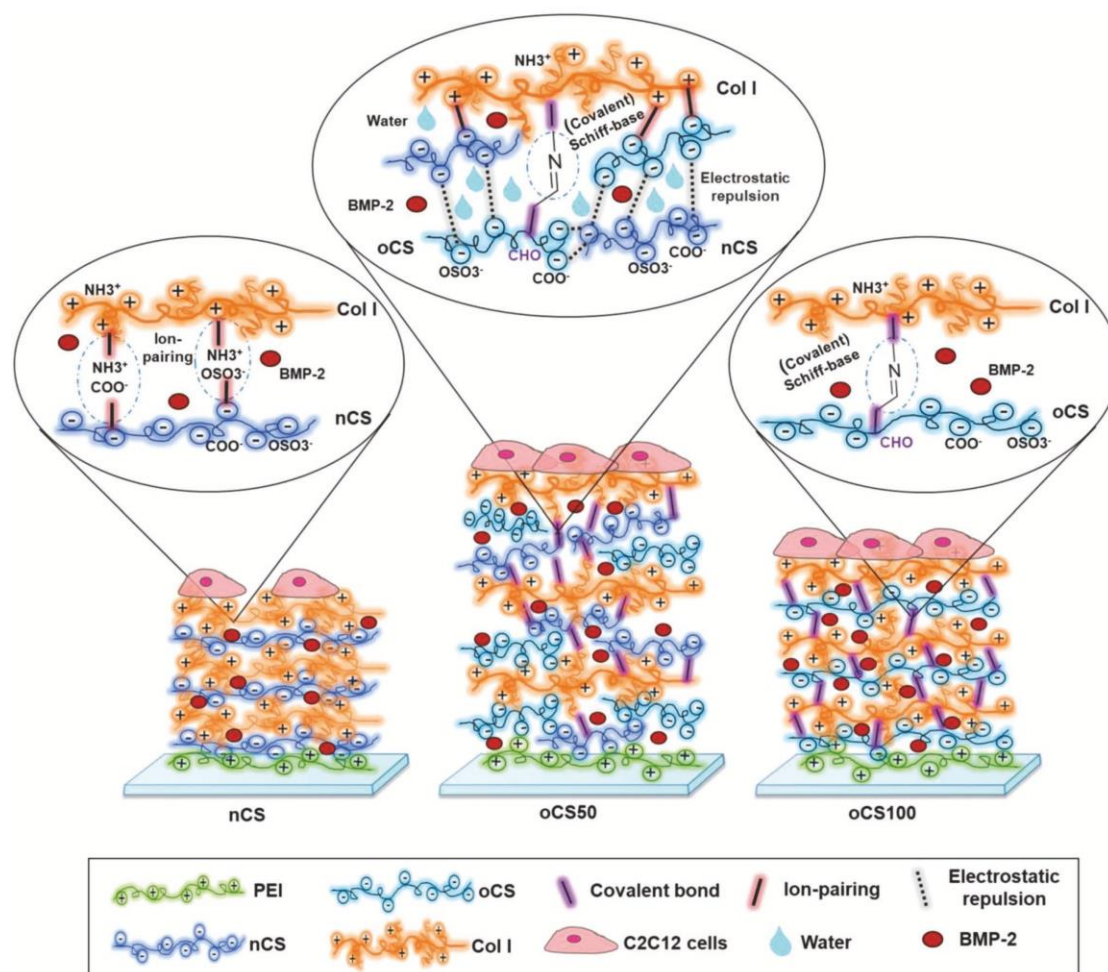
Figure 1. Illustration of the multilayers used in this study. Total of 17 layers. nCS is nCS/Col I multilayers, oCS50 is oCS50/Col I multilayers, and oCS100 is oCS100/Col I multilayers with oCS having oxidation degree of 2.77%. nCS depends mainly on ion pairing while oCS50 relies mainly on covalent binding and to a smaller extent on ion pairing, resulting in free negatively charged groups that lead to electrostatic repulsion, attraction of more water, and swelling. oCS100 is depending only on covalent binding.

The detected change in resonance frequency as a function of multilayers' build-up has been converted to the Sauerbrey adsorbed amount, as shown in Figure 2D. Further, by assuming that the density of the layer, viscosity of the bulk liquid, and fixed density layer are 1000 kg m^{-3}, 1 mPas, and 1400 kg m^{-3}, respectively,[27] it was possible to estimate the thickness as a function of the number of layers during the build-up of the PEMs as shown in Figure 2C. Value of $\approx$155, 140, and 128 nm for the final thickness was obtained for oCS50, oCS100, and nCS PEMs, respectively.

2.1.2. Wettability and Dry Thickness Measurements

As shown in **Figure 3**, all PEM systems showed moderate water contact angle (WCA) values around 50°, indicating that all

PEMs are moderately hydrophilic compared to the plain glass (control) that showed WCA below 35°. Further, after measuring the dry thickness via ellipsometry, significantly thicker multilayers were obtained for oCS100 PEMs ($\approx$32 nm) and oCS50 ($\approx$31 nm) in comparison to nCS PEMs ($\approx$24 nm).

2.1.3. Topography, Stiffness, and Roughness of PEMs

The surface topography, stiffness, and roughness of clean Si wafers and all PEMs were analyzed by atomic force microscopy (AFM) in wet state and under ambient laboratory conditions. **Figure 4**A shows that the topography of final layers of all PEM systems was characterized by the presence of Col I fibers. The fibrillization of Col I was supported on all BMP-2
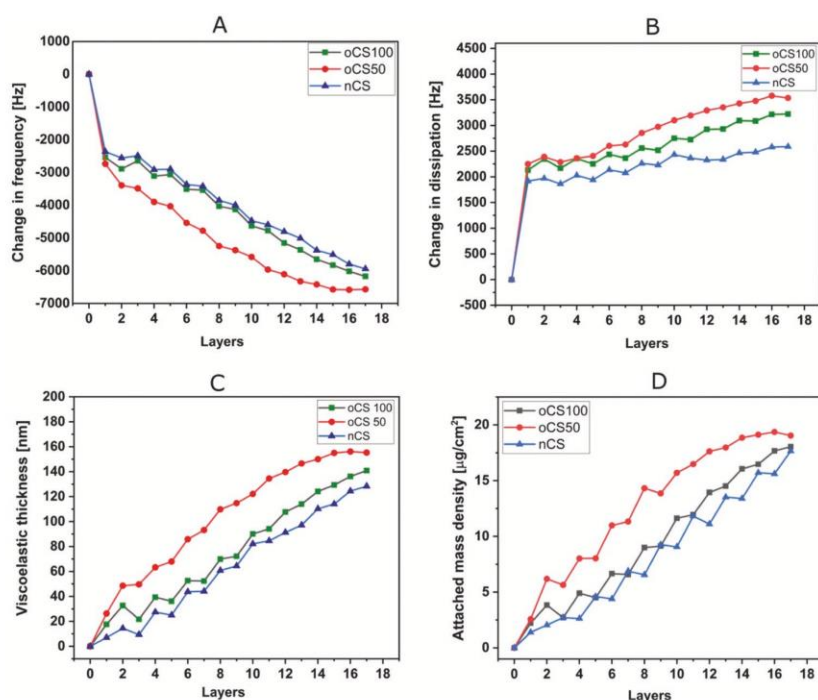
Figure 2. Film growth monitored in situ by QCM-D for oCS100, oCS50, and nCS multilayers. PEMs of oxidized chondroitin sulfate (oCS100), native chondroitin sulfate (nCS), or a mixture of both (oCS50) were prepared with Col I as polycation. A) Change in frequency shifts. B) Change in dissipation. C) Representation of viscoelastic thickness calculated in (nm) using voigt-based model. D) Representation of the attached mass calculated using Sauerbrey equation. The 1st layer is PEI, even numbers refer to native or oxidized CS and odd numbers refer to Col I. $n = 2$.

nonloaded multilayers with slight differences. oCS100 and oCS50 PEMs had significantly thicker Col I fibers than nCS PEMs (Figure 4B). On nonloaded samples (*BMP-2-*), oCS100 PEMs were showing the highest stiffness and roughness while oCS50 PEMs had the softest surface. A noticeable decrease in Col I fibers' thickness was observed after BMP-2 loading on all BMP-2-loaded PEMs. This decrease was reflected in a decrease in Young's modulus as well. However, oCS100 and oCS50

PEMs were more resistant and stable than nCS PEMs which were prone to complete loss of Col I fibers after BMP-2 loading. This Col I loss on nCS PEMs could have led to some rearrangement making the silicone substrate more prominent, which was reflected in a false positive increase in Young's modulus of nCS PEMs (Figure 4C). Further, the roughness of nonloaded PEMs was the highest for oCS100 PEMs, lesser for oCS50, and the least for nCS PEMs. The dissolution of Col I fibers
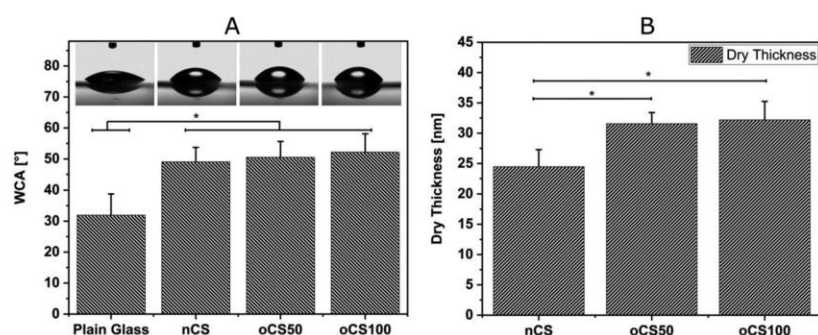
Figure 3. A) Static WCA measurements after multilayers formation up to 17 layers. Multilayers of oxidized chondroitin sulfate (oCS100), native chondroitin sulfate (nCS), or a mixture of both (oCS50) were prepared with Col I as polycation. Results are presented as means ± SD of four measurements taken from each sample for each multilayers system. B) Measurements of dry thickness taken by ellipsometry after formation of 17 layers of the various multilayers. Results represent means ± SD. $n = 4$. (*) data are significantly different.
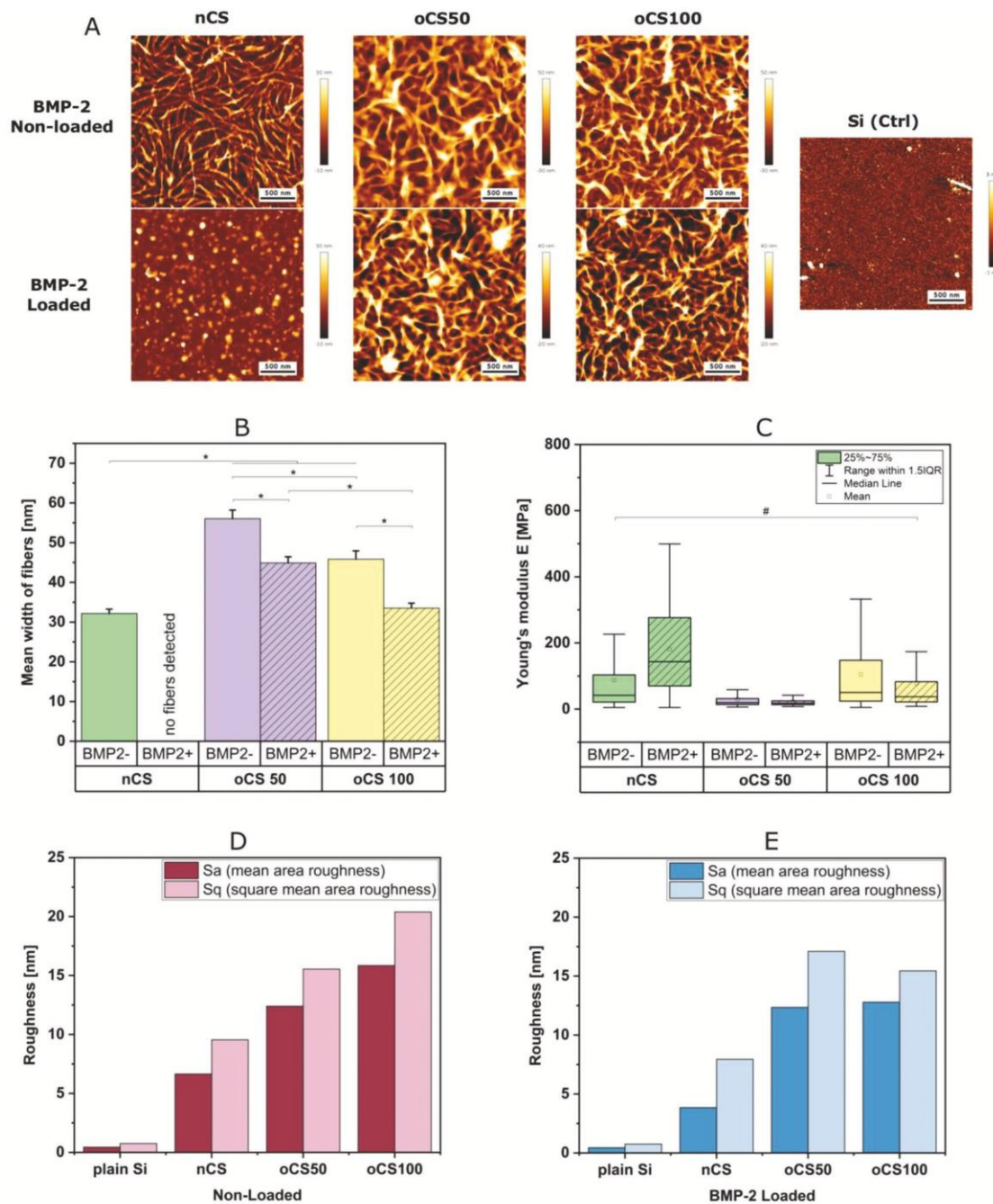
Figure 4. A) Surface topography of type I collagen (Col I) terminated multilayers (17th layer) visualized by atomic force microscopy (AFM)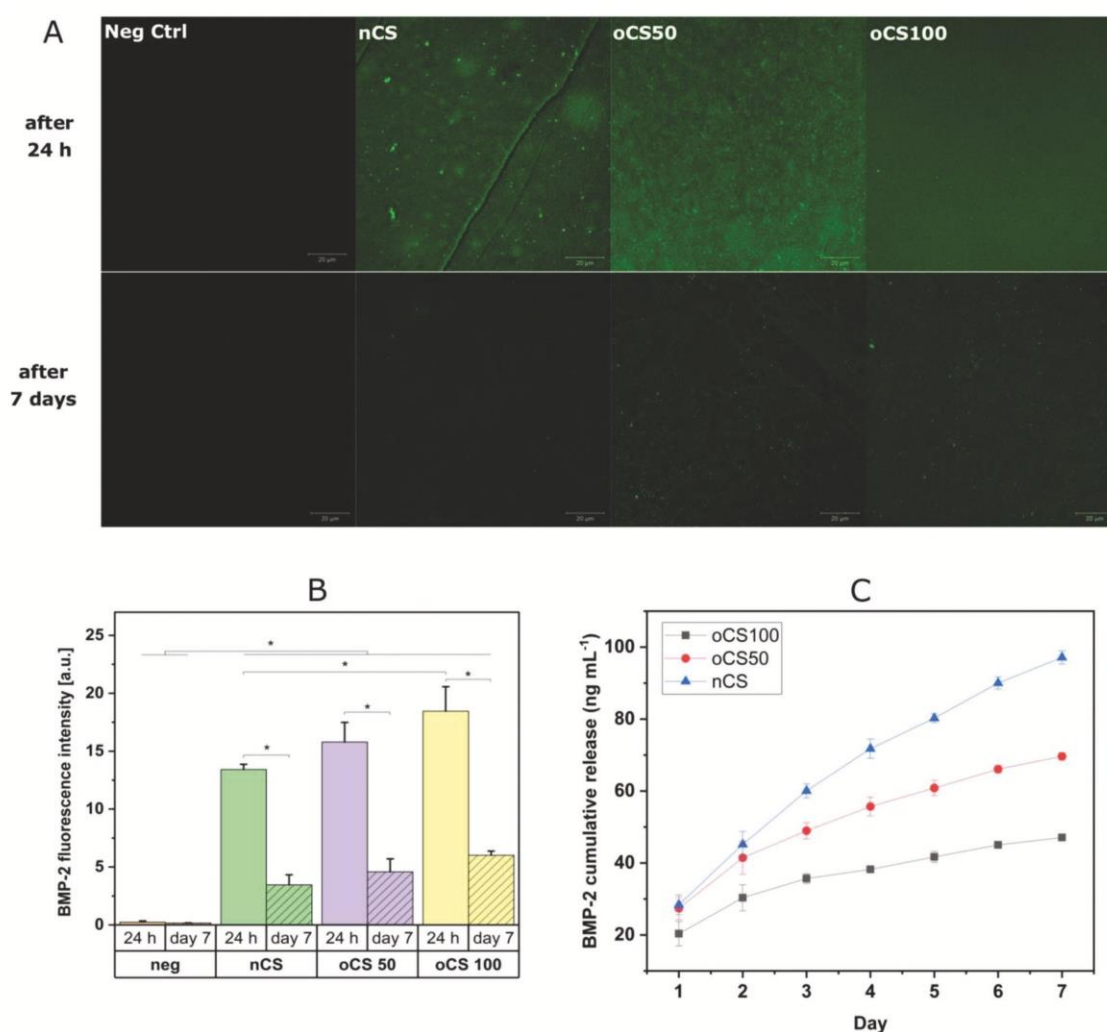. Multilayers of oxidized chondroitin sulfate (oCS100), native chondroitin sulfate (nCS), or a mixture of both (oCS50) were prepared with Col I as polycation. (Scale bar: 500 nm.) (✳) data are significantly different. B) Quantification of Col I fibers diameter on the various multilayers using *FSegment* program. The program traces all fibers and measures the width of each fiber every 5 pixel (equals 48.5 nm). All measuring points per sample were then cumulated and analyzed. *BMP+* refers to BMP-2 loaded multilayers and *BMP-* refers to BMP-2 nonloaded multilayers. C) Young's modulus (elasticity) measurements by AFM. The Young's modulus E for each pixel was determined. All data are significant to each other except # ($p \leq 0.05$ Kruskal–Wallis-ANOVA, Dunn post hoc, $n = 131.072$). D) Surface roughness measurements of BMP-2 nonloaded multilayers. E) Surface roughness measurements of BMP-2 loaded multilayers.

affected the surface roughness, hence, a decrease in roughness was observed after loading BMP-2 to all types of PEMs (Figure 4D,E).

2.2. BMP-2 Adsorption and Release Studies

From the confocal laser scanning microscopy (CLSM) images and the quantification of BMP-2 adsorbed by the multilayers' surfaces (**Figure** 5A,B), it was concluded that BMP-2 adsorbed the most on oCS100 PEMs followed by oCS50 while the least was on nCS PEMs. However, a significant decrease of adsorbed BMP-2 was noticed after 7 days of incubation in Dulbecco's modified Eagle's medium (DMEM) for all PEMs. Further, regarding BMP-2 release, all PEMs were releasing the loaded BMP-2 over time in a sustained release manner. However, oCS100 PEMs with intrinsic cross-linking were able to store and present the majority of the loaded BMP-2 to the cells in a matrix-bound manner through releasing the least amounts over time (47 ng mL^{-1} on day 7) compared to oCS50 and nCS PEMs;

Figure 5. Multilayers of oxidized chondroitin sulfate (oCS100), native chondroitin sulfate (nCS), or a mixture of both (oCS50) were prepared with Col I as polycation. Neg Ctrl is plain glass and no BMP-2 was added. A) CLSM images of BMP-2 adsorbed at the various multilayers surfaces, after 24 h (the first row) and 7 days (the second row) of incubation in DMEM. (Scale bar: 20 µm.) B) Semiquantification of BMP-2 adsorbed on multilayers surface by quantifying the fluorescence intensity in CLSM images. The mean intensity was extracted by ImageJ 1.53c. (*) refers to significant difference, $p \leq 0.05$. C) Cumulative BMP-2 release from the various multilayers measured by ELISA over 7 days after loading BMP-2 (10 µg mL^{-1}) for overnight. Results are means ± SD. $n = 6$ replicates of each multilayers system.

as illustrated in Figure 5C. Released GFs have short life-time[28] while matrix-bound is the effective form of GFs presentation to cells, as shown in previous studies by the group of Picart.[29] Further, since the initial differentiation of C2C12 cells into functional osteoblasts is detectable during the first 3–7 days, characterized by upregulation of ALP,[26] BMP-2 release was only measured for 7 days. Despite that all PEMs were having a similar first release value (between 20 and 29 ng mL^{-1}), nCS PEMs, which lack intrinsic cross-linking and are mainly dependent on ion pairing, could not retain the loaded BMP-2 but rather released it much faster to the solution (97 ng mL^{-1} on day 7). However, oCS50 PEMs, partially depending on ion pairing and more on covalent binding, could balance this high release to a more moderate behavior (≈70 ng mL^{-1} on day 7). Moreover, after checking the BMP-2 release kinetics fitting from the multilayers, it was concluded that the BMP-2 release in this study fits to the Higuchi model (see the Supporting Information). This means that the release was diffusion dependent and was not relying on the degradation of the matrix or the multilayers.[30] Therefore, the type of binding inside the multilayers is mainly affecting and controlling the BMP-2 release and presentation.

2.3. BMP-2 Internalization Study

BMP-2 was internalized into the cells on all PEMs in general (**Figure 6**). However, more staining of BMP-2 molecules was observed on oCS PEMs than on nCS PEMs indicating more internalization on intrinsically cross-linked PEMs (oCS100, oCS50) due to the presentation of BMP-2 to cells in a matrix-bound manner. Further, lesser BMP-2 internalization was observed on pos Ctrl where BMP-2 is present to the cells in a soluble state and not as matrix-bound like in the oCS PEMs, indicating much slower internalization of soluble BMP-2. Similar results were for nCS PEMs which were offering most of the BMP-2 in a released (soluble) state. The neg Ctrl

containing no BMP-2 showed no staining of BMP-2. On all PEMs, the internalization of BMP-2 in permeabilized cells after 24 h was clear in the form of dots (green) representing BMP-2 molecules.

2.4. C2C12 Cell Adhesion Study

To explore whether the loaded BMP-2 has any effect on cell adhesion, two sets of samples were used, original (nonloaded) and BMP-2-loaded multilayers, as shown in **Figure 7**. All original PEMs supported cell adhesion in general with small variances regarding the number of C2C12 cells (Figure 7A). However, on original PEMs (nonloaded), cell spreading was higher on intrinsically cross-linked PEMs (i.e., on oCS100 and oCS50 PEMs) than on nCS PEMs and pos Ctrl, characterized by more spread and elongated cells with significantly longer actin filaments (red) which could be seen from the CLSM images as well as from the quantification of cell area and actin filaments length per cell. Nevertheless, no organization of vinculin molecules (green) in focal adhesions (FAs) could be detected there.

Interestingly, after BMP-2 loading, a general increase in cell adhesion and spreading was observed on all BMP-2-loaded PEMs, including the pos Ctrl, indicating a promoting effect of BMP-2 on cell adhesion and spreading. This enhancement was characterized by more spread elongated cells showing more alignment of longitudinal actin filaments (red) and organization of vinculin (green) in FA plaques, as illustrated in the CLSM images (Figure 7E, 2nd and 3rd row). Further, the increase of total length of actin filaments on loaded PEMs was significant for all PEMs compared to nonloaded ones (Figure 7D). Nonetheless, oCS100 PEMs were still superior to oCS50 and nCS PEMs even after loading BMP-2. This was proven not only by showing the longest total actin filaments (Figure 7D) but also by the pronounced organization of the most vinculin in FA (Figure 7C) compared to oCS50 and nCS PEMs.
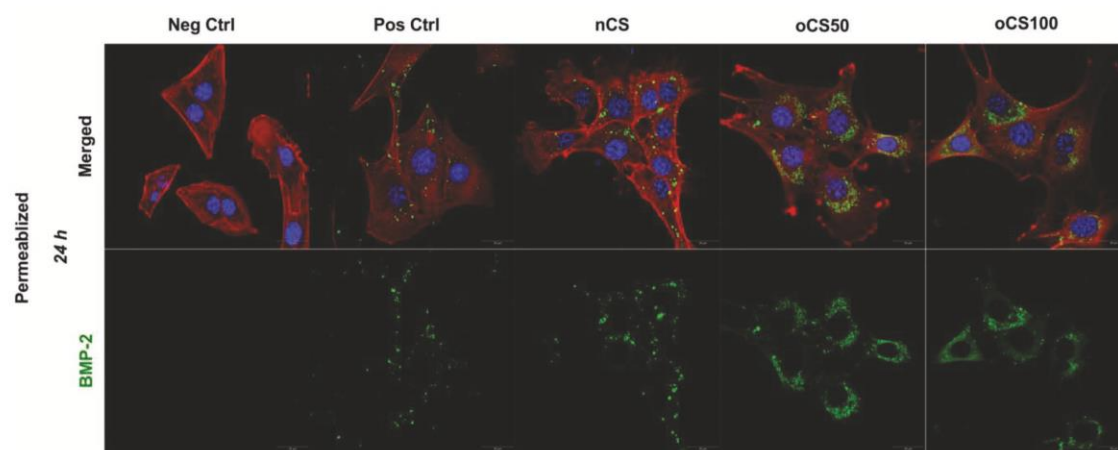

Figure 6. CLSM images show BMP-2 internalization into permeabilized C2C12 cells after 24 h of incubation on BMP-2-loaded PEM. PEMs of oxidized chondroitin sulfate (oCS100), native chondroitin sulfate (nCS), or a mixture of both (oCS50) were prepared with Col I as polycation. The samples were stained for BMP-2 (green) being internalized into the cells, filamentous actin (red), and nucleus (blue). As controls, cells were seeded on plain glass slides either without (neg Ctrl) or with BMP-2 (pos Ctrl) in the medium. Cells were imaged with CLSM 63× oil immersion objective (scale bar: 20 μm).
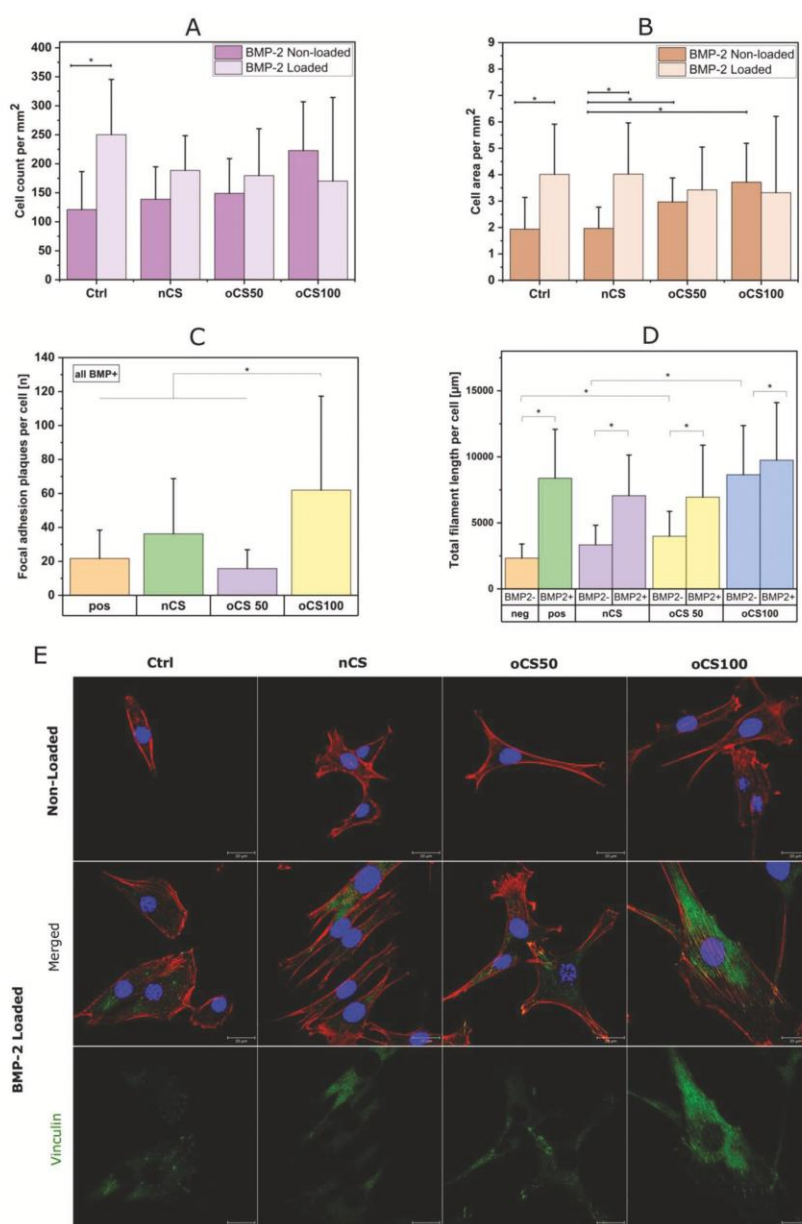
Figure 7. Adhesion of C2C12 cells seeded on native and various cross-linked multilayers, after 24 h of incubation. PEMs of oxidized chondroitin sulfate (oCS100), native chondroitin sulfate (nCS), or a mixture of both (oCS50) were prepared with Col I as polycation. A) Quantification of cell count, B) and cell area obtained using ImageJ. C) Quantification of vinculin in FA plaques. Calculated FA plaques were related to the individual cell area and detected with a custom cell profiler pipeline. $n > 15$, $*p \leq 0.05$ ANOVA, post-Tukey. D) Actin filament length quantification on both BMP-2-loaded and nonloaded multilayers. All actin fibers were detected by phalloidin. Filament sensor 0.1.7 was used to detect all fibers in each cell. $n > 15$, $*p \leq 0.05$ ANOVA, post-Tukey. (*) data are significantly different. E) CLSM images show C2C12 cells adhesion after 24 h incubation on various native and cross-linked multilayers. The cells were stained for vinculin (green) present in FAs, filamentous actin (red), and nucleus (blue) on multilayers without BMP-2 (upper row) and with BMP-2 loading (lower row). As a control, cells were seeded on plain glass slides either without (nonloaded) or with BMP-2 (BMP-2 loaded) in the medium. Cells were imaged with CLSM 63× oil immersion objective (scale bar: 20 μm).

2.5. Quantitative and Qualitative Osteogenic Differentiation Studies

To understand whether it is the released BMP-2 or the matrix-bound BMP-2 that is bioactive and able to trigger osteogenesis, quantitative real-time polymerase chain reaction (qRT-PCR) was performed to evaluate the expression of specific osteogenic markers (**Figure 8**). ALP was significantly upregulated in C2C12 cells grown on oCS100 PEMs (≈4.5-fold increase) and oCS50 PEMs (≈3.5-fold increase) compared to the weak increase (≈1.5) in gene expression on nCS PEMs. One exception was for pos Ctrl, where the high concentration (10 µg mL^{-1}) of soluble BMP-2 in the medium triggered very high expression of ALP gene (≈11-fold increase). Further, Col I was also found to be strongly expressed in cells grown on oCS100 PEMs (≈3.5-fold increase) followed by oCS50 PEMs with 2.5-fold increase in Col I gene expression, while reduced expression was measured for cells on nCS PEMs (≈0.5-fold). Interestingly, the soluble BMP-2 in pos Ctrl could not trigger high Col I gene expression. Furthermore, the osteogenic marker Runx2 was upregulated in cells grown on all PEMs in general, with being more pronounced in cells on nCS PEMs and on pos Ctrl with ≈2.5-fold and twofold increase, respectively, and less on oCS100 (≈1.5-fold increase) and oCS50 PEMs (≈1.25-fold increase). Similar finding goes for Osterix which was significantly more upregulated in cells cultured on nCS PEMs and pos Ctrl than on oCS100 and oCS50 PEMs. Noggin which acts as a BMP-2 antagonist[31] was downregulated in cells grown on oCS100 and oCS50 PEMs (≈0.5-fold increase) and upregulated in cells on nCS PEMs and pos Ctrl. It is worth mentioning that a balanced BMP-2/ Noggin level is very important in regulating osteogenesis.[31] The more Noggin is expressed, the less osteogenesis occurs. However, since the expression of genes does not guarantee their translation into proteins,[32] further osteogenic markers on the protein or ECM level were screened.

In **Figure 9**A, it is worth noticing that significantly high ALP activity was observed in cells grown on oCS100 and oCS50 PEMs and not on nCS or pos Ctrl which confirms the PCR data of ALP and Col I expression. These findings were also reflected in the ALP staining and alizarin red staining of the mineralized matrix (Figure 9B) at which the most ALP staining (purple color) was observed for cells on oCS100 and oCS50 PEMs while very little ALP staining (purple) was observed for nCS PEMs and even for pos Ctrl. The same was noted for alizarin red. Big dark red oily spots, representing the mineralized matrix, were observed on oCS100 and oCS50 PEMs compared to the absence of this positive staining on nCS PEMs. Moreover, in the immune staining of Col I and Runx2 (Figure 9C), oCS100 and oCS50 PEMs were also superior to nCS PEMs at which more Col I and Runx2 staining existed on oCS100 and oCS50 PEMs, as visualized in the single channels of Col I (green) and Runx2 (red), while very faint staining is observed on nCS PEMs.

3. Discussion

3.1. Physical Studies on Multilayers Formation and Properties

The multilayers build-up was investigated by QCM-D, which provides information on the total adsorbed mass (containing water) and permits the study of the viscoelastic properties of the multilayers. In all PEMs, more deposition of Col I than of the polyanion was observed, which is probably related to the higher molecular weight of Col I. ΔD increased after addition of Col I followed by a decrease after addition of polyanion, indicating stiffening of PEM after CS adsorption. This is due to the diffusion of CS into the underlying layers of Col I leading to compaction and displacement of water. A similar effect was observed by others for heparin/poly(L-lysine) (PLL) and heparin/chitosan PEMs.[33,34] When an additional Col I layer is adsorbed and the system takes up water, the multilayers swell and become softer again.[35] The PEM assembly was performed at pH 4 at which Col I acquires a net positive charge since its isoelectric point is about 5.5[36] while CS is considered a polyanion with a pK_a value of 2.5.[37] Therefore, our assumption is that the formation of nCS PEMs was mainly depending on ion pairing[38] between positively charged Col I and negatively charged CS whereas in oCS PEMs an additional covalent pairing mechanism was involved, which is the imine bond formation between the aldehyde groups in oCS and the amino groups of Col I.[21] Therefore, in oCS50 PEMs, it is suggested that the polymer binding was mainly depending on the covalent pairing mechanism between oCS and Col I while most of other negatively charged groups on nCS and oCS are remaining free, causing electrostatic repulsion that leads to more swelling and attraction of water. The latter could be the reason behind the higher dissipation and viscoelastic thickness calculated for oCS50 PEMs. This was also proven when comparing the viscoelastic thickness to the dry thickness measured by ellipsometry. Here, oCS50 PEMs had a comparable dry thickness to oCS100 PEMs when water was excluded.

Surface properties of PEMs were studied with WCA and AFM measurements. This is related to the fact that both wetting properties and topography have an effect on cell adhesion and fate.[39] Biophysical cues such as topographical and mechanical features of ECM result in profound effects on cellular morphology and function, through mechanotransduction mechanisms.[40] Cells possess the ability to recognize and respond to the nano- and microscale organization of molecular signals in their ECM.[41] On nanostructured surfaces, cells tend to spread more on the smallest nanostructures accompanied by increased expression of FA while less spreading occurs on macrostructures.[39] Here in our study, the Col I fibers with the various densities and diameters represent both the chemical and topographical cues. The observed moderate wettability of all studied PEMs is favorable for cell adhesion.[42] While CS is known to be highly hydrophilic, Col I is more hydrophobic as a pure film (WCA ~ 110°).[43] Thus, the reason behind these WCA values could be the high mass contribution of Col I in all studied multilayers. A similar WCA was observed by Zhao et al. for CS-based PEMs compared to HA-based PEMs showing lower WCA for the latter due to lesser Col content.[21,22]

Col as ECM molecule plays an important role in cell adhesion, spreading, and differentiation.[44] The soft nature of oCS50 PEMs detected by QCM-D with higher dissipation was confirmed by AFM measurements, which revealed that oCS50 PEMs have the lowest elastic modulus. The intrinsic cross-linking of oCS100 PEMs together with the observed density and
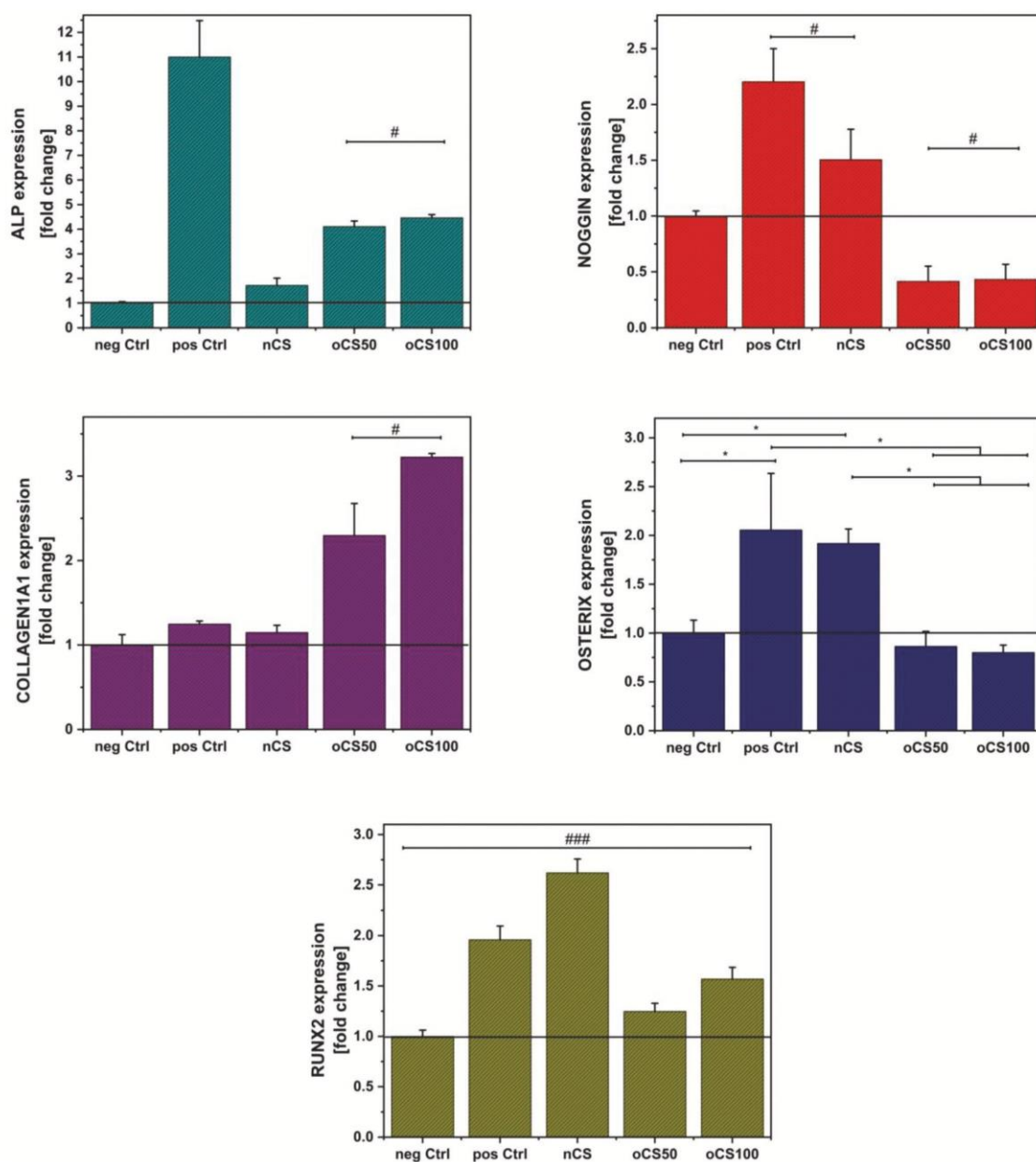
Figure 8. Relative expression of mRNA of osteogenic markers (ALP, Col I, Runx2, Osterix, and Nogging) after 14 days of C2C12 incubation on the various native and cross-linked multilaye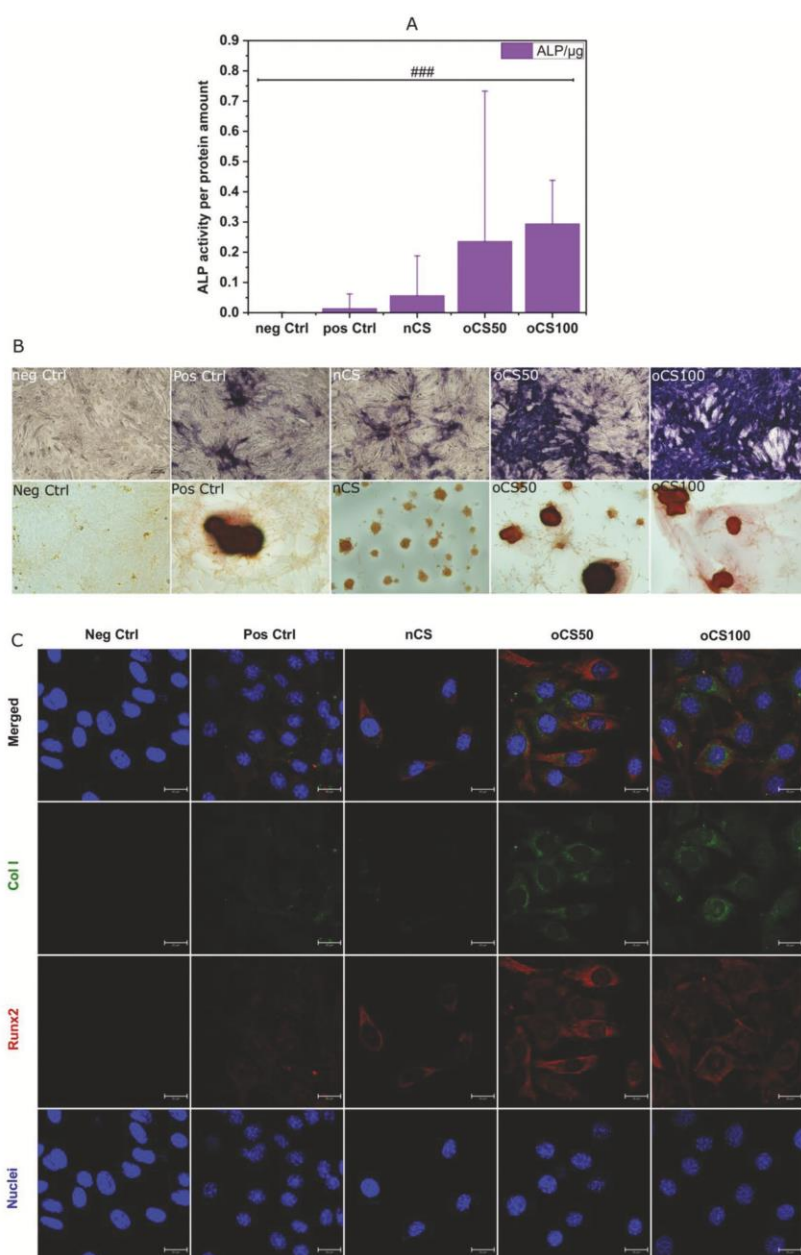rs. PEMs of oxidized chondroitin sulfate (oCS100), native chondroitin sulfate (nCS), or a mixture of both (oCS50) were prepared with Col I as polycation. qRT-PCR analyses were performed as described in the Experimental Section. Data represent mean ± SD values, $n = 6$, $p \leq 0.05$ and Scheffe post hoc test. (*) data are significantly different. (#) all data are significantly different except. (###) all data are significantly different.

thickness of Col I fibers contributed to its high elastic modulus and roughness compared to nCS PEMs. Further, Col I is self-assembling to form fibrils both in vivo and in vitro.[45] Col I

fibrillization results from two successive processes. One is happening during the lag period (nucleation) and the other occurring during the growth phase where nuclei grow into fibrils.[46]

　　　2201596 (10 of 17)

Figure 9. PEMs of oxidized chondroitin sulfate (oCS100), native chondroitin sulfate (nCS), or a mixture of both (oCS50) were prepared with Col I as polycation. A) Measurements of ALP activity in C2C12 cells seeded directly on top of BMP-2-loaded multilayers fabricated in 24-well plate, determined via absorbance measurements at 405 nm after 7 days' incubation time, using a plate reader. Measurements are normalized to the total protein amount (BCA values). ### indicates that all data are significantly different to each other. B) Bright-field images (10×) of C2C12 cells seeded on various native and cross-linked multilayers and stained after 7 days for ALP, and after 14 days with alizarin red-S solution to investigate the formation of mineralized matrix (scale bar: 100 µm). C) CLSM images show C2C12 cells after 14 days incubation on BMP-2-loaded multilayers. The cells were stained for Col I (green), Runx2 (red), and nucleus (blue). As a control, cells were seeded on plain glass slides either without (neg Ctrl) or with BMP-2 (pos Ctrl) in the medium. Cells were imaged with CLSM 63× oil immersion objective (scale bar: 20 µm).

Col I fibrillogenesis is affected by several factors such as ionic strength, pH, temperature, and the presence of GAGs.[47] It was found that a pH value less than 5.5 enhances the formation of globular Col I structures while a pH value above 5.5 promotes fibrillogenesis.[47,48] However, since the fibrillogenesis occurred in our study even at pH 4, CS seems to play a remarkable role in regulating this process through facilitating the organization of mature Col I fibrils by enhancing Col I concentration.[49] While nCS PEMs rely mainly on ion pairing, it has been suggested that strong electrostatic interaction between the used polyanion and Col I can produce a high number of nucleation sites, which in turn results in a long and retarded lag phase that results in fibers with smaller diameter.[50,51] On the other hand, in oCS50 PEMs, the electrostatic repulsion and steric hindrance resulting from the free charged groups in the mixture of nCS and oCS lead to less induction of nucleation making Col I more available. This higher availability of Col I permits then more lateral aggregation of it and shorter lag phase ending up with fibers of larger diameters.[51,50] Furthermore, the Col I fibrils were prone to either complete or partial dissolution after loading BMP-2, which is due to the acidic pH at which Col I has a net positive charge and is present in a soluble state.[36] However, oCS100 and oCS50 PEMs could save the fibrillar structure of Col I to a certain degree which could be related to the successful crosslinking of Col I in those PEMs. Further, this partial dissolution of Col I fibers led to a decrease in elastic modulus and roughness on all PEMs. One exception was the nCS PEMs, which showed an increase in elastic modulus after BMP-2 loading. We relate this to the function of the AFM cantilever, which interacts with the surface, hence, it could have given a false positive result after the dissolution of Col I fibers and started rather sensing the silicon substrate instead.

3.2. Biological Studies

BMP-2 was expected to be bound to CS in all multilayers via its heparin binding domain, at which positively charged amino acids bind to negatively charged groups on GAGs.[52] Indeed, intrinsic cross-linking of oCS PEMs not only increased sequestering of BMP-2 compared to nCS PEMs as visualized by antibody staining of bound BMP-2, but also resulted in lesser BMP-2 release over time. Since the release of BMP-2 was fitting to the Higuchi model,[30] the release seems to be depending on the cross-linking density related to the mechanism of binding. In nCS PEMs, the multilayers formation (at pH 4) is based on ion pairing[38] and the BMP-2 can be easily entrapped inside the multilayers. When the pH is increased to physiological value (pH 7.4), Col I will be less charged with reduction of ion pairing[38] which leads to faster release of BMP-2. The faster the release is, the more BMP-2 in a soluble state exists (similar to pos Ctrl). Hence, less matrix-bound BMP-2 remains in the multilayers to be presented to the cells, which led to less BMP-2 internalization in cells on nCS PEMs. Further, the imine bonds in oCS PEMs can be partly hydrolyzed at acidic pH permitting uptake of BMP-2 during loading (pH 4) while these bonds are formed and are more stable at neutral and basic pH.[53] Therefore, the loaded BMP-2 is entrapped when the imine bonds are formed. This resulted in the very little release of BMP-2 from

oCS100 PEMs and here it is worth pointing out that this very little release indicates that the majority of the loaded BMP-2 is still stored and available to cells in a matrix-bound manner, which is the effective way of GF presentation to the cells that is similar to what happens in the native ECM.[10] The availability of BMP-2 as matrix-bound in oCS100 PEMs allowed its presentation in a spatial/temporal manner to the cells at their ventral side which resulted in more BMP-2 internalization. However, it has been found that BMP-2 signaling can be independent of BMP-2 internalization where signaling can still take place at the plasma membrane even in the absence of BMP-2 internalization.[16,54] Moreover, the swelling and the aqueous nature of oCS50 PEMs indicated previously by AFM and QCM data, resulted in more diffusion of BMP-2 compared to oCS100 PEMs, i.e., more soluble BMP-2. This highlights the strong contribution of the intrinsic cross-linking in oCS100 PEMs in increasing the stability of the multilayers under physiological conditions,[21] and controlling BMP-2 release and presentation.[8]

Cell adhesion is considered as a prerequisite for a variety of cellular function including cell growth and differentiation.[55] C2C12 cells adhered generally on all nonloaded PEMs due to their moderate wettability, observed by WCA that is usually preferred by cells (WCA 40°–70°),[56] and the presence of Col I.[22] Moreover, Col I fibrils are known to promote the adhesion of a variety of cells via integrin-mediated interaction,[57] where $\alpha2\beta1$ is the main functioning integrin receptor for Col I fibrils.[58] Thus, on nonloaded PEMs, the thick Col I fibers present on oCS PEMs contributed to significant more cell spreading than on nCS PEMs, as shown by quantification of cell area. In addition, on BMP-2 nonloaded multilayers, cell attachment on control surfaces was the lowest which indicates that there is no intrinsic toxicity of multilayers particularly when using oxidized CS. Necrotic of apoptotic cells have a rather round shape[59] which was not seen there. Furthermore, more elongated cells and more cell spreading characterized by expression of longitudinal actin filaments and vinculin molecules in FA sites were observed on all BMP-2-loaded samples indicating a promoting effect of BMP-2 on cell adhesion.[54] A crosstalk between BMP-2 and integrin-dependent signaling pathways which promotes the formation of FA and stress fibers, was observed in other studies.[54] Additionally, the mechanical properties of the ECM or the substrata are strong modulators of cellular behavior.[60] On stiff surfaces, the cells exert stress by expansion of their FA and increase recruitment of vinculin.[61] This results in an extended and spread shape of cells together with alteration of stress fibers,[62] which goes on well with our findings regarding oCS100 PEMs (both loaded and nonloaded). Vinculin plays a role in strengthening adhesion by increasing the local membrane stiffness, modulating by that bond stressing in the contact area.[63] On the other hand, cell adhesion and spreading are suppressed on soft substrata because of suppressing signaling via integrins regarding mechanotransduction.[35] Since oCS50 PEMs are the softest and most water containing, less vinculin organization was observed compared to oCS100 and even nCS PEMs. Such effect of PEM stiffness on FA and actin organization of C2C12 cells was already shown previously by others using PLL/HA PEM and ethyl-3-(3-dimethylaminopropyl) carbodiimide (EDC) for cross-linking[15] which fits to our findings here. In this study, it was made clear that not only

the topography matters but also the stiffness and the molecular composition together affect the behavior of cells.

The bioactivity of PEMs including the effect of BMP-2 on osteogenic differentiation of C2C12 myoblasts was investigated by qRT-PCR via studying the expression of early osteogenic markers ALP and Col I.[64] These markers were highly upregulated in cells grown on both oCS PEMs compared to the ones on nCS PEMs and pos Ctrl. Ligation of collagen integrin receptors $\alpha 2\beta 1$ and $\beta 1$ integrins in general is required for ALP induction as it increases ALP mRNA triggered by BMP-2.[65] Hence, the presence of thick Col I fibers and the more cell adhesion and spreading could be the reason triggering more osteogenesis in cells grown on oCS100 and oCS50 PEMs compared to nCS PEMs. In addition, the ALP gene expression levels from the qRT-PCR were closely related to ALP staining and activity except for the positive control. The reason for the lack of ALP gene translation could be phosphorylation, proteolysis of core components of the translation machinery, or specific factors such as RNA-binding proteins and miRNA.[32] Moreover, it has been reported that the activity but not the expression of Runx2 is enhanced with osteoblast differentiation in some hMSCs,[66] which could, on one side, explain the reason behind the lower expression of Runx2 in cells grown on oCS PEMs compared to nCS PEMs and pos Ctrl. On the other side, post-transcriptional regulation by miRNAs may affect the expression of Runx2 and Osterix,[67] which could explain the lower level of Osterix expression in cells grown on oCS PEMs compared to nCS. Furthermore, Noggin is a specific antagonist of BMPs that was found to be expressed by osteoblasts to regulate the extracellular exposure to BMP as part of the negative feedback mechanism that prevents the interaction of BMP with its receptor. Therefore, achieving a balance between BMPs and Noggin plays a critical role in regulating osteogenesis.[31] On pos Ctrl and nCS PEMs, cells are exposed to high amounts of soluble BMP-2, triggering by that the expression of osteogenic gene markers together with high Noggin expression. By contrast, matrix-bound BMP-2 presented to cells from oCS PEMs triggered higher expression of osteogenic genes but reduced Noggin. Therefore, this balanced BMP-2/Noggin ratio in oCS PEMs is expected to enable complete osteogenesis in comparison to the unbalanced ratio in pos Ctrl. Osteoblasts start synthesizing their ECM which consists mainly of Col I followed by ALP production and later-stage ECM calcification occurs.[65] Hence, Col I expression and secretion is important for starting and increasing the mineralization process.[66,68] Referring back to the qRT-PCR data, Col I and ALP expression were highly upregulated in cells grown on oCS PEMs while it was almost like the neg Ctrl on nCS PEMs. Thus, more mineralization is expected to occur on oCS PEMs. The latter was proven when looking at Alizarin red staining of the mineralized matrix that was more pronounced in cells cultured on oCS than on nCS PEMs. The findings of qRT-PCR go well with the results detected from CLSM images of immune-staining where more Col I and Runx2 staining were detectable for cells on oCS compared to nCS PEMs and pos Ctrl. Altogether, this confirms that the osteogenic markers expressed in cells grown on oCS PEMs were efficiently translated into proteins and were accompanied with real osteoblast development while this was absent on nCS and pos Ctrl despite offering the soluble BMP-2 in larger amounts.

4. Conclusion and Outlook

The oCS PEMs with intrinsic cross-linking are superior to nCS PEMs in supporting cell adhesion, spreading, and triggering osteogenesis through storage and presentation of the loaded BMP-2 to the cells in a matrix-bound manner rather than releasing it in a soluble state. The intrinsic cross-linking supports the presence of an ECM-like microenvironment through enhancing the stiffness and stability of PEMs and preserving the structure of Col I fibers that represent an ECM-like topographical and chemical cue. The key to achieve the targeted cell differentiation is not only about the quantities of GF released but requires rather a combination between the availability of matrix-bound GF and a slow release profile. Moreover, the moderate releasing profile and the soft nature of oCS50 PEMs could allow their use for articular cartilage regeneration using the growth and differentiation factor-5 (GDF-5) that supports cell differentiation into chondrocytes. Overall, these multilayers with intrinsic cross-linking can be further used as coatings for implants to deliver GFs to the site of defects for bone regeneration application and other tissue defects.

5. Experimental Section

Materials: Cell culture flasks and polystyrene well-plates were purchased from Greiner Bio-one GmbH & Co.KG (Frickenhausen, Germany). Round glass (Ø12 mm) were purchased from VWR (Germany) and glass object holders were provided by Karl Hecht GmbH & Co (Sondheim, Germany). Glutaraldehyde was obtained from AppliChem (Darmstadt, Germany). Collagen I was obtained from Sichuan Mingrang Bio-Tech (Sichuan, China). Chondroitin sulfate (CS), PEI, Triton X-100, and sodium periodate (NaIO4) were provided by Sigma-Aldrich Chemie GmbH (Steinheim, Germany). Trypsin/ethylenediaminetetraacetic acid (EDTA) solution and fetal bovine serum (FBS) were provided by Biochrom (Berlin, Germany). Penicillin/ streptomycin (pen/strep) was from Lonza (Walkersville, MD, USA). Sodium chloride (NaCl), bovine serum albumin (BSA), 4-nitrophenylphosphate disodium salt hexahydrate (*p*-NPP), hydrogen peroxide 35% (H2O2), and alizarin red-S were provided by Carl Roth GmbH & Co. KG (Karlsruhe, Germany). Schiff's reagent was from Merck KGaA (Darmstadt, Germany). DMEM (phenol red) and paraformaldehyde 4% (PFA) were provided by Roth (Germany). Dialysis bags (Spectra/Por membrane, M_w cutoff = 3500) were provided by Spectrum Labs (CA, USA). 5-Brom-4-chlor-3-idolylphosphate-*p*-toluidinsalt (BCIP) was purchased from Roth, Germany. While, *p*-Nitro blue tetrazolium chloride (NBT) was purchased from Applichem, Germany. AMP buffer was provided by Roth, Germany. 2-phospho-L-ascorbic acid trisodium salt was from Sigma-Aldrich, Germany and β-glycerol phosphate was from Alfa Aesar, Germany. Mowiol was obtained from Calbiochem (Darmstadt, Germany).

Synthesis of oCS: Native CS (nCS) was used as a polyanion and as a native glycosaminoglycan (nGAG) in all experiments. According to previously published protocol, oxidized CS (oCS) was synthesized.[8] In short, to get 100% theoretical oxidation degree, 1 g of nCS (nCS $M_w \approx 75$ kDa) was dissolved in (200 mL) of ultrapure water and left to react with 0.5 g of NaIO4 for 3 h at room temperature (RT) under stirring and protection from light. Dialysis against distilled water using membrane of 3.5 kDa cut-off was used for 3 days at RT to purify the reacted CS and the final product was obtained by freeze-drying (ALPHA 1–2 LDplus, Christ, Osterode am Harz, Germany) and stored at 4 °C for further use. A photometric detection method known as "Schiff's test" was used, as described previously,[69] to quantify the aldehyde groups present in oCS. Oxidation degree of 2.77% was obtained for oCS.

Preparation of Substrata: Glass coverslips, silicon wafers, polystyrene well plates, and quartz chip Au were used when appropriate as substrate surface in the preparation of PEMs systems. Si wafers (Silicon Materials, Kaufering, Germany) with a size of 10×10 mm^2 were used for ellipsometry, while round glass coverslips (ø12 mm) were used as substrata for WCA and cell experiments. Both glass and silicon were cleaned using RCA-1 cleaning method which aimed to removing organic contaminants, thin oxide layer, and ionic contamination.[70] Quartz chip Au purchased from 3T Analytik (Germany) were used for QCM-D studies and were cleaned with 70% ethanol and ultrapure water and dried with a stream of nitrogen before use. Ethanol 70% was used for 15 min to sterile glass before the formation of multilayers.

Preparation of Solutions and Formation of PEMs: The multilayers were built up by dip coating method on the previously mentioned substrata which were selected appropriately depending on the experiment to be done. PEI was dissolved in 0.15 mol L^{-1} sodium chloride (NaCl) solution at a concentration of 2 mg mL^{-1}. Native chondroitin sulfate (nCS), oxidized chondroitin sulfate (oCS100), and oxidized/native chondroitin sulfate mixture (oCS50) were used as polyanions. oCS100 and nCS were dissolved in 0.15 mol L^{-1} NaCl solution at a concentration of 2 mg mL^{-1}. oCS50 solution was obtained by mixing oCS100 and nCS in a 1:1 ratio to get a mixture which contained 50% oCS and 50% nCS. Collagen I (Col I) was used as a polycation and was dissolved at a concentration of 2 mg mL^{-1} in a 0.15 mol L^{-1} NaCl solution containing 0.2 mol L^{-1} acetic acid and stirred at 4 °C overnight followed by centrifugation for 10 min at max speed to eliminate insoluble precipitates. A final working concentration of 0.5 mg mL^{-1} working solution was obtained by diluting the stock solution in 0.15 M sodium chloride and 0.2 mol L^{-1} acetic acid solution.[21] 0.15 mol L^{-1} NaCl was used as a washing solution. All polyelectrolytes were adjusted to pH 4 with exception to PEI with pH 7.4. A 0.2 µm pore size membrane filter (Whatman) was used to filter all polyelectrolytes and washing solution before use.

PEI was used as the first binding layer to obtain a net positive charge and was adsorbed for 30 min on the substrates. Then, for the various systems, alternating layers of polyanions (nCS, oCS100, or oCS50) and polycation (Col I) were used until reaching a total number of 17 layers with Col I being the terminating layer. Polyanions and polycation were alternatively incubated for 15 min followed by 2 × 4 min washing steps using 0.15 mol L^{-1} NaCl solution. All multilayers formation procedures were carried out at RT under gentle shaking (Heidolph, Polymax 1040, at 30 rpm).

Measurement of Multilayers Growth: The layer growth and multilayers formation were investigated via QCM-D monitoring, as previously described.[38] A qCell T temperature-controlled quartz crystal microbalance from 3T analytik (Tuttlingen, Germany) was used for QCM-D measurements. The principle of QCM-D was based on the sensitivity of the quartz sensor to the mass and properties of materials deposited on the surface. During the deposition of materials on the sensor or when an alternating voltage was applied, there was a change in resonant frequency and damping (dissipation). The change in frequency and damping was captured by the device in real-time.[71] Multilayers were built up in the QCM-D flow cell by injecting alternating polyanion/polycation solutions and this was monitored in real-time using quartz chip Au as the substrate surface. The change in frequency and evaluation of layer thickness were carried out using the qCell T device and qGraph software.

WCA Measurements: After the formation of multilayers on glass coverslips, they were stored in a desiccator before carrying out WCA measurements. The wettability properties of multilayer surfaces were determined by static WCA measurements using an OCA15+ device (Dataphysics, Filderstadt, Germany), as previously described.[72] The sessile drop method was implemented using five droplets of 3 µL ultrapure water for each sample. The software of OCA15+ device recorded for each droplet at least ten independent measurements. Measurements were fitted with the ellipse-fitting method and mean and standard deviations for all measurements were calculated.

Characterization of PEMs Dry Thickness: The thickness of PEMs built up on cleaned Si wafers was determined using an M-2000 V scanning ellipsometer (J.A Woollam Co. Inc., Lincoln, NE, USA) with an angle of incidence of 70°. The thickness of formed multilayers was determined by fitting the experimental data to an additional Cauchy layer and a refractive index of 1.36 was used to calculate layer thickness. Finally experimental data obtained were analyzed with the device' software (WVase32).

Measurement of PEMs Surface Topography and Elastic Modulus: Topographical imaging as well as measuring local elasticity of the multilayers (deposited on silicon substrates) was performed using AFM (nanowizard IV, JPK-Instruments, Berlin, Germany) in quantitative imaging mode (QI). Here, a silicon cantilever (FMR, Nanosensors) in a standard liquid cell (JPK-Instruments) containing 0.15 mol L^{-1} NaCl was employed. *JPK Data Processing V5.0.85* and (*Gwyddion V2.49*) software were used for postprocessing, calculation of elasticity, and analyzing roughness parameters. To measure the diameter of the Col I fibers present on the surface, the program *FSegment* was used.[73] While this program was originally developed for actin fiber detection, its line tracing algorithm was also successfully used to detect the Col I fibers found on top of the samples. All settings were kept equal for all samples. The program traced all fibers and measured the width of each fiber every 5 pixel (equals 48.5 nm). All measuring points per sample were then cumulated and analyzed.

Uploading of Recombinant Human Bone Morphogenetic Protein 2 (rhBMP-2) to Multilayers for Cell and Release Studies: After the formation of multilayers, rhBMP-2, produced in a heterologous host of *Escherichia coli (E. coli)* according to Hillger et al.,[74] was loaded onto the multilayers. A concentration of 10 µg mL^{-1} rhBMP-2 was used for all experiments and was obtained by diluting the stock solution (50 µg mL^{-1}) with 1 mmol HCl. 200 µL rhBMP-2 was added to each PEM sample and incubated at 4 °C overnight 1 day prior to cell seeding/enzyme-linked immunosorbent assay (ELISA) samples collecting. After incubation, rhBMP-2 was aspirated and layers were washed quickly with 0.15 mol L^{-1} NaCl solution pH 7.4. For positive controls in cell experiments, 10 µg mL^{-1} rhBMP-2 was added directly to the medium and the stock solution was diluted using DMEM cell culture medium instead of 1 mmol HCl.

BMP-2 Release Studies via ELISA: 10 µg mL^{-1} BMP-2 in 1 mmol HCl (50 µL each well) was loaded for overnight at 4 °C to the PEMs which were fabricated in a 96-well plate. Samples were collected over 7 days, each time followed by adding new fresh phosphate-buffered saline (PBS, pH 7.4). An ELISA kit from PeproTech (Hamburg, Germany) was used to check the released amounts of BMP-2. A series of BMP-2 concentrations was used to obtain a standard curve which was used later to calculate the released amounts from the PEMs according to the absorbance values measured at 405 nm.

BMP-2 Staining on Multilayers for Semiquantification: Multilayers were fabricated on glass cover slips and loaded with BMP-2 as mentioned previously. After loading, the samples were incubated in DMEM + 10% FBS (the same medium used for cell experiments) at 37 °C. After 24 h (the first set) and 7 days (the second set), samples were washed with PBS and fixation was done for 15 min using 4% PFA and further 1% BSA was used as a blocking agent with two washing steps with PBS in between. Then, the staining of BMP-2 was done using a primary BMP-2 mouse monoclonal antibody (1:50, Invitrogen) and a secondary CY2-conjugated goat anti-mouse antibody (1:100, Jackson Immuno Research Laboratory, Inc.) for 30 min incubation each, and 3×5 washing times with PBS after each staining step. The samples were then mounted on cover slips with Mowiol (Calbiochem, Darmstadt, Germany) and placed on an object holder. After storage for overnight at 4 °C, samples were visualized with a CLSM (LSM 710, Carl Zeiss, Oberkochen, Germany). The samples were fixed completely flat on the sample holder of the CLSM. Pictures were taken using a 20× objective, open pinhole, and low laser energy to avoid bleaching and gather as much signal as possible. For each measurement, an area of 2125×2125 µm was evaluated by using the tiles add-in of Zen 2008 to take a matrix of 5 × 5 individual pictures. The focus was set where the highest mean intensity was reached. Under- or overexposure was avoided carefully. All settings were kept constant during measurements. Finally, the mean intensity of the 8 bit image was extracted by ImageJ 1.53c.

C2C12 (Mouse Myoblast Cell Line) Cell Culture: Cryopreserved C2C12 cells were thawed in a water bath at 37 °C and cultured in DMEM (phenol red) supplied with 10% FBS and 1% penicillin/streptomycin (pen/strep) in a F75 culture flask and incubated in a humidified 5% CO_2/95% air atmosphere in a NUAIRE DH autoflow air-jacketed incubator (NuAire Corp., Plymouth, USA). When cells were about 80% confluence, cells were washed with PBS pH 7.4 and detached from the flask using 0.25% trypsin/EDTA for 3 min at 37 °C, then trypsin action was blocked using DMEM medium containing 10% FBS + 1% pen/strep. Cells were collected in a 15 mL falcon tube and centrifuged at 250 g for 5 min, the supernatant was collected and pellet was re-suspended in 1 mL (DMEM + 10% FBS + 1% pen/strep). A 1:100 dilution was made and cells were counted using the Neubauer counting chamber and seeded as needed.

C2C12 Cell Adhesion Studies: C2C12 cells were seeded on the various PEM made on glass cover slips and loaded with BMP-2 as mentioned previously. Two sets of samples were used here; BMP-2-loaded ones and non-BMP-2-loaded ones using positive and negative controls samples as defined above. The density of C2C12 used for each samples was 50 000 cells mL^{-1} in DMEM medium supplemented with 10% FBS. After incubating for 24 h at 37 °C, the same fixation, permeabilization, and blocking steps mentioned above, were employed. For the immune staining, cells were stained with ToPro3 (1:500, Invitrogen) for nucleus, Bodipy-Phalloidin (1:50, Invitrogen) for actin filaments and a primary mouse antibody against vinculin (1:50, Santa Cruz Biotechnology) which was followed by incubation with a CY2-conjugated goat anti-mouse antibody (1:100, Jackson Immuno research Laboratory, Inc.). Samples were incubated with each staining agent/antibody for 30 min in the dark at RT. After each staining step, 3 × 5 min rinsing steps with PBS were performed. Samples were mounted on cover slips with Mowiol as described before. Images were visualized using CLSM with 10x, 20x, and 63x oil immersion objective lenses. Images were analyzed with ZEN 2011 software (Carl Zeiss) and later with ImageJ (1.53c) for cell count and area. For actin length quantification, at least 15 pictures per condition were taken. Contrast of pictures was enhanced with the "Enhance Contrast" function of ImageJ 1.53c. Additionally, all cells touching the image borders as well as dead cell fragments were removed from each picture manually with ImageJ. Afterward, the program filament sensor 0.1.7 developed by Eltzner et al.[75] was used to detect the actin fibers automatically. The settings were kept the same for all samples of the experiment.

The detection of FA was carried out with a custom cell profiler pipeline using Cell Profiler 2.2. The individual cells were segmented with the help of TwoPro3 staining, which was associated with the nuclei and phalloidin staining, which was used to quantify the cytoplasm area. This was done by an automatic thresholding of both areas, a subsequent deduction of the nucleus area from the cytoplasm area, and a parent–child association of the cytoplasm of each cell. FA plaques were made visible by a primary vinculin antibody and subsequent cy2 secondary antibody. To increase the contrast, an enhance feature texture function was used and the FA plaques were detected by thresholding in the individual cell cytoplasm areas. All settings were kept constant over all samples.

BMP-2 Internalization: Multilayers were fabricated on glass cover slips and loaded with BMP-2 as mentioned previously. After overnight incubation, BMP-2 was aspirated and PEMs were washed quickly with NaCl pH 7.4. C2C12 cells were seeded on the various multilayers at a density of 50 000 cells mL^{-1} in (DMEM + 10% FBS) for 24 h at 37 °C. Positive and negative controls were cells seeded directly on glass, with adding the 10 µg mL^{-1} BMP-2 directly to the medium and without adding any BMP-2, respectively. After 24 h, the medium was removed and cells were washed quickly with PBS followed by a fixation step using PFA 4% for 15 min. After that, the samples were divided into two sets: permeabilized and nonpermeabilized. The cell permeabilization was performed using 0.1% triton for 10 min. Thereafter, 1% BSA solution was used as blocking agent for both sets of samples for 1 h. Two washing times using PBS were employed after each step. Afterward, incubation with each antibody for 30 min took place, starting with a primary BMP-2 mouse monoclonal antibody (1:50, Invitrogen), a secondary CY2-conjugated goat anti-mouse antibody (1:100, Jackson Immuno

Research Laboratory, Inc.), Bodipy-Phalloidin (1:50, Invitrogen) for actin filaments and ToPro3 (1:1000, Invitrogen) for the nucleus staining. 3×5 washing times with PBS after each incubation step was performed. Stained samples were mounted on cover slips with Mowiol and placed on an object holder and stored at 4 °C for the next day. Using a CLSM, samples were visualized with 63x oil immersion objective lens. Images were processed with the ZEN 2011 software (Carl Zeiss).

Osteogenic Cell Differentiation Studies: ALP Assay: C2C12 cells were seeded at a density of 50 000 cells mL^{-1} in (DMEM + 10% FBS + 1% Pen/strep) on PEMs fabricated directly in a 24-well plate and loaded with BMP-2 as mentioned before. Positive/negative controls were cells seeded directly on well plate with and without BMP-2 addition, respectively, as mentioned previously. After 7 days of incubation, cells were washed with PBS and cell lysis was performed using 1% Triton X-100 for 30 min under slow shaking. Afterward, 1 mg mL^{-1} *p*-NPP was incubated with 50 µL of cell lysate in a 96-well plate for 30 min at 37 °C and the absorbance was measured using a plate reader (FLUOstar OPTIMA, BMG LABTECH) at 405 nm wavelength. The alkaline phosphatase values were normalized to the total protein content that was measured using a Pierce BCA Protein Assay Kit from Thermo scientific (Rockford, IL, USA).

ALP Staining: The same cell seeding procedure used for ALP assay was used here. After 7 days of incubation, cells were washed with PBS and fixed using 2.5% glutaraldehyde solution for 10 min followed by a washing step with AMP buffer. ALP staining mixture included: 25 mg mL^{-1} NBT and 25 mg mL^{-1} BCIP that were prepared in 70% and 100% dimethylformamide, respectively. For every 5 mL AMP buffer, 33 µL NBT and 16 µL BCIP were added to form the ALP staining reagents mixture. After fixation, cells were incubated with the staining reagents mixture in the dark for 1 h at RT. The reaction was then stopped with $20 × 10^{-3}$ M EDTA and images were taken using a bright-field NIKON microscope 10x lens and analyzed using NIS element imaging software version 5.10.00.

Alizarin Red Staining: Alizarin red staining was done to determine the deposition of mineralized matrix after 14 days following the same cell seeding procedure and BMP-2 loading, on PEMs made on glass. 1 g of alizarin red was dissolved in 50 mL ultrapure water and pH was adjusted to 4.1–4.3 with 0.5% NH3 and filtered before use. Cells were rinsed once with PBS and fixed with 4% PFA for 15 min then rinsed twice with water. 1 mL of alizarin red was used to stain the fixed cells and incubated in the dark for 45 min at RT. After the incubation period, the stained cells were rinsed twice with ultrapure water and 1 mL PBS was added. Bright-field images were taken using NIKON microscope with 10x lens and analyzed with NIS element imaging software version 5.10.00.

Immune Staining for Osteogenic Differentiation: PEMs made on glass were loaded with BMP-2 and C2C12 cells were seeded, fixed, permeabilized, blocked, and immune-stained as mentioned in the cell adhesion studies paragraph. For osteogenic differentiation, cells were incubated for 14 days and were stained with ToPro3 for the nucleus, a primary mouse antibody against collagen I (Col I A2) (1:50, Santa Cruz) followed by a CY2-conjugated goat anti-mouse antibody (1:100, Jackson Immuno research Laboratory, Inc.) and a primary rabbit antibody against Runx-related transcription factor 2 (Runx2) (1:50, Biorbyt) followed by a CY3-conjugated goat anti-rabbit antibody (1:100, Jackson Immuno research Laboratory, Inc.). Images were visualized using CLSM with 63x oil immersion objective lens and later were analyzed with ZEN 2011 software (Carl Zeiss).

Extraction of RNA and qRT-PCR: C2C12 cells were seeded at a density of 50 000 cell mL^{-1} on the various multilayers surfaces that were fabricated in a 24-well plate. After incubation of cells in DMEM medium supplemented with 2% FBS and 1% Pen/Strep for 14 days, RNA was extracted from the cultured C2C12 cells according to the manufacturer's protocol using the Aurum Total RNA Mini Kit from BioRad (Hercules, CA, USA). The first strand of cDNA was synthesized in 20 µL reactions using an iScript Advanced cDNA Synthesis Kit for RT-qPCR according to manufacturer's procedure (Biorad, Hercules, CA, USA). Quantitative Real-Time PCR was carried out under standard enzyme and cycling state on a CFX Connect Real-Time PCR Detection system (Biorad, Hercules, CA, USA). Primer sets were confirmed by PrimePCR Probe Assays for the transcription factors (ALP, COL1A1, Runx2, SP7, and Nog), mentioned in **Table 1**. RPLP0 housekeeping gene was used in this analysis. Data were

ADVANCED SCIENCE NEWS
www.advancedsciencenews.com

ADVANCED MATERIALS INTERFACES
www.advmatinterfaces.de

Table 1. Primers of osteogenic transcription factors and housekeeping gene used for qRT-PCR.

Symbol	Transcription factor/Name	Assay ID
ALP	Alkaline phosphatase	qMmuCIP0028321
COL1A1	Collagen type 1 alpha 1	qMmuCEP0052648
Runx2	Run-related transcription factor 2	qMmuCEP0057696
SP7	Osterix	qMmuCEP0042201
Nog	Noggin	qMmuCEP0058332
Housekeeping gene RPLP0	60S acidic ribosomal protein P0	qMmuCEP0042968

analyzed using the BioRad CFX Manager Software 3.0 (Hercules, CA, USA). qRT-PCR was carried out under the following conditions: 95 °C for 30 s, then 39 cycles at 95 °C for 15 s and 60 °C for 30 s. The relative gene expression levels were calculated and normalized to the housekeeping gene RPLP0 by the DDCt method ($2-\Delta\Delta Ct$).

Statistics: Statistical calculations were carried out with Origin 8 software. Mean, standard deviation, analysis of significance (analysis of variance (ANOVA)), Kruskal–Wallis, and Dunn post hoc were calculated and described in the respective figures. A value of $p \leq 0.05$ was considered to be significantly different and was indicated by (*). On the other hand, (#) was used to indicate that all data were significantly different except the indicated ones. (###) meant that all data were significantly different to each other. Further, box-whisker diagrams were shown where appropriate. The box indicated the 25th and 75th percentiles, the median (line), and the mean value (square).

Supporting Information

Supporting Information is available from the Wiley Online Library or from the author.

Conflict of Interest

The authors declare no conflict of interest.

Data Availability Statement

The data that support the findings of this study are available in the supplementary material of this article.

[1] A. Mansour, M. A. Mezour, Z. Badran, F. Tamimi, *Tissue Eng., Part A* **2017**, *23*, 1436.
[2] A. Khojasteh, H. Behnia, N. Naghdi, M. Esmaeelinejad, Z. Alikhassy, M. Stevens, *Oral Surg., Oral Med., Oral Pathol. Oral Radiol.* **2013**, *116*, e405.
[3] B. D. Ratner, A. S. Hoffman, F. J. Schoen, J. E. Lemons, *MRS Bull.* **2006**, *31*, 59.
[4] R. O. Hynes, *Science* **2009**, *326*, 1216.
[5] C. Frantz, K. M. Stewart, V. M. Weaver, *J. Cell Sci.* **2010**, *123*, 4195.
[6] A. D. Theocharis, S. S. Skandalis, C. Gialeli, N. K. Karamanos, *Adv. Drug Delivery Rev.* **2016**, *97*, 4.
[7] A. Köwitsch, G. Zhou, T. Groth, *J. Tissue Eng. Regener. Med.* **2018**, *12*, e23.
[8] R. Anouz, A. Repanas, E. Schwarz, T. Groth, *Macromol. Biosci.* **2018**, *18*, 1800283.
[9] T. Katagiri, A. Yamaguchi, M. Komaki, E. Abe, N. Takahashi, T. Ikeda, V. Rosen, J. M. Wozney, A. Fujisawa-Sehara, T. Suda, *J. Cell Biol.* **1994**, *127*, 1755.
[10] R. Anouz, T. Groth, in *Soft Matter for Biomedical Applications* (Eds: H. S. Azevedo, J. F. Mano, J. Borges), Royal Society of Chemistry, London **2021**, pp. 326.
[11] M. S. Niepel, D. Peschel, X. Sisquella, J. A. Planell, T. Groth, *Biomaterials* **2009**, *30*, 4939.
[12] K. Kirchhof, A. Andar, H. Yin, N. Gadegaard, M. Riehle, T. Groth, *Lab Chip* **2011**, *11*, 3326.
[13] J. Borges, J. F. Mano, *Chem. Rev.* **2014**, *114*, 8883.
[14] C. Monge, J. Almodóvar, T. Boudou, C. Picart, *Adv. Healthcare Mater.* **2015**, *4*, 811.
[15] K. Ren, T. Crouzier, C. Roy, C. Picart, *Adv. Funct. Mater.* **2008**, *18*, 1378.
[16] F. Gilde, L. Fourel, R. Guillot, I. Pignot-Paintrand, T. Okada, V. Fitzpatrick, T. Boudou, C. Albiges-Rizo, C. Picart, *Acta Biomater.* **2016**, *46*, 55.
[17] G. Apte, A. Repanas, C. Willems, A. Mujtaba, C. E. Schmelzer, A. Raichur, F. Syrowatka, T. Groth, *Macromol. Biosci.* **2019**, *19*, 1900181.
[18] G. V. Martins, E. G. Merino, J. F. Mano, N. M. Alves, *Macromol. Biosci.* **2010**, *10*, 1444.
[19] S. Ber, G. T. Köse, V. Hasırcı, *Biomaterials* **2005**, *26*, 1977.
[20] Y. Yang, A. Köwitsch, K. Ma, K. Mäder, I. Pashkuleva, R. L. Reis, T. Groth, *J. Bioact. Compat. Polym.* **2016**, *31*, 191.
[21] M. Zhao, L. Li, C. Zhou, F. Heyroth, B. Fuhrmann, K. Maeder, T. Groth, *Biomacromolecules* **2014**, *15*, 4272.
[22] M. Zhao, G. Altankov, U. Grabiec, M. Bennett, M. Salmeron-Sanchez, F. Dehghani, T. Groth, *Acta Biomater.* **2016**, *41*, 86.
[23] A. D. Theocharis, D. Manou, N. K. Karamanos, *FEBS J.* **2019**, *286*, 2830.
[24] J. Bonor, E. L. Adams, B. Bragdon, O. Moseychuk, K. J. Czymmek, A. Nohe, *J. Cell. Physiol.* **2012**, *227*, 2880.
[25] T. Crouzier, K. Ren, C. Nicolas, C. Roy, C. Picart, *Small* **2009**, *5*, 598.
[26] J. A. Phillippi, E. Miller, L. Weiss, J. Huard, A. Waggoner, P. Campbell, *Stem Cells* **2008**, *26*, 127.
[27] N. M. Alves, C. Picart, J. F. Mano, *Macromol. Biosci.* **2009**, *9*, 776.
[28] A. Weltrowski, M. L. da Silva Almeida, D. Peschel, K. Zhang, S. Fischer, T. Groth, *Macromol. Biosci.* **2012**, *12*, 740.
[29] T. Crouzier, L. Fourel, T. Boudou, C. Albigès-Rizo, C. Picart, *Adv. Mater.* **2011**, *23*, H111.
[30] S. Dash, P. N. Murthy, L. Nath, P. Chowdhury, *Acta Pol. Pharm.* **2010**, *67*, 217.
[31] J. Fan, H. Park, S. Tan, M. Lee, *PLoS One* **2013**, *8*, e72474.
[32] R. de Sousa Abreu, L. O. Penalva, E. M. Marcotte, C. Vogel, *Mol. BioSyst.* **2009**, *5*, 1512.
[33] T. Crouzier, C. Picart, *Biomacromolecules* **2009**, *10*, 433.

[34] M. Lundin, F. Solaqa, E. Thormann, L. Macakova, E. Blomberg, *Langmuir* **2011**, *27*, 7537.

[35] N. Aggarwal, N. Altgärde, S. Svedhem, G. Michanetzis, Y. Missirlis, T. Groth, *Macromol. Biosci.* **2013**, *13*, 1327.

[36] N. Barbani, L. Lazzeri, C. Cristallini, M. G. Cascone, G. Polacco, G. Pizzirani, *J. Appl. Polym. Sci.* **1999**, *72*, 971.

[37] K. E. Kuettner, A. Lindenbaum, *Biochim. Biophys. Acta* **1965**, *101*, 223.

[38] N. Aggarwal, N. Altgärde, S. Svedhem, K. Zhang, S. Fischer, T. Groth, *Langmuir* **2013**, *29*, 13853.

[39] B. K. Ekambaram, M. S. Niepel, B. Fuhrmann, G. Schmidt, T. Groth, *ACS Biomater. Sci. Eng.* **2018**, *4*, 1820.

[40] a) G. Chu, Z. Yuan, C. Zhu, P. Zhou, H. Wang, W. Zhang, Y. Cai, X. Zhu, H. Yang, B. Li, *Acta Biomater.* **2019**, *92*, 254; b) M. Aragona, T. Panciera, A. Manfrin, S. Giulitti, F. Michelin, N. Elvassore, S. Dupont, S. Piccolo, *Cell* **2013**, *154*, 1047; c) Y. Xia, X. Fan, H. Yang, L. Li, C. He, C. Cheng, R. Haag, *Small* **2020**, *16*, 2003010.

[41] N. M. Alves, I. Pashkuleva, R. L. Reis, J. F. Mano, *Small* **2010**, *6*, 2208.

[42] J. H. Lee, G. Khang, J. W. Lee, H. B. Lee, *J. Colloid Interface Sci.* **1998**, *205*, 323.

[43] F. Taraballi, S. Zanini, C. Lupo, S. Panseri, C. Cunha, C. Riccardi, M. Marcacci, M. Campione, L. Cipolla, *J. Colloid Interface Sci.* **2013**, *394*, 590.

[44] E. Gurdak, P. G. Rouxhet, C. C. Dupont-Gillain, *Colloids Surf., B* **2006**, *52*, 76.

[45] Z. Keresztes, P. Rouxhet, C. Remacle, C. Dupont-Gillain, *J. Biomed. Mater Res., Part A* **2006**, *76*, 223.

[46] G. Wood, *Biochem. J.* **1960**, *75*, 605.

[47] M. Raspanti, M. Viola, M. Sonaggere, M. E. Tira, R. Tenni, *Biomacromolecules* **2007**, *8*, 2087.

[48] F. Gobeaux, G. Mosser, A. Anglo, P. Panine, P. Davidson, M.-M. Giraud-Guille, E. Belamie, *J. Mol. Biol.* **2008**, *376*, 1509.

[49] A. J. Kvist, A. E. Johnson, M. Mörgelin, E. Gustafsson, E. Bengtsson, K. Lindblom, R. Aszodi, R. Fässler, T. Sasaki, R. Timpl, *J. Biol. Chem.* **2006**, *281*, 33127.

[50] D. Stamov, M. Grimmer, K. Salchert, T. Pompe, C. Werner, *Biomaterials* **2008**, *29*, 1.

[51] D. A. Parry, M. H. Flint, G. C. Gillard, A. S. Craig, *FEBS Lett.* **1982**, *149*, 1.

[52] E. M. Munoz, R. J. Linhardt, *Arterioscler., Thromb., Vasc. Biol.* **2004**, *24*, 1549.

[53] Y. Tao, S. Liu, Y. Zhang, Z. Chi, J. Xu, *Polym. Chem.* **2018**, *9*, 878.

[54] E. Migliorini, A. Valat, C. Picart, E. A. Cavalcanti-Adam, *Cytokine Growth Factor Rev.* **2016**, *27*, 43.

[55] T. Groth, Z.-M. Liu, M. Niepel, D. Peschel, K. Kirchhof, G. Altankov, N. Faucheux, in *Advances in Regenerative Medicine: Role of Nanotechnology, and Engineering Principles* (Eds: V. P. Shastri, G. Altankov, A. Lendlein), Springer, New York **2010**, pp. 253–284.

[56] Y. Arima, H. Iwata, *Biomaterials* **2007**, *28*, 3074.

[57] N. M. Coelho, C. González-García, J. Planell, M. Salmerón-Sánchez, G. Altankov, *Eur. Cells Mater.* **2010**, *19*, 262.

[58] J. Jokinen, E. Dadu, P. Nykvist, J. Käpylä, D. J. White, J. Ivaska, P. Vehviläinen, H. Reunanen, H. Larjava, L. Häkkinen, *J. Biol. Chem.* **2004**, *279*, 31956.

[59] W. Lieberthal, V. Triaca, J. Levine, *Am. J. Physiol.: Renal Physiol.* **1996**, *270*, F700.

[60] M. S. Niepel, B. K. Ekambaram, C. E. Schmelzer, T. Groth, *Nanoscale* **2019**, *11*, 2878.

[61] W. H. Ziegler, R. C. Liddington, D. R. Critchley, *Trends Cell Biol.* **2006**, *16*, 453.

[62] J. Blacklock, A. Vetter, A. Lankenau, D. Oupický, H. Möhwald, *Biomaterials* **2010**, *31*, 7167.

[63] D. W. Dumbauld, H. Shin, N. D. Gallant, K. E. Michael, H. Radhakrishna, A. J. García, *J. Cell. Physiol.* **2010**, *223*, 746.

[64] P. J. Marie, O. Fromigué, *Regener. Med.* **2006**, *1*, 539.

[65] A. Jikko, S. E. Harris, D. Chen, D. L. Mendrick, C. H. Damsky, *J. Bone Miner. Res.* **1999**, *14*, 1075.

[66] R. Marom, I. Shur, R. Solomon, D. Benayahu, *J. Cell. Physiol.* **2005**, *202*, 41.

[67] M. T. Valenti, L. Dalle Carbonare, M. Mottes, *Int. J. Mol. Sci.* **2017**, *18*, 41.

[68] A. M. Ferreira, P. Gentile, V. Chiono, G. Ciardelli, *Acta Biomater.* **2012**, *8*, 3191.

[69] M. Muhammad, C. Willems, J. Rodríguez-Fernández, G. Gallego-Ferrer, T. Groth, *Biomolecules* **2020**, *10*, 1185.

[70] W. Kern, *J. Electrochem. Soc.* **1990**, *137*, 1887.

[71] D. Kömpf, J. Held, S. F. Müller, H. R. Drechsel, S. C. Tschan, H. Northoff, B. Mordmüller, F. K. Gehring, *Malar. J.* **2016**, *15*, 317.

[72] A. Köwitsch, Y. Yang, N. Ma, J. Kuntsche, K. Mäder, T. Groth, *Biotechnol. Appl. Biochem.* **2011**, *58*, 376.

[73] H. Rogge, N. Artelt, N. Endlich, K. Endlich, *J. Microsc.* **2017**, *268*, 129.

[74] F. Hillger, G. Herr, R. Rudolph, E. Schwarz, *J. Biol. Chem.* **2005**, *280*, 14974.

[75] B. Eltzner, C. Wollnik, C. Gottschlich, S. Huckemann, F. Rehfeldt, *PLoS One* **2015**, *10*, e0126346.

Chapter 4

Summary - Effect of microenvironment on adhesion and differentiation of murine
C3H10T1/2 cells cultured on multilayers containing collagen I and glycosaminoglycans:

Since the interactions of C3H10T1/2 cells with polyelectrolyte multilayers have not been studied yet, this study offered a chance to explore that and to test if those cells could be used instead of mesenchymal stem cells for further studies. This study was not focused on growth factors release and presentation but was rather dedicated to comparing the effect of the multilayers' composition only (native *versus* oxidized) on C3H10T1/2 cells in the presence of either basal (BM), osteogenic (OM) or chondrogenic (CM) medium. The native glycosaminoglycans (GAGs) chondroitin sulfate (CS), hyaluronic acid (HA) and their oxidized versions were combined with collagen I (Col I) to fabricate the various native and intrinsically cross-linked (oxidized) GAGs multilayers. The physiochemical characterization of the multilayers showed that the intrinsically cross-linked GAGs multilayers had more mass adsorption during the multilayer formation process compared to the native ones. Further, the oxidized GAGs multilayers had stiffer surfaces compared to the natives which exhibited softer surfaces with a higher water content. The ability of multilayers to promote the natural Col I fibrilization was studied *via* Labelling the Col I *in situ* with FITC, which concluded that CS-based multilayers (both native and oxidized) promoted longer Col I fibers compared to HA-based multilayers that had short fibrils and aggregates. Testing the direct interaction of C3H10T1/2 cells with the multilayers was achieved by culturing the cells on the multilayers in the absence of serum to prevent any interaction with other proteins. In that regard, cells seeded on CS-based multilayers were larger and more spread and elongated compared to cells on HA-based multilayers. Moreover, the differentiation studies concluded that; in the presence of BM, the differentiation of C3H10T1/2 cells was completely relying on the molecular composition of multilayers at which osteogenesis was more triggered on CS-based multilayers while chondrogenesis was more enhanced on HA-based ones. Thus, the type of GAG can be used for controlling the lineage specification of cells. OM and CM had inhibitory effects on C3H10T1/2 cells in term of differentiation towards osteogenesis and chondrogenesis, respectively. The OM and the soluble BMP-2 (100 ng mL^{-1}) showed significant induction effect on cells towards adipogenesis, especially on oxidized GAGs multilayers. Therefore, the choice of cell model is as important as controlling the matrix composition.

Original Article

Effect of microenvironment on adhesion and differentiation of murine C3H10T1/2 cells cultured on multilayers containing collagen I and glycosaminoglycans

Mingyan Zhao[1] (ID)**, Reema Anouz**[2] **and Thomas Groth**[2,3,4]

Abstract

Polyelectrolyte multilayer coating is a promising tool to control cellular behavior. Murine C3H10T1/2 embryonic fibroblasts share many features with mesenchymal stem cells, which are good candidates for use in regenerative medicine. However, the interactions of C3H10T1/2 cells with polyelectrolyte multilayers have not been studied yet. Hence, the effect of molecular composition of biomimetic multilayers, by pairing collagen I (Col I) with either hyaluronic acid or chondroitin sulfate, based primarily on ion pairing and on additional intrinsic cross-linking was studied regarding the adhesion and differentiation of C3H10T1/2 cells. It was found that the adhesion and osteogenic differentiation of C3H10T1/2 cells were more pronounced on chondroitin sulfate-based multilayers when cultured in the absence of osteogenic supplements, which corresponded to the significant larger amounts of Col I fibrils in these multilayers. By contrast, the staining of cartilage-specific matrixes was more intensive when cells were cultured on hyaluronic acid-based multilayers. Moreover, it is of note that a limited osteogenic and chondrogenic differentiation were detected when cells were cultured in osteogenic or chondrogenic medium. Specifically, cells were largely differentiated into an adipogenic lineage when cultured in osteogenic medium or $100\,\text{ng}\,\text{mL}^{-1}$ bone morphogenic protein 2, and it was more evident on the oxidized glycosaminoglycans-based multilayers, which corresponded also to the higher stiffness of cross-linked multilayers. Overall, polyelectrolyte multilayer composition and stiffness can be used to direct cell–matrix interactions, and hence the fate of C3H10T1/2 cells. However, these cells have a higher adipogenic potential than osteogenic or chondrogenic potential.

Introduction

In vivo, cells reside in an extracellular matrix (ECM)-based microenvironment consisting of fibril-forming proteins, such as collagens, laminin, and fibronectin,[1] making the insoluble protein component of the ECM and polysaccharide-based on glycosaminoglycans (GAGs) in particular hyaluronan and proteoglycans, which contain other GAGs such as chondroitin sulfate (CS), heparan sulfate, and others.[2] In addition, various cytokines as soluble protein components are contained in the ECM or bound to the cell surface by support from sulfated GAGs.[3] The ECM proteins can interact with cells via integrin

[1]Stem Cell Research and Cellular Therapy Center, Affiliated Hospital of Guangdong Medical University, Zhanjiang, China
[2]Department Biomedical Materials, Institute of Pharmacy, Martin Luther University Halle Wittenberg, Halle (Saale), Germany
[3]Laboratory of Biomedical Nanotechnologies, Institute of Bionic Technologies and Engineering, I.M. Sechenov First Moscow State University, Moscow, Russian Federation
[4]Interdisciplinary Center of Materials Research, Martin Luther University Halle Wittenberg, Halle (Saale), Germany

Corresponding author:
Mingyan Zhao, Stem Cell Research and Cellular Therapy Center, Affiliated Hospital of Guangdong Medical University, Zhanjiang 524001, China.
Email: mingyan.zhao@gdmu.edu.cn

adhesion receptors,[4] which are involved in cell signaling transduction, and thus influencing cell adhesion, growth, and differentiation.[5] Moreover, interaction of proteoglycans having GAGs side-chains of heparin and CS, but also fibronectin with growth factors (GFs) including bone morphogenic proteins (BMPs) provides the basis for GF-related signal transduction processes, too.[2,6] Hence, the ECM acts not only as a structural support of cells, but provides chemical and mechanical cues involved in the regulation of cellular responses.[6,7]

Biomaterials for use as scaffolds in tissue engineering should meet important characteristics, such as bioactivity and biodegradability. Many synthetic materials such as polylactic or polyglycolic acids have been widely used because of their good mechanical properties, low cost, and biodegradability.[8] However, those synthetic materials have poor bioactive properties, because they lack the necessary cues to guide cellular behavior in a desired manner.[9] Furthermore, the bio-integration, which is the interaction between an implant and the host tissue, occurs always at the interface or surface of the implant materials.[10] Therefore, despite the importance of bulk properties of a biomaterial, the surface properties arise to play a critical role in the process.[11] Hence, several physiochemical surface modification methods have been established to alter the surface properties of biomaterials in a desired manner. While physical and chemical treatments of implant materials often modulate biocompatibility to improve engrafting or reduce adverse effects, biomimetic modifications aim at reestablishing an ECM-like microenvironment for tissue cells[12] to resemble the mechanical and chemical cues required to control cell behavior and tissue regeneration.[13]

Among a variety of methods for surface modification, layer-by-layer (LbL) assembly of polyelectrolytes has emerged as a very simple, cost-efficient, and versatile strategy in fabricating biogenic thin films and for the immobilization of bioactive molecules such as growth factors on biomaterial surfaces.[14–16] Matrix components such as fibrillar glycoproteins (e.g. collagens, fibronectins, laminins) and GAGs such as CS, heparin, and HA have gained an increasing interest for making of bioactive surface coatings and three-dimensional (3D) systems,[15,17,18] implementing that as a step toward mimicking the native ECM. However, some of these polysaccharide and protein-based multilayer systems have been found to be relatively unstable under physiological conditions[19] that may require subsequent or concurrent cross-linking to improve their stability. To enhance stability of multilayers from biogenic polyelectrolytes, we introduced recently intrinsic cross-linking by formation of imine bonds between aldehydes of oxidized GAGs with pendant amino groups of proteins resulting in improved stability.[20]

Mesenchymal stem cells (MSCs) represent a multipotent type of cells, which lineages result in all kinds of connective tissues. Hence, they have been considered for regenerative therapies of musculoskeletal diseases and traumata.[21] Indeed, programming of MSCs differentiation has been done by tailoring physical and chemical cues expressed by man-made material surfaces including application of ECM components[22] and growth factors.[23] However, proliferative capacity of MSCs is limited to a few passages[24] and studies of fundamental effects of surface modifications may be hampered by use of several passages and donors. However, cell lines derived from multipotent mesenchymal cells such as the C3H10T1/2 cell line established in 1973 from C3H mouse embryos of 14- to 17-day-old mice[25] that share many features of MSCs, may be an alternative source of cells for studies on development of biomimetic surfaces for tissue engineering of bone, cartilage, and other types of connective tissues. In fact, C3H10T1/2 cells are able to develop into different cell lineages under specific cell culture induction media including osteoblasts,[26] chondrocytes,[27] and also adipocytes.[28] For example, bone morphogenic protein 4 (BMP-4) has been found to promote the adipogenic differentiation of C3H10T1/2 cells[28] while a high cell density micro-mass culture with a specific medium (supplemental with a purified mixture of osteoinductive proteins, ascorbic acid, and β-glycerophosphate) regulates commitment to the chondrogenic lineage.[27] In addition, previous studies found that BMP-2 was capable of triggering commitment of multipotent C3H10T1/2 cells to adipocyte[29] and osteocyte[26] lineages. Moreover, others observed that these cells respond to chemical and mechanical cues differentiating into osteoblasts, chondrocytes, and tenoblasts.[30] Hence, they seem to represent a suitable model to study the effect of biomimetic surface modifications on differentiation of multipotent cells.

So far, the effect of composition of biomimetic multilayers that resemble matrix composition of connective tissues such as bone and cartilage using collagen and either CS or HA on differentiation of C3H10T1/2 cells has not been studied yet. In addition, no studies exist that investigate the effect of intrinsic cross-linking of multilayers on adhesion, growth, and differentiation of C3H10T1/2 cells. Hence, in the present work, biomimetic multilayers prepared by pairing collagen I (Col I) with HA or CS in either native or oxidized form were used as substrate for studying adhesion, growth, and multipotent differentiation of C3H10T1/2 cells to learn about the effect of ECM-like microenvironment of differentiation of multipotent cells into mesenchymal tissues.

Materials and methods

Materials

Glass coverslips (Roth, Germany) of size ∅12 mm and ∅15 mm were treated with 0.5 M sodium hydroxide (Roth) dissolved in 96% ethanol (Roth) to clean the surfaces for
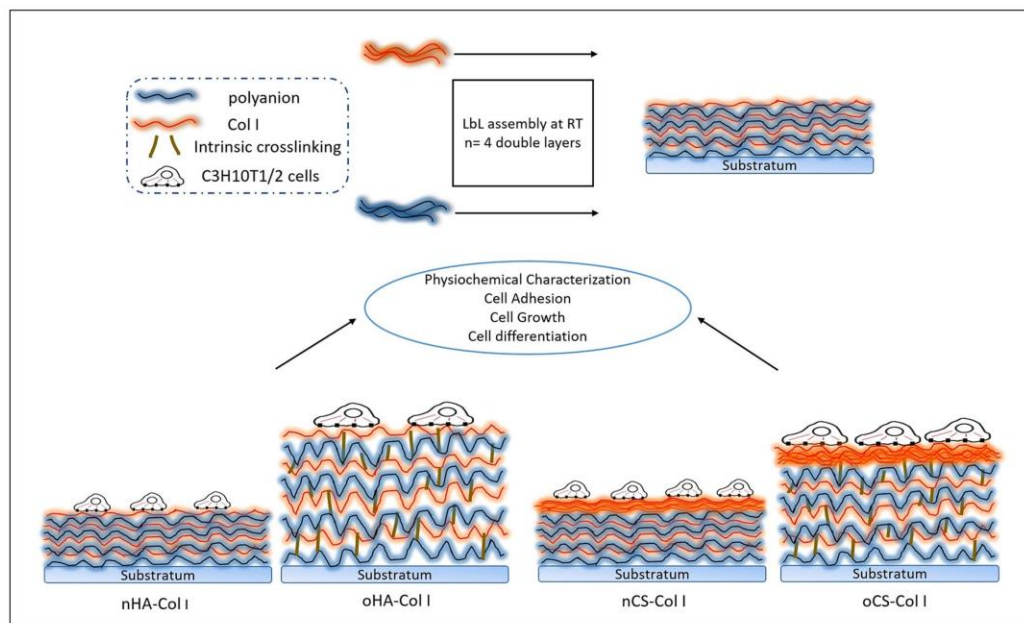
Figure 1. A concept figure illustrating the differences among the four multilayer systems.

2 h at room temperature. Subsequently, the samples were thoroughly washed with ultrapure water and dried under nitrogen flow. Silicon wafers (Silicon materials, Germany) were cut to a size of (10×10) mm² and (37×17) mm² and cleaned with a solution of hydrogen peroxide (35%, Roth), ammonium hydroxide (25%, Roth), and ultrapure water (1:1:5, v/v/v) at 75°C for 15 min.[31] Thereafter, the wafers were thoroughly rinsed with ultrapure water and dried with nitrogen. New gold-coated quartz sensors (QT Quarztechnik GmbH, Germany) for quartz crystal microbalance (QCM) measurements were cleaned with ethanol p.a. (99.8%, Roth), and extensively rinsed with ultrapure water. After drying with nitrogen, the sensors were kept in 2 mM mercaptoundecanoic acid (MUDA, 95%, Sigma, Germany) diluted in ethanol p.a. at room temperature to obtain a negatively charged surface overnight owing to the formation of carboxylate-terminated monolayer.[32]

Native hyaluronic acid (nHA MW ∼ 1.3 MDa) was provided by Innovent (Jena, Germany) while native chondroitin sulfate (nCS, MW ∼ 25 kDa) was purchased from Sigma. Polyelectrolyte solutions were prepared as follows: poly (ethylene imine) (PEI, MW ∼ 750 kDa, Sigma, Germany) was dissolved in a 0.15 M sodium chloride (NaCl, Roth) solution at a concentration of 5 mg mL⁻¹ and adjusted to a pH value of 7.4. The native and oxidized GAGs (nGAGs and oGAGs) were used as polyanions and were dissolved under stirring in a 0.15 M sodium chloride to obtain a final concentration of 0.5 mg mL⁻¹. Collagen I (Col I) from porcine skin (polycation, MW ∼ 100 kDa, Sichuan Mingrang Bio-Tech, China) was used as

polycation and was dissolved in 0.2 M acetic acid (Roth) at a concentration of 2 mg mL⁻¹ at 4°C. After dissolution, the Col I solution was centrifuged at 9000*g* for 10 min and then diluted to a final concentration of 0.5 mg mL⁻¹ using 0.2 M acetic acid supplied with NaCl (final concentration to 0.15 M NaCl). The pH value of the polyelectrolyte solutions was adjusted to pH 4.0.

Polyelectrolyte multilayer assembly

Cleaned glass coverslips or silicon wafers were used as substrate for deposition of polyelectrolyte multilayers. A first anchoring layer of PEI was formed on the substrate to obtain a surface with positive charge, which was then followed by adsorption of nGAGs (nCS, nHA) or oGAGs (oCS, oHA) as the anionic layer and then Col I as the cationic layer. Polyelectrolyte multilayers were fabricated by immersing the glass coverslips in polyanions for 15 min while in polycation for 20 min followed by three times rinsing with a solution of NaCl (0.15 M, pH 4.0) for 5 min. By alternating adsorption of Col I and nGAGs or oGAGs, multilayers with eight total layers (eighth) on top of the PEI layer were fabricated. The four different systems (Col I terminated, see Figure 1) were designated as: nHA–Col I, oHA–Col I, nCS–Col I, and oCS–Col I.

Physicochemical characterization of multilayers

The layer growth was monitored in situ using surface plasmon resonance (SPR, iSPR from IBIS Technologies,

Hengelo, The Netherlands), which is based on the detection of changes in the refractive index (RI) caused by the adsorption of molecules at the gold–liquid interface of the sensor. The resulting change in the SPR angle shift (m°) is proportional to the mass (Γ_{SPR}) of adsorbed molecules on the surface given as[33]

$$122 \, m° \approx 1 \, ng \, mm^{-1} \qquad (1)$$

The measurements were performed in situ in the flow cell of the device using gold sensors treated with MUDA (see above). Shifts in resonance angles from 10 regions of interest (ROI) defined on the sensor surface were recorded using the IBIS SPR software. To obtain a stable baseline, 0.15 M NaCl (pH 4.0) was injected into the flow cells. Then, the polyelectrolyte solution was brought to the sensor surface for 15 min followed by 15 min rinsing with 0.15 M NaCl solution (pH 4.0). Afterwards, polyelectrolyte solutions of nGAGs or oGAGs and Col I were adsorbed up to eight layers with incubation times of 15 min for nGAGs and oGAGs, while 20 min for Col I. Each adsorption step was followed by a rinsing step described above to remove unbound or loosely bound material.

QCM measurements were conducted using a LiquiLab 21 (ifak e.V., Germany) with MUDA-modified gold sensors mounted in the flow cells of the device to monitor the damping shift after each single adsorption step. The damping shift reflects the mechanical properties of multilayers with higher values for softer adsorbed mass.[34,35] The flow regime (3 μL s^{-1}) and time periods for pumping the different polyelectrolyte and washing solutions from reservoirs were programmed with the device.

The presence and organization of Col I in multilayers was characterized after in situ labelling with fluorescein isothiocyanate (FITC, Sigma)[36] using a confocal laser scanning microscope (CLSM 710, Carl Zeiss Micro-Imaging GmbH, Germany). Briefly, the multilayer-coated glass slides were placed in 24-well plates (Greiner, Germany). Then, 500 μL of 0.6 mg mL^{-1} FITC (Sigma) dissolved in pure dimethyl sulfoxide (DMSO, Sigma) solution was added to each well, followed by incubation at room temperature for 10 h. Then, samples were washed extensively with 0.15 M NaCl to remove any residual FITC. After a final short washing with water, samples were mounted with Mowiol (Merck, Germany) and examined with CLSM.

Cell culture

C3H10T1/2 embryonic fibroblasts (Clone 8) were purchased from ATCC (CCL-226, LGC Standards GmbH Wesel, Germany) and grown in Dulbecco's modified Eagle's medium (DMEM, Biochrom AG, Germany) supplemented with 10% fetal bovine serum (FBS, Biochrom AG) and 1% antibiotic–antimycotic solution (AAS,

Promocell, Germany) at 37°C in a humidified 5% CO$_2$/95% air atmosphere. Prior to reaching confluence, the cells were harvested from the culture flasks by treatment with 0.25% trypsin/0.02% EDTA (Biochrom AG) followed by subsequent centrifugation and re-suspending in DMEM at a concentration of 20,000 cells mL^{-1}.

Short-term interaction of C3H10T1/2 cells with multilayers

Cell adhesion and spreading. Adhesion of C3H10T1/2 cells was studied on glass coverslips coated with multilayer coatings of polyanion (nHA, oHA, nCS, oCS) and Col I. The serum-free C3H10T1/2 cell suspensions (1×10^4 cells), were prepared as mentioned above, and seeded on samples and incubated for 4 h. After incubation, the cells were stained with crystal violet (Roth; 0.5% (w/v)) in methanol (Roth) at room temperature for 30 min, and then carefully washed with water and dried in air. Images were taken in transmission mode with an Axiovert 100 (Carl Zeiss MicroImaging GmbH, Germany) equipped with a charge-coupled device (CCD) camera (Sony, MC-3254, AVT-Horn, Germany). Cell count, cell area, and aspect ratio were calculated from five images per sample using image processing software "ImageJ 1.41o, NIH."

Focal adhesion complex formation and organization of cellular integrins. The C3H10T1/2 cell suspensions (1×10^4 cells) were prepared and placed on samples and incubated for 24 h. After incubation, the cells attached to the multilayers were fixed with 4% paraformaldehyde solution (Roth) for 10 min followed by rinsing with phosphate-buffered saline (PBS). Thereafter, the cells were permeabilized with 0.1% Triton X-100 in PBS (v/v; Sigma) for another 10 min and washed again with PBS. The samples were further blocked by incubation with 1% (w/v) bovine serum albumin (BSA, Merck) at room temperature for 1 h. To study the formation of focal adhesions (FA) and distribution of integrins, the samples were stained by incubation with a rabbit polyclonal antibody against α2 (1:100, Santa Cruz, USA) and a mouse monoclonal antibody against vinculin (1:100, sigma), or incubated with a mouse monoclonal antibody against CD44 (1:100, Dianova, Germany) at room temperature for 30 min. After rinsing with PBS, the samples were treated with a goat Cy2-conjugated anti-mouse or goat Cy3-conjugated anti-rabbit secondary antibody (1:100, Dianova) for another 30 min. In addition, actin cytoskeleton was labeled by incubating the samples with BODIPY-phalloidin (1:50, Invitrogen, Germany) at room temperature for 30 min. The samples were then rinsed again with PBS and mounted with Mowiol. Subsequently, the samples were examined using CLSM and images were processed with the ZEN2011 software (Carl Zeiss). The vinculin level in cells was quantified using ImageJ as described in our previous work.[17]

Growth of C3H10T1/2 cells

A total 500 µL (2×10^4 cells mL^{-1}) C3H10T1/2 cells suspended in DMEM with 10% FBS were seeded either on multilayers or plain glass coverslips and cultured for 1, 2, and 3 days. Growth of cells was monitored using a phase contrast microscopy equipped with a CCD camera (Leica, Germany). Images were taken at the different days of culture. The quantity of cells was measured the same day with a Qblue fluorescence assay (BioChain, USA), which quantifies the amount of metabolic active cells. On the measuring day, the old medium was carefully removed and the samples were washed with sterile PBS once. Then, 400 µL of phenol red free DMEM supplemented with 40 µL of Qblue assay reagent was added to each well. After 2 h of incubation at 37°C, 100 µL of supernatant of each well was transferred to a black 96-well plate, and fluorescence intensity (excitation wavelength 544 nm, emission wavelength 590 nm) was measured using a plate reader (BMG LABTECH, Fluostar OPTIMA, Germany).

Cell differentiation

Multi-lineages differentiation induction. For differentiation experiments, 1 mL C3H10T1/2 cells were plated on plain or multilayer-coated glass coverslips at a density of 2.5×10^4 cells mL^{-1}. After the cells reached almost confluence, differentiation was induced with 100 ng mL^{-1} BMP-2; or with osteogenic media (OM) consisting of basal medium (BM, 10% FBS and 1% penicillin–streptomycin-containing DMEM) supplemented with 10 nM dexamethasone (Sigma), 20 mM β-glycerophosphate (Alfa Aesar, USA), 50 µM L-ascorbic acid (Sigma), and 50 ng mL^{-1} BMP-2 (Speed Biosystem, USA); or with chondrogenic media (CM) consisting of BM supplemented with 0.1 µM dexamethasone, 50 µg mL^{-1} L-ascorbic acid, 40 µg mL^{-1} L-proline, and 1% ITS (Sigma). The medium was changed every 3 days until end-point assay. Images were taken using a phase contrast microscopy during the different days of induction.

Alkaline phosphatase activity detection. At day 10 of induction with BM or OM, alkaline phosphatase activity (ALP) was measured to evaluate the osteoblastic differentiation of C3H10T1/2 cells. Cell lysates were obtained by treatment with 0.2% (v/v) Triton X-100 (Sigma) in PBS at 4°C for 20 min, and then incubated with 2 mM *p*-nitrophenyl phosphate (*p*NPP, Sigma) in 1 M diethanolamine at pH 9.8 in the dark at 37°C for 30 min. The absorbance at 405 nm was measured with a plate reader. The total protein content of the lysates was evaluated by BCA assay (Pierce, USA). The ALP activity was calculated by normalization to the protein content of the lysates.

Cytochemical staining

ALP staining. At day 24 of induction with BM or OM, ALP staining was performed. The samples were washed once with PBS and fixed with 5% glutaraldehyde for 15 min. After washing twice with distilled water, a mix solution of BCIP (0.17 mg mL^{-1}, Applichem, Germany) and NBT (0.33 mg mL^{-1}, Applichem) in 0.375 M AMP buffer was added into each well, and left for 1 h in the dark at room temperature. The reaction was stopped by washing with 20 mM EDTA (Biochrom AG), and then thoroughly washed with distilled water to remove the excess dye. Images were taken in transmission mode with an Axiovert 100 equipped with a CCD camera.

Alizarin red and Sudan black staining. Alizarin red staining was performed to observe the calcium phosphate deposition of C3H10T1/2 cells. At day 24 of induction with BM or OM, the samples were washed once with PBS and fixed with 4% paraformaldehyde for 15 min. Thereafter, staining with Alizarin red (2%, pH 4.2, Roth) was performed for 45 min in the dark, and the excess dye was removed by rinsing twice with distilled water. Images were taken in transmission mode with an Axiovert 100 equipped with a CCD camera.

Sudan black staining was further performed to counterstain adipocyte-containing osteogenic cultures whose mineralized matrix has been stained with Alizarin red.[37] Briefly, the Alizarin red staining samples were incubated with 1.2% (w/v) Sudan black solution for 30 min in the dark followed by extensive washing with distilled water. Finally, images were taken in transmission mode with an Axiovert 100 equipped with a CCD camera.

Alcian blue staining. At day 24 of chondrogenic induction, the samples were fixed as described above and incubated with 0.5% (w/v) Alcian blue (Roth) in 3% acetic acid for 1 h in the dark to detect the secretion of GAGs and mucopolysaccharides by C3H10T1/2 cells. The excess dye was removed by washing with distilled water and images were taken with an Axiovert 100 equipped with a CCD camera.

Oil red staining. Oil red staining was performed to investigate the presence of lipid vacuoles in C3H10T1/2 cells. Briefly, at day 14 of induction with 100 ng mL^{-1} BMP-2, the samples were fixed as described above and stained with 0.5% (w/v) Oil red (Roth) for 30 min in the dark. Then, the excess dye was removed by thoroughly washing with distilled water and images were taken in transmission mode with an Axiovert 100 equipped with a CCD camera.

Statistics

All the data are provided as mean values ± standard deviations (SDs) from at least three independent experiments. Statistical analysis was performed using Origin with analysis of variance (ANOVA) test (one way) followed by post hoc Tukey testing. The number of samples has been indicated in the respective figures and tables captions.
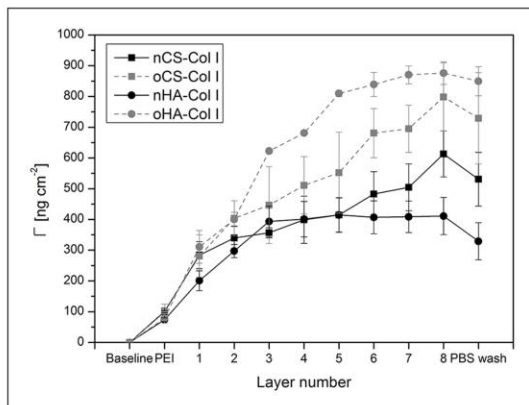
Figure 2. Surface plasmon resonance (SPR) measurements of the layer-by-layer assembly of polyelectrolyte multilayers up to eight layers. Multilayer mass Γ calculated from angle shifts are mean ± SD values of three independent experiments, the initial layer is poly (ethylene imine) (PEI), odd numbers refer to native or oxidized glycosaminoglycans (nGAG or oGAG), even numbers refer to collagen I (Col I).
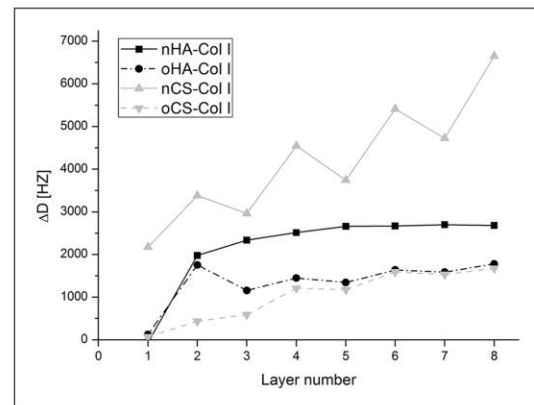
Figure 3. Quartz crystal microbalance (QCM) measurements of damping shift with each polyelectrolyte adsorption steps. The odd numbers refer to native (nGAGs) or oxidized glycosaminoglycans (oGAGs) and even numbers refer to collagen I (Col I). Four bilayers of native hyaluronic acid (nHA), oxidized hyaluronic acid (oHA), native chondroitin sulfate (nCS), or oxidized chondroitin sulfate (oCS) were prepared with collagen I (Col I) as terminal layer.

Statistical significance was considered for $p < 0.05$ and is indicated by asterisks.

Results and discussion

Physicochemical characterization of polyelectrolyte multilayers

The multilayer growth was performed under pH 4 condition as in some of our previous work.[16] Considering the isoelectric point (p*I*) of Col I of around 5.5, it should possess a net positive charge at this pH condition. By contrast, both CS and HA represent polyanions at pH 4, because of the pKa values of about 2–2.5 for CS[38] and 2.9 for HA.[39] Hence, the formation of nGAGs and Col I multilayers at pH 4 should be predominantly dependent on ion pairing. The multilayer growth, based on ion pairing for nGAGs–Col I systems and additional cross-linking via the formation of Schiff's base in oGAGs–Col I systems, was monitored using the surface-sensitive SPR technique. The accumulated layer mass of adsorbed polyelectrolytes with increasing layer number was calculated according to equation (1). The results are depicted in Figure 2. In general, the trend in layer growth was similar for polyelectrolyte multilayers based on the same GAG, either nHA–Col I and oHA–Col I, or nCS–Col I and oCS–Col I. However, slight differences were found in the growth regimes of HA-based multilayers when compared to CS-based multilayers.

For nHA–Col I and oHA–Col I systems, a linear increase in adsorbed mass was found up to three (nHA) or five adsorbed layers (oHA) on top of the PEI priming layer. After that, adsorption reached a plateau indicating

that mass adsorption reached an equilibrium. It was visible that multilayer mass of oHA–Col I system was significantly higher due to additional chemical cross-linking.

The multilayer growth of the nCS–Col I and oCS–Col I systems here was roughly linear; this trend was in agreement with a previous report for other polyelectrolytes.[40] Again, a higher mass increase was observed for the multilayer system when fabricated with oCS. Furthermore, here the SPR curves revealed a much larger amount of Col I (even numbers) in comparison to nCS and oCS deposition (odd numbers), which was in contrast to HA-based systems, probably due to the higher charge density of CS compared to HA, which enabled the CS-based systems to bind more Col I. Indeed, the fibrillization of Col I was strongly influenced by the type of GAG as studied by CLSM (see Figure 4). Similar findings were shown in previous work comparing heparin to CS-based multilayers regarding the layer growth and polycation adsorption.[41] Furthermore, the increase in angle shifts was higher for multilayers based on oGAGs compared to their natives, indicating that the intrinsic cross-linking capability makes a major contribution to multilayer formation.[41]

QCM measurements were performed to evaluate mechanical properties of polyelectrolyte multilayers on the sensor surface after each adsorption step. According to the damping shift, assumptions on the mechanical properties of multilayers can be drawn because the higher the damping shift, the softer is the substratum.[34] As shown in Figure 3, the damping shift values for nGAGs and oGAGs multilayer systems varied significantly after each layer adsorption, indicating different mechanical properties of
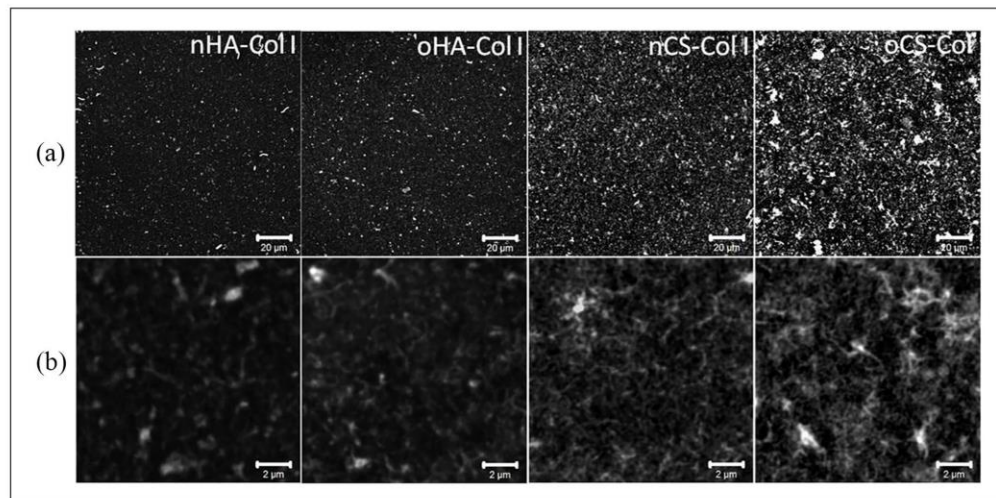
Figure 4. Overall morphology of in situ FITC-labeled collagen I (FITC-Col I) terminated polyelectrolyte multilayers viewed with confocal laser scanning microscopy (CLSM) at (a) lower (scale 20 μm) and (b) higher (scale 2 μm) magnification. Four bilayers of native hyaluronic acid (nHA), oxidized hyaluronic acid (oHA), native chondroitin sulfate (nCS), or oxidized chondroitin sulfate (oCS) were prepared with Col I as polycation.

the polyelectrolyte multilayers. Softer multilayers were obtained when nGAGs were used, as indicated by the pronounced higher damping shifts for both nHA and nCS. Conversely, multilayers made of oGAGs were more rigid because dampening shifts were much lower. Overall, the results demonstrate that the cross-linking significantly affects mechanical features of multilayers, giving rise to stiffer substrata.

To learn more about the ability of GAGs to support fibrillization of Col I in multilayers, the protein was labeled in situ by FITC and multilayers were viewed with CLSM (see Figure 4). Although Col I aggregates were present in all multilayer systems, a prominent fibrous structure was found mostly in CS-based multilayers (both nCS and oCS), showing a tendency to form a network-like structure. Conversely, rather sparse and short fibrils were observed in both nHA and oHA-based multilayers where Col I seemed to form rather discrete aggregates than fibers. Col I fibrillogenesis is known to be affected not only by several environmental parameters such as collagen concentration[42] and pH value,[43] but also by the presence of GAGs such as CS and other naturally derived polyanions.[44] Generally, a pH value above 5.5 normally supports fibrillogenesis of Col I, while at pH value below 5.5 Col I forms more globular structures.[43] Nevertheless, the presence of GAGs, particularly CS, seems to support Col I fibril formation as happened even at pH 4. Furthermore, the concentration of Col I also affects strongly fibril formation as found previously.[42] Presumably CS binds to Col I molecules and promotes the organization of mature fibrils by increasing Col I concentration, as it was observed in the

presence of 4,6-disulfated disaccharides structures, previously.[44] In line with this, here, fibril formation in both nCS and oCS-based multilayers was observed, when more Col I was adsorbed.

Adhesion of C3H10T1/2 cells

C3H10T1/2 cells were seeded on the test samples in the absence of serum to allow a direct cell–surface interaction avoiding the interference with other proteins. The quantitative data of cell adhesion and morphology visualized by crystal violet staining and image analysis are shown in Figure 5 and Table 1. It was observed that cells show a superior spreading on the multilayer-coated surfaces, compared to cells on plain glass coverslips, which were used here as additional control to assure normal adhesion of cells. Furthermore, the cells were larger and more elongated on CS-based multilayers in general, and more specifically on oCS-based multilayers when compared to HA-based systems, where cell spreading was significantly lower than on CS-based multilayers. Indeed, significantly more cells adhered on the CS-based multilayer systems (where Col I was dominating) when compared to HA-based systems, while no obvious differences were observed for multilayer systems based on the same GAG type (e.g. nHA and oHA, or nCS and oCS; see Table 1).

Adhesion and spreading of cells are considered as promoters of gene expression and subsequent cell differentiation.[45] To learn more about the organization of C3H10T1/2 cells adhesive machinery, the formation of FA was visualized by staining of vinculin (green, see Figure 6(a)) and the
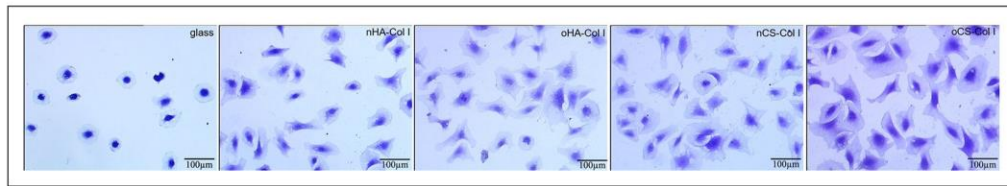
Figure 5. Transmitted light microscopic images of crystal violet staining C3H10T1/2 cells adherent on different test surfaces for 4 h. The cells were seeded in serum-free medium. The four types of polyelectrolyte multilayers are the same as described in Figure 4.

Table 1. Quantification of cell count, area, and aspect ratio of C3H10T1/2 cells seeded on the various multilayers and glass as a control. Results are mean ± SD values of three independent experiments. The four types of polyelectrolyte multilayers are the same as described in Figure 4.

Samples	Cell count (mm^{-2})	Cell area (μm^2)	Aspect ratio (a.u.)
Glass	36.7 ± 9.6	3127.9 ± 1602.4	0.73 ± 0.12
nHA–Col I	41.3 ± 6.3	4875.5 ± 2232.0	0.56 ± 0.14
oHA–Col I	42.6 ± 7.1	5292.0 ± 2952.4	0.53 ± 0.16
nCS–Col I	56.1 ± 6.2	5840.8 ± 2838.1	0.57 ± 0.14
oCS–Col I	54.7 ± 6.2	6025.5 ± 3412.6	0.51 ± 0.15

nHA: native hyaluronic acid; Col I: collagen I; oHA: oxidative hyaluronic acid; nCS: native chondroitin sulfate; oCS: oxidative chondroitin sulfate.
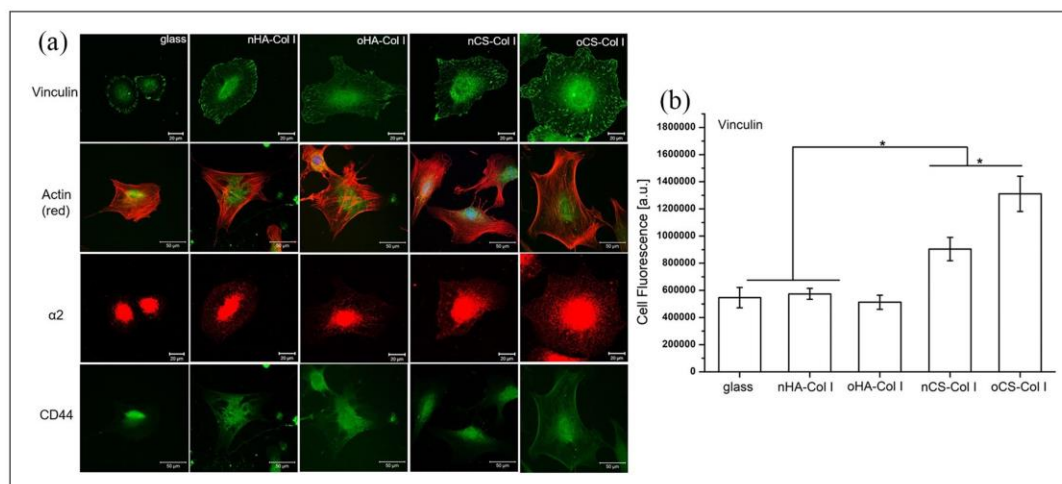
Figure 6. Confocal laser scanning micrographs (CLSM) of C3H10T1/2 cells on different test surfaces. (a) Staining of vinculin, α2, actin (red), and CD44 of C3H10T1/2 cells after 24 h of incubation on different polyelectrolyte multilayers; (b) fluorescence signals of vinculin in focal adhesions quantified by ImageJ and corrected total cell fluorescence was calculated by fluorescence signal with elimination of background signal. The four types of polyelectrolyte multilayers are the same as described in Figure 4.

development of actin cytoskeleton (red, see Figure 6(a)) after 24 h of incubation. Cells cultured on plain glass coverslips displayed short length of vinculin-positive streaks (Figure 6(a)), which were weak in comparison to the cell plated on the multilayers. Though a pronounced cell spreading was observed on all multilayer-coated surfaces, the overall appearance of FA plaques was different. The FA plaques formed on HA-based multilayers were lesser and

weaker, which were mainly present at the cell periphery. Conversely, more elongated FA plaques were found on CS-based multilayers and distributed all over the ventral cell side, which is again well in line with the presence of higher quantity and more fibrillar Col I since collagen promotes cell adhesion via integrin-mediated mechanism.[46] Furthermore, the FA plaques were much more pronounced when cells adhered on oCS–Col I (Figure 6(a)). Particularly,
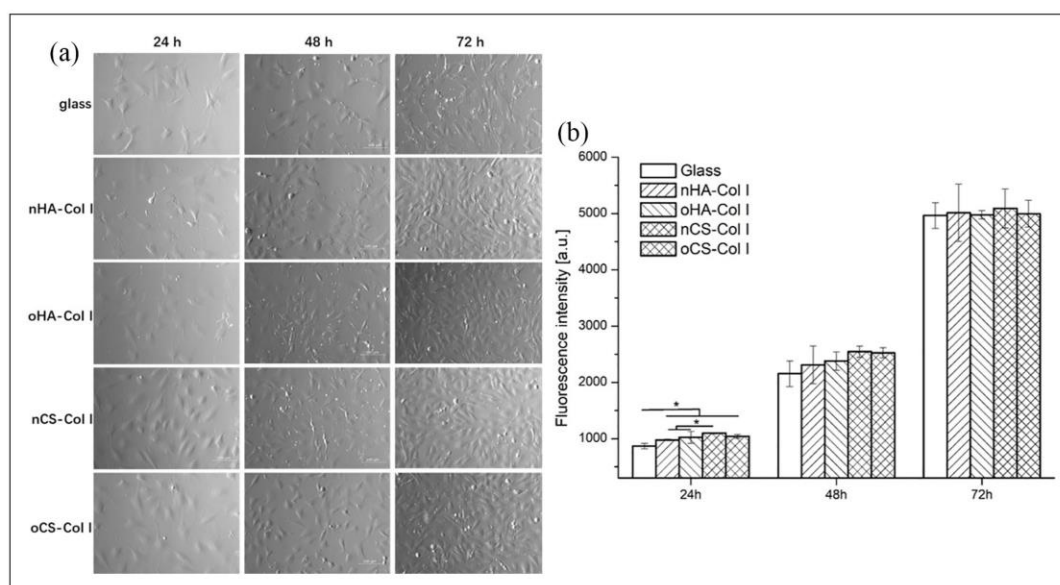
Figure 7. Phase contrast images (a; 100× magnification) and (b) proliferation of long-term C3H10T1/2 cells cultured on plain glass and Col I-terminated multilayers prepared with nHA, oHA, nCS, or oCS as polyanion for 24, 48, and 72 h. Proliferation of C3H10T1/2 cells was assessed by the Qblue assay for determination of metabolically active cells. Results are mean ± SD values of three independent experiments.

the quantitative analysis of vinculin-positive FA showed higher quantities in cells grown on CS–Col I compared to HA–Col I (Figure 6(b)). In addition, more vinculin was pronounced on oCS–Col I compared to the native system nCS–Col I, which is related to the stiffness resulting from intrinsic cross-linking occurring in oGAGs systems, as found by QCM studies (as shown in Figure 6(b)).

Since integrins play a pivotal role in connecting ECM proteins with the cell cytoskeleton and signaling complexes, we further studied the expression and organization of $\alpha2$ that is regarded as a main collagen receptor[47] and CD44 that is known as a main HA receptor.[48] As shown in Figure 6(a), $\alpha2$ was more expressed and organized in C3H10T1/2 cells adhering on CS multilayer surfaces (either nCS–Col I or oCS–Col I), while on HA-based surfaces, a weaker expression of $\alpha2$ with a tendency for peri-nuclear accumulation was observed (see Figure 6(a) as well). In addition, no large difference was found on the multilayer-coated samples with respect to the expression of CD44, where Col I was used as the terminating layer (Figure 6(a)). However, the expression of $\alpha2$ and CD44 were always weaker in cells placed on the plain glass coverslips, due to the lack of integrin receptor sites.

Overall, the adhesion, spreading, and $\alpha2$ integrin organization of C3H10T1/2 cells were increased on CS-based multilayers, which can be explained with the composition of these multilayer systems. First, more Col I was assembled in the CS-based multilayers and formed a well-interconnected fibrillar structure, resembling the natural Col I

environment. Col I fibrils have been found to promote the adhesion of a variety of cells via $\alpha2$ integrin-mediated interaction,[46] which explains also the apparently higher organization of this integrin on CS-based multilayer surfaces. Conversely, apparently lower expression of integrin $\alpha2$ was found on HA-based multilayers where GAG was dominant as shown also in our previous work leading to the formation of lower quantity of Col I fibrils. In addition, the increased hydrophilicity of HA-based coatings[20] may also lead to the reduced adhesion and spreading of C3H10T1/2 cells, as cells prefer to adhere on surfaces with moderate wettability.[49] It is of note that both spreading and organization of cell adhesion complexes was more pronounced on oCS surfaces when compared to nCS-based multilayers. The additional covalent cross-linking in oGAGs-based systems increased the multilayer stiffness (proven by QCM study), thus, effects on adhesion and spreading of cells can be expected.[50] Nevertheless, the lack of such obvious difference between nHA and oHA multilayers may be due to the higher hydrophilicity of these systems that reduces spreading, and thus overriding the effect of different stiffness of native and oxidized HA-based systems.

Growth of C3H10T1/2 cells on multilayers

To see the effect of multilayers during longer culture of cells, proliferation studies were done with C3H10T1/2 cells for 24, 48, and 72 h. Figure 7(a) shows the morphology and growth of cells during the culture period on plain

glass and Col I-terminated multilayers. As can be seen in Figure 7(a), cells were able to grow on all substrata and cell number increased over time from 24 (left lane) to 72 (right lane) hours, while the cell number was always lower on the plain glass. It was also obvious that cell spreading was improved on CS-based multilayers and combined with a higher cell number as well.

Quantitative data on cell proliferation were obtained with Qblue assay, which determines the metabolic activity of cells. Results in Figure 7(b) show a coincidence with that of adhesion studies and found the quantity of metabolically active cells on plain glass coverslips was lower than that of multilayer-coated surfaces. In addition, improved cell proliferation was detected on CS-based multilayers in comparison to surfaces containing HA, during the first 48 h of incubation. This suggests that surfaces containing higher amounts of Col I fibrils mimic the ECM and thus, support initial cell attachment and growth. However, no obvious differences in amount of metabolically active cells were found between both types of GAG-based multilayers after 48 h incubation. It is assumed that the ability of cells to secrete matrix proteins such as fibronectin may contribute to the lower differences.[51] Furthermore, no significant differences in cell growth were observed between native and oGAGs multilayers, which also indicate that the intrinsic cross-linking ability due to presence of aldehyde groups in oGAGs systems did not have any toxic or other adverse effects on cell proliferation.

Multi-lineages differentiation of C3H10T1/2 cells

Osteogenic differentiation investigation. To see the effect of multilayers on osteogenic differentiation of C3H10T1/2 cells, change of cell morphology was recorded after 24 days of incubation. As can be seen in Figure 8(a), no big difference could be found between the cells cultured in BM, while aggregated vacuoles-like structures resembling probably lipid droplets were observed under OM conditions, especially on the multilayer-coated surfaces.

To evaluate the osteogenic differentiation of C3H10T1/2 cells on the various surfaces, ALP activity was normalized to protein content and investigated at day 10 of post-differentiation (Figure 8(b)). The ALP activity of C3H10T1/2 cells cultured in BM or OM was always lower on the plain glass as compared to the multilayer-coated surfaces. In addition, a higher activity of ALP was found on CS-based multilayers when cells were cultured in BM, though no significant difference was observed. Moreover, it is of note that cells in BM showed significantly higher ALP activity compared to OM, indicating an inhibitory effect of osteogenic supplements on driving osteogenic differentiation of C3H10T1/2 cells (Figure 8(b)). The staining of ALP (Figure 8(c)) was always weaker in cells growing on the plain glass, which is well in line with the quantitative

study. Though no intensive staining of ALP could be found on all the samples (either in BM or OM), a slightly stronger staining was observed on CS-based multilayers when cells were cultured in BM that could be related to the higher expression of α2 integrin observed on CS multilayers. The collagen receptors signaling via α2β1 and β1 integrins is required for ALP induction process.[52]

Furthermore, at a later stage of osteogenesis, ECM calcification occurs,[52] hence, the deposition of calcium phosphate at day 24 post-differentiation was studied by Alizarin red staining. Figure 8(d) shows that no significant staining was observed when cells cultured in either BM or OM, indicating the limited osteogenic differentiation potential of C3H10T1/2 cells under these conditions. Since pronounced lipid vacuoles were detected in C3H10T1/2 cells when cultured in OM (see in Figure 8(a)), we further studied the adipogenic differentiation of C3H10T1/2 cells by Sudan black staining to counterstain adipocyte-containing osteogenic cultures whose mineralized matrix has been stained with Alizarin red.[37] Indeed, significant staining with Sudan black was observed when C3H10T1/2 cells were cultured in OM (Figure 8(d)), where no positive staining of Alizarin red was found. In addition, the staining with Sudan black was more intensive on oGAGs-based surfaces. This finding provided a hint to a dominating adipogenic compared to osteogenic differentiation of C3H10T1/2 cells, when exposed to medium with osteogenic supplements, such as dexamethasone and BMP-2. By contrast, no significant staining with Sudan black was observed when C3H10T1/2 cells were cultured in BM (Figure 8(d)) indicating that the adipogenesis occurred because of an induction effect caused by the supplements added in case of OM. Previous studies found that BMPs such as BMP-2[29] and BMP-4[53] are capable of triggering commitment of multipotent C3H10T1/2 cells to the adipocyte lineage, which might explain the positive Sudan black staining compared to the negative staining of mineralized matrix that was observed. Furthermore, the synthetic glucocorticoid dexamethasone has a regulatory effect on mesenchymal cells commitment to various cell lineages.[54] The promoting effect of dexamethasone on adipogenesis has been described by others.[55] In cells that are not committed to osteogenic differentiation only, dexamethasone had a stimulatory effect on adipogenesis.[56] Therefore, we concluded that both dexamethasone and BMP-2 supplements in OM might trigger C3H10T1/2 cells more toward adipogenesis.

As the addition of BMP-2 might push C3H10T1/2 cells more toward adipogenesis, we further investigated the effect of BMP-2 alone (no OM or CM supplements) on driving C3H10T1/2 cells differentiation. The cells were cultured in 100 ng mL^{-1} BMP-2 and incubated for 14 days, and then histochemical staining was carried out to view the ECM deposition. As can be seen in Figure 9, no positive staining of Alizarin red or Alcian blue was observed in
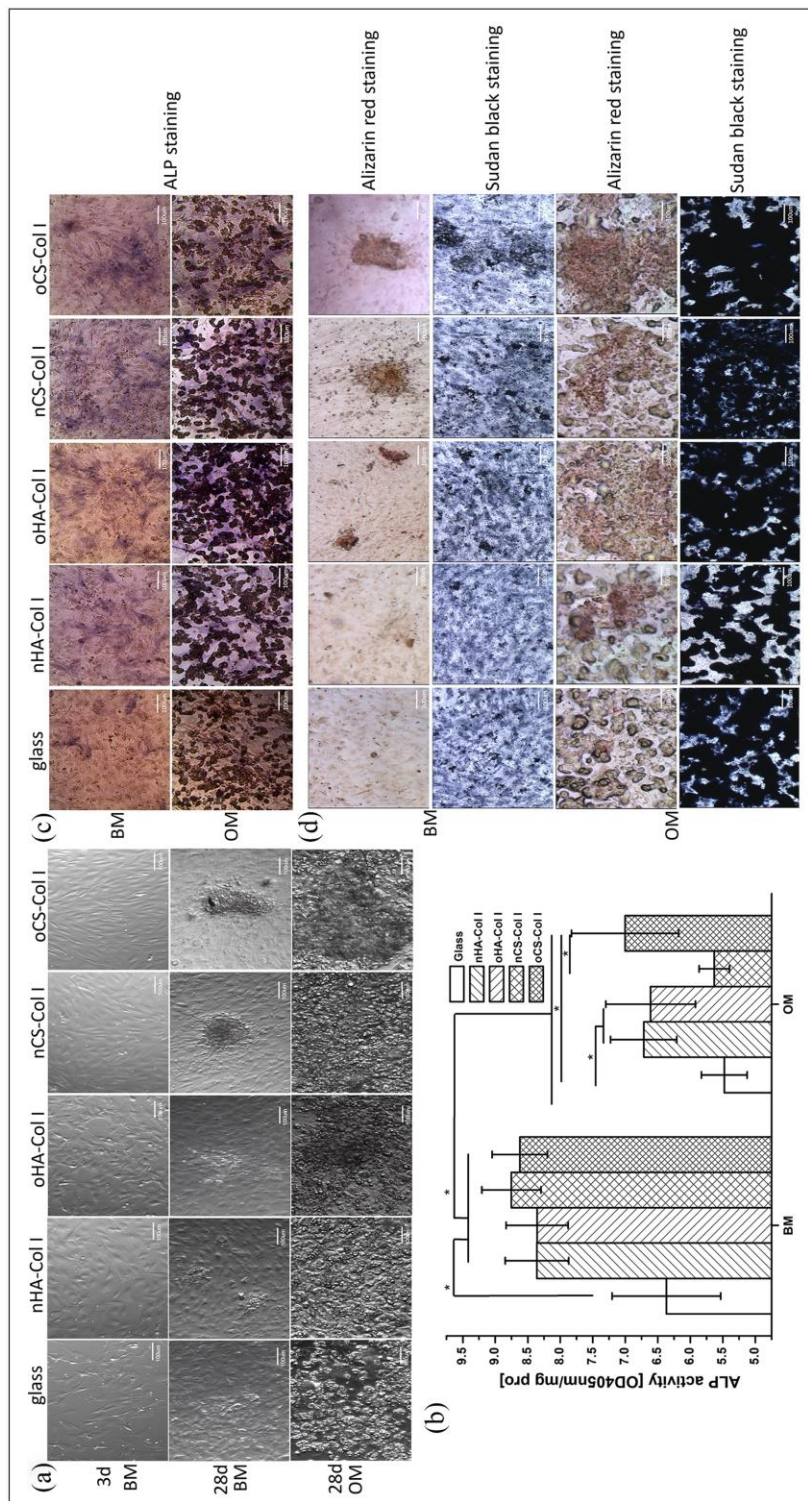
Figure 8. Phase contrast images (a), ALP activity (b), and histochemistry staining ((c) and (d)) of C3H10T1/2 cells cultured on various test samples with basal medium (BM) and osteogenic medium (OM). ALP activity of cells was determined at day 10 post-differentiation; ALP staining and Alizarin red staining were performed at day 24 post-differentiation; Sudan black staining was performed to counterstain adipocyte-containing osteogenic cultures whose mineralized matrix has been stained with Alizarin red. The four types of polyelectrolyte multilayers are the same as described in Figure 4.
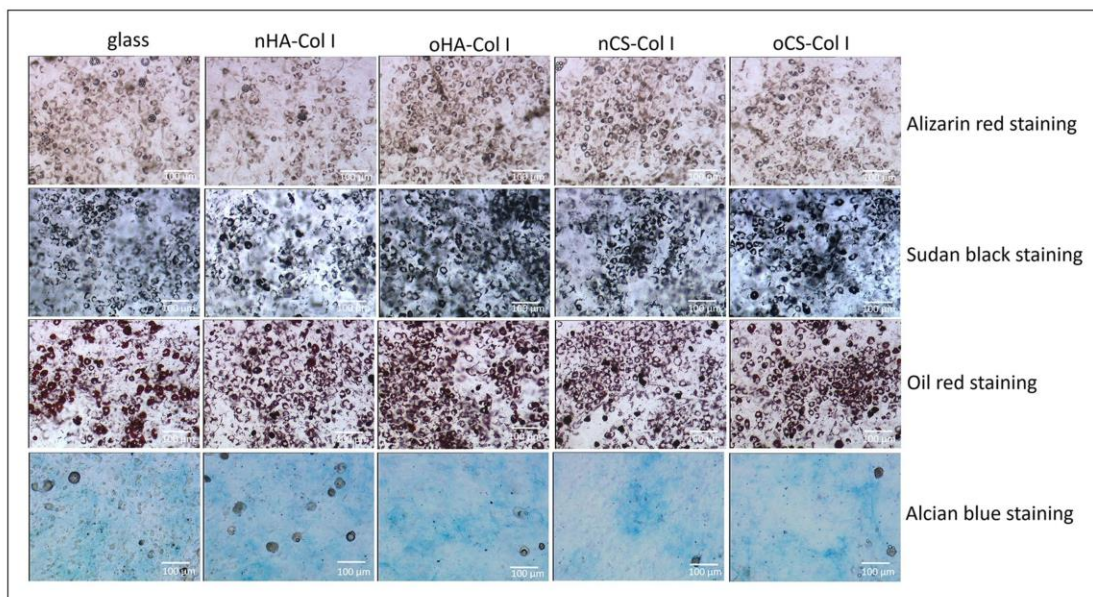
Figure 9. Histochemistry staining of C3H10T1/2 cells placed on various test samples with 100 ng mL^{-1} BMP-2 up to 14 days. The four types of polyelectrolyte multilayers are the same as described in Figure 4.

samples indicating no osteogenic or chondrogenic differentiation of C3H10T1/2 cells. By contrast, with respect to adipogenic markers, Oil red and Sudan black staining revealed lipid vacuoles in cells, especially when they were cultured on the multilayer-coated surfaces. This shows the effect of BMP-2 in directing C3H10T1/2 cells commitment to adipogenesis, as it has also been observed by others, too.[57] BMP-2 initiates this adipogenic commitment via activating of downstream signaling intermediates of BMP signaling pathway through increasing their expression and phosphorylation.[57] Moreover, the development of fat droplets was more pronounced on the oGAGs multilayers.

Chondrogenic differentiation investigation. To see the effect of multilayers on chondrogenic differentiation of C3H10T1/2 cells, cell morphology was recorded after 24 days of incubation. No large differences could be found between cells cultured in BM as shown in Figure 10(a). However, in note contrast, only few cells adhered and mostly presented a round-shaped morphology under CM condition as it has been observed for MSCs in other studies.[58]

To further view the deposition of a cartilage-specific matrix, C3H10T1/2 cells were stained with Alcian blue at day 24 post-differentiation (Figure 10(b)). A positive staining with Alcian blue was observed on multilayer-coated surfaces when cells were cultured in BM. This staining was more intensive on HA-based multilayers, especially on nHA surfaces. In note contrast, no significant staining

could be detected when cells were grown in CM, most of the cells seemed to detach or shrink on the multilayer-coated surfaces, suggesting that chondrogenic supplements, probably dexamethasone, impeded chondrogenic differentiation of C3H10T1/2 cells. Treatment of tendon stem cells with dexamethasone has been found to increase the expression of PPARγ gene, which is a specific marker for adipogenesis of adult stem cells.[59] Other studies also showed that dexamethasone suppressed chondrocytes differentiation when it was in combination with ITS by modulating the local environment,[60] which could be the case here since our chondrogenic medium was supplemented with ITS together with dexamethasone.

Overall, the osteogenic differentiation of C3H10T1/2 cells was increased on CS-based multilayers, while the chondrogenic differentiation was more pronounced on HA-based systems, but only when cells were cultured in BM. Conversely, C3H10T1/2 cells displayed a limited differentiation potential toward osteogenic and chondrogenic lineages when cultured in media with osteogenic or chondrogenic supplements. C3H10T1/2 cells differentiated more into an adipogenic lineage, when cultured in OM or with addition of 100 ng mL^{-1} BMP-2 to BM, and it was more pronounced on oGAGs multilayers. We assumed that the differed differentiation potential of C3H10T1/2 cells in BM, toward osteogenic and chondrogenic lineages on multilayer-coated surfaces, was mostly dependent on the molecular composition of the multilayers where the observed effect on cells was only because of the intrinsic
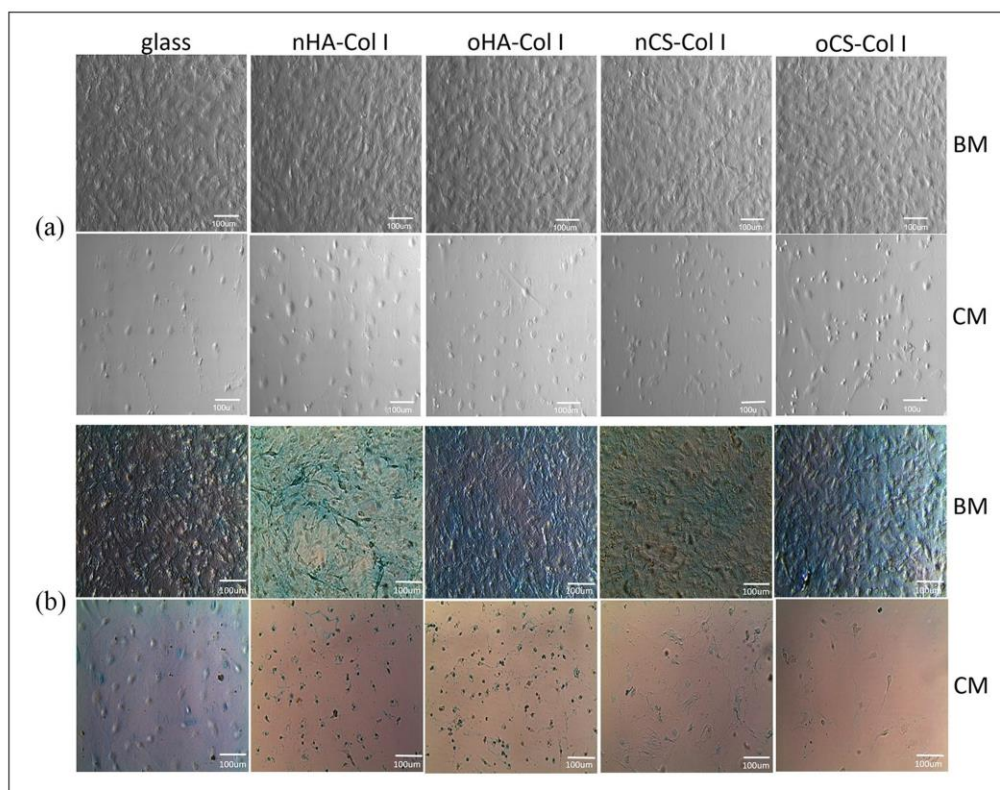
Figure 10. Phase contrast images (a) and Alcian blue staining (b) of C3H10T1/2 cells placed on various test samples supplied with basal medium (BM) and chondrogenic medium (CM), respectively. Staining was performed at day 24 post-differentiation. The four types of polyelectrolyte multilayers are the same as described in Figure 4.

properties of the multilayer surfaces without any external addition. The larger quantity and fibrillar structure of Col I, which is also a key component of bone, contributed to more osteogenic differentiation of C3H10T1/3 cells on CS-based multilayers. This was also evidenced by enhanced cell-material interactions, such as FA formation and $\alpha 2$ integrin clustering, while interaction of cells with Col I via $\alpha 2$ integrin has been shown to be important in regulating osteogenic differentiation.[61] However, many studies demonstrated the benefits of HA and CS on cartilage formation and bone regeneration, respectively.[62] It was found that the type of GAG can be used for controlling the lineage specification of MSCs, whereby CS enhanced the osteogenic differentiation of MSCs, and HA promoted chondrogenic differentiation.[62] In addition, the differentiation of C3H10T1/2 cells toward adipocytes might be attributed to the presence of BMP-2,[29] and dexamethasone,[56] which have been found to promote adipogenesis. Furthermore, the ALP activity of cells in OM (Figure 8(b)) despite their adipogenic differentiation behavior observed by histochemical staining (Figure 8(d)), does not contradict the overall findings. ALP has

been shown to be upregulated during osteogenic and adipogenic differentiation. It cannot be considered as lineage specific marker as it only proves the starting of differentiation.[63] Presumably, the most pronounced adipogenesis observed on oGAGs multilayers might be related to a different interaction of BMP-2 with oxidized multilayers, where the activity of the growth factor is extremely enhanced as shown in a previous study from our group.[41]

Conclusion

It was shown that the adhesion and differentiation of C3H10T1/2 cells were largely affected by the composition of polyelectrolyte multilayers. The CS-based multilayers rich in larger quantity and fibrillar structure of Col I have a superior effect on promoting cell adhesion in terms of increased FA formation and $\alpha 2$ integrin clustering, and osteogenic differentiation, when cultured in BM without any osteogenic supplements. It was also found that multilayers made of oGAGs and Col I possessed a higher rigidity resulting from intrinsic cross-linking, which affected spreading of cells. By contrast, the chondrogenic

differentiation of C3H10T1/2 cells was more pronounced on HA-based polyelectrolyte multilayers. Furthermore, it is of note that the CM and OM supplemented with BMP-2 and dexamethasone, impeded the chondrogenic and osteogenic differentiation of C3H10T1/2 cells. Conversely, the BMP-2 and dexamethasone supplemented OM and BMP-2 alone directed adipogenic differentiation of C3H10T1/2 cells, which was more evident on oGAGs multilayers. These findings provided new insights to our understanding not only the importance of controlling matrix composition as an approach to manipulate cell fates but also the selection of C3H10T1/2 cells for differentiation investigations. Cautions are needed when using C3H10T1/2 cells for osteogenic and chondrogenic studies.

Declaration of conflicting interests

The author(s) declared no potential conflicts of interest with respect to the research, authorship, and/or publication of this article.

Funding

ORCID iD

Mingyan Zhao [iD] https://orcid.org/0000-0003-4063-8351

References

1. Frantz C, Stewart KM and Weaver VM. The extracellular matrix at a glance. *Journal of Cell Science* 2010; 123: 4195.
2. Schnabelrauch M, Scharnweber D and Schiller J. Sulfated glycosaminoglycans as promising artificial extracellular matrix components to improve the regeneration of tissues. *Curr Med Chem* 2013; 20(20): 2501–2523.
3. Schaefer LSR. Proteoglycans: from structural compounds to signaling molecules. *Cell Tissue Res* 2010; 339(1): 237–246.
4. Kechagia JZ, Ivaska J and Roca-Cusachs P. Integrins as biomechanical sensors of the microenvironment. *Nat Rev Mol Cell Biol* 2019; 20(8): 457–473.
5. Sainio A and Järveläinen H. Extracellular matrix-cell interactions: focus on therapeutic applications. *Cell Signal* 2020; 66: 109487.
6. Hynes RO. The extracellular matrix: not just pretty fibrils. *Science* 2009; 326: 1216.
7. Liu ZM, Gu Q, Xu ZK, et al. Synergistic effect of polyelectrolyte multilayers and osteogenic growth medium on differentiation of human mesenchymal stem cells. *Macromol Biosci* 2010; 10: 1043–1054.
8. Liu Z-M, Lee S-Y, Sarun S, et al. Biocompatibility of poly (L-lactide) films modified with poly (ethylene imine) and polyelectrolyte multilayers. *J Biomater Sci Polym* 2010; 21(6–7): 893–912.
9. Ma Z, Mao Z and Gao C. Surface modification and property analysis of biomedical polymers used for tissue engineering. *Colloid Surf B: Biointerf* 2007; 60: 137–157.
10. Hao L and Lawrence J. *Laser surface treatment of bioimplant materials*. Chichester: Wiley, 2005.
11. Roach P, Eglin D, Rohde K, et al. Modern biomaterials: a review—bulk properties and implications of surface modifications. *J Mater Sci Mater Med* 2007; 18(7): 1263–1277.
12. Rahmany MB and Van Dyke M. Biomimetic approaches to modulate cellular adhesion in biomaterials: A review. *Acta Biomater* 2013; 9(3): 5431–5437.
13. Niepel MS, Almouhanna F, Ekambaram BK, et al. Cross-linking multilayers of poly-l-lysine and hyaluronic acid: Effect on mesenchymal stem cell behavior. *Int J Artif Organs* 2018; 41(4): 223–235.
14. Ren KF, Hu M, Zhang H, et al. Layer-by-layer assembly as a robust method to construct extracellular matrix mimic surfaces to modulate cell behavior. *Progress in Polymer Science* 2019; 92: 1–34.
15. Silva JM, Reis RL and Mano JF. Biomimetic extracellular environment based on natural origin polyelectrolyte multilayers. *Small* 2016; 12(32): 4308–4342.
16. Guillot R, Gilde F, Becquart P, et al. The stability of BMP loaded polyelectrolyte multilayer coatings on titanium. *Biomaterials* 2013; 34(23): 5737–5746.
17. Zhao M, Altankov G, Grabiec U, et al. Molecular composition of GAG-collagen I multilayers affects remodeling of terminal layers and osteogenic differentiation of adipose-derived stem cells. *Acta Biomaterialia* 2016; 41: 86–99.
18. Aggarwal N, Altgärde N, Svedhem S, et al. Tuning cell adhesion and growth on biomimetic polyelectrolyte multilayers by variation of pH during layer-by-layer assembly. *Macromol Biosci* 2013; 13(10): 1327–1338.
19. Chaubaroux C, Vrana E, Debry C, et al. Collagen-based fibrillar multilayer films cross-linked by a natural agent. *Biomacromolecules* 2012; 13: 2128–2135.
20. Zhao M, Li L, Zhou C, et al. Improved stability and cell response by intrinsic cross-linking of multilayers from collagen I and oxidized glycosaminoglycans. *Biomacromolecules* 2014; 15: 4272–4280.
21. Tuan RS, Boland G and Tuli R. Adult mesenchymal stem cells and cell-based tissue engineering. *Arthritis Res Ther* 2002; 5: 32.
22. Uygun BE, Stojsih SE and Matthew HW. Effects of immobilized glycosaminoglycans on the proliferation and differentiation of mesenchymal stem cells. *Tissue Eng Part A* 2009; 15(11): 3499–3512.
23. Danišovič I, Varga Ľ and Polák Š. Growth factors and chondrogenic differentiation of mesenchymal stem cells. *Tissue and Cell* 2012; 44: 69–73.
24. Trivanović D, Jauković A, Popović B, et al. Mesenchymal stem cells of different origin: comparative evaluation of

Zhao et al.   15

proliferative capacity, telomere length and pluripotency marker expression. _Life Sci_ 2015; 141: 61–73.

25. Reznikoff CA, Brankow DW and Heidelberger C. Establishment and characterization of a cloned line of C3H mouse embryo cells sensitive to postconfluence inhibition of division. _Cancer Res_ 1973; 33(12): 3231–3238.

26. Katagiri T, Ikeda T, Yoshiki S, et al. The non-osteogenic mouse pluripotent cell line, C3H10T1/2, is induced to differentiate into osteoblastic cells by recombinant human bone morphogenetic protein-2. _Biochem Biophys Res Commun_ 1990; 172: 295–299.

27. Atkinson BL, Benedict JJ, Huffer WE, et al. Combination of osteoinductive bone proteins differentiates mesenchymal C3H/10T1/2 cells specifically to the cartilage lineage. _J Cell Biochem_ 1997; 65: 325–339.

28. Tang QQ, Otto TC and Lane MD. Commitment of C3H10T1/2 pluripotent stem cells to the adipocyte lineage. _Proc Natl Acad Sci USA_ 2004; 101: 9607–9611.

29. Chun XCQ, Yang S, Sun F, et al. BMP2 Induces Adipogenic Differentiation of C3 H10T1/2 Cells. _Chin J Biochem Mol Biol_ 2008; 24: 142–147.

30. Baudequin T, Gaut L, Mueller M, et al. The osteogenic and tenogenic differentiation potential of C3H10T1/2 (Mesenchymal Stem Cell Model) cultured on PCL/PLA electrospun scaffolds in the absence of specific differentiation medium. _Materials_ 2017; 10: 1387.

31. Fung CD, Cheung PW, Ko WH, et al. _Micromachining and micropackaging of transducers_. Amsterdam: Elsevier, 1985.

32. Niepel MS, Peschel D, Sisquella X, et al. pH-dependent modulation of fibroblast adhesion on multilayers composed of poly(ethylene imine) and heparin. _Biomaterials_ 2009; 30(28): 4939–4947.

33. Schasfoort RBM and Tudos Anna J. _Handbook of Surface Plasmon Resonance_. Cambridge: Royal Society of Chemistry, 2008, pp. 35–80.

34. Kirchhof K, Andar A, Yin HB, et al. Polyelectrolyte multilayers generated in a microfluidic device with pH gradients direct adhesion and movement of cells. _Lab Chip_ 2011; 11: 3326–3335.

35. Höök F. _Development of a Novel QCM Technique for Protein Adsorption Studies_. PhD thesis, Chalmers University of Technology and Göteborg University, Gothenburg, 1997.

36. McSwain BS, Irvine RL, Hausner M, et al. Composition and distribution of extracellular polymeric substances in aerobic flocs and granular sludge. _Appl Environ Microbiol_ 2005; 71(2): 1051–1057.

37. Vemuri MC, Chase LG and Rao MS. Mesenchymal stem cell assays and applications. In: Walker JM (ed.) _Methods in molecular biology_. Totowa, NJ: Humana Press, 2011.

38. Kuettner KE and Lindenbaum A. Analysis of mucopolysaccharides in partially aqueous media. _Biochim Biophys Acta_ 1965; 101: 223–225.

39. Almodóvar J, Place LW, Gogolski J, et al. Layer-by-layer assembly of polysaccharide-based polyelectrolyte multilayers: a spectroscopic study of hydrophilicity, composition, and ion pairing. _Biomacromolecules_ 2011; 12: 2755–2765.

40. Mhanna RF, Vörös J and Zenobi-Wong M. Layer-by-Layer Films Made from Extracellular Matrix Macromolecules on Silicone Substrates. _Biomacromolecules_ 2011; 12: 609–616.

41. Anouz R, Repanas A, Schwarz E, et al. Novel surface coatings using oxidized glycosaminoglycans as delivery systems of bone morphogenetic protein 2 (BMP-2) for bone regeneration. _Macromol Biosci_ 2018; 18(11): e1800283.

42. Raspanti M, Viola M, Sonaggere M, et al. Collagen fibril structure is affected by collagen concentration and decorin. _Biomacromolecules_ 2007; 8(7): 2087–2091.

43. Jiang F, Hörber H, Howard J, et al. Assembly of collagen into microribbons: effects of pH and electrolytes. _J Struct Biol_ 2004; 148(3): 268–278.

44. Kvist AJ, Johnson AE, Mörgelin M, et al. Chondroitin sulfate perlecan enhances collagen fibril formation. Implications for perlecan chondrodysplasias. _J Biol Chem_ 2006; 281: 33127–33139.

45. McBeath R, Pirone DM, Nelson CM, et al. Cell shape, cytoskeletal tension, and RhoA regulate stem cell lineage commitment. _Dev Cell_ 2004; 6(4): 483–495.

46. Coelho NM, González-García C, Planell JA, et al. Different assembly of type IV collagen on hydrophilic and hydrophobic substrata alters endothelial cells interaction. _Eur Cell Mater_ 2010; 19: 262–272.

47. Gullberg DE and Lundgren-Åkerlund E. Collagen-binding I domain integrins—what do they do? _Prog Histochem Cytochem_ 2002; 37: 3–54.

48. Ouasti S, Kingham PJ, Terenghi G, et al. The CD44/integrins interplay and the significance of receptor binding and re-presentation in the uptake of RGD-functionalized hyaluronic acid. _Biomaterials_ 2012; 33(4): 1120–1134.

49. Köwitsch A, Yang Y, Ma N, et al. Bioactivity of immobilized hyaluronic acid derivatives regarding protein adsorption and cell adhesion. _Biotechnol Appl Biochem_ 2011; 58(5): 376–389.

50. Richert L, Engler AJ, Discher DE, et al. Elasticity of native and crosslinked polyelectrolyte multilayer films. _Biomacromolecules_ 2004; 5: 1908–1916.

51. Altankov GGT. Fibronectin matrix formation by human fibroblasts on surfaces varying in wettability. _J Biomater Sci Polym_ 1996; 8(4): 299–310.

52. Jikko A, Harris SE, Chen D, et al. Collagen integrin receptors regulate early osteoblast differentiation induced by BMP-2. _J Bone Miner Res_ 1999; 14(7): 1075–1083.

53. Zhao GL, Li G, Chan KM, et al. Comparison of multipotent differentiation potentials of murine primary bone marrow stromal cells and mesenchymal stem cell line C3H10T1/2. _Calcif Tissue Int_ 2009; 84(1): 56–64.

54. Ghali O, Broux O, Falgayrac G, et al. Dexamethasone in osteogenic medium strongly induces adipocyte differentiation of mouse bone marrow stromal cells and increases osteoblast differentiation. _BMC Cell Biology_ 2015; 16: 9.

55. Lee SY, Lim J, Khang G, et al. Enhanced Ex vivo expansion of human adipose tissue–derived mesenchymal stromal cells by fibroblast growth factor-2 and dexamethasone. _Tissue Eng Part A_ 2009; 15(9): 2491–2499.

56. Ito S, Suzuki N, Kato S, et al. Glucocorticoids induce the differentiation of a mesenchymal progenitor cell line, ROB-C26 into adipocytes and osteoblasts, but fail to induce terminal osteoblast differentiation. _Bone_ 2007; 40(1): 84–92.

57. Huang H, Song TJ, Li X, et al. BMP signaling pathway is required for commitment of C3H10T1/2 pluripotent stem cells to the adipocyte lineage. _Proc Natl Acad Sci_ 2009; 106: 12670–12675.

58. Chen G, Akahane D, Kawazoe N, et al. Chondrogenic differentiation of mesenchymal stem cells in a leakproof collagen sponge. *Mater Sci Eng: C* 2008; 28: 195–201.

59. Zhang J, Keenan C and Wang JH. The effects of dexamethasone on human patellar tendon stem cells: Implications for dexamethasone treatment of tendon injury. *J Orthop Res* 2013; 31(1): 105–110.

60. Naito M, Ohashi A and Takahashi T. Dexamethasone inhibits chondrocyte differentiation by suppression of Wnt/β-catenin signaling in the chondrogenic cell line ATDC5. *Histochem Cell Biol* 2015; 144(3): 261–272.

61. Salasznyk RM, Klees RF, Hughlock MK, et al. ERK signaling pathways regulate the osteogenic differentiation of human mesenchymal stem cells on collagen I and vitronectin. *Cell Commun Adhes* 2004; 11(5–6): 137–153.

62. Murphy CM, Matsiko A, Haugh MG, et al. Mesenchymal stem cell fate is regulated by the composition and mechanical properties of collagen–glycosaminoglycan scaffolds. *J Mech Behav Biomed Mater* 2012; 11: 53–62.

63. Köllmer M, Buhrman JS, Zhang Y, et al. Markers are shared between adipogenic and osteogenic differentiated mesenchymal stem cells. *J Develop Biol Tissue Eng* 2013; 5: 18.

Chapter 5

Summary and future perspectives

This PhD thesis was aimed to develop stable biomimetic surface coatings with intrinsic cross-linking property that enables controlling the activity and release of bone morphogenetic protein-2 (BMP-2) in order to promote osteogenic differentiation of cells for bone regeneration applications. The layer-by-layer technique (LbL) was applied to fabricate the various multilayers surface coatings. The multilayers consisted of natural biopolymers called glycosaminoglycans (GAGs) that were used to mimic the composition of the natural extracellular matrix (ECM) and provide the cells with the ECM-like chemical cues. Hence, the GAGs heparin (H), chondroitin sulfate (CS) and hyaluronic acid (HA) were combined with either chitosan (Chi) or collagen I (Col I) as polycations to fabricate the native GAGs multilayers. The intrinsic cross-linking strategy was achieved by functionalizing the GAGs with an aldehyde group, *via* oxidation process, which can then bind to the amino groups on Chi or Col I and create a covalent imine bond (Schiff's base). This strategy was used to increase the multilayers' stability and stiffness and to control BMP-2 activity and release. The oxidized GAGs multilayers with intrinsic cross-linking were based mainly on covalent binding while their native counterparts were based mainly on ion pairing. The physiochemical characterization demonstrated that intrinsically cross-linked multilayers (especially CS multilayers) had a higher polyelectrolyte adsorption, thicker multilayers, stiffer surface and enabled the natural Col I fibrilization in the form of thick long fibers which were preserved even in acidic environment. On the other hand, the native GAGs multilayers had softer surfaces and could not preserve the Col I fibers. Additionally, the intrinsic cross-linking in oxidized GAGs multilayers contributed greatly the storage and activity of BMP-2. BMP-2 from oxidized CS multilayers was delivered to cells as a matrix bound BMP-2 since only little amounts got released. On the contrary, native GAGs multilayers delivered most of the loaded BMP-2 as soluble (released). Furthermore, it has been found that despite the very small amounts of BMP-2 released from oxidized GAGs multilayers, more BMP-2 internalization to cells has been detected indicating that BMP-2 delivery to cells is not about release but rather about the BMP-2 stored in the multilayers and being presented to cells in an active matrix-bound state. In addition, using a 50:50 mixture of native and oxidized CS enabled having a new multilayers system with enhanced water content and efficient BMP-2 release profile which permits its use for further applications. Further, the stiff surface

offered by intrinsically cross-linked multilayers together with the enhanced Col I fibrilization, led to an enhanced cell adhesion and spreading on those multilayers compared to their natives. The osteogenic differentiation studies concluded that; the matrix-bound BMP-2 delivered from the oxidized GAGs multilayers was active and succeeded in triggering osteogenesis which was proven by the detected higher alkaline phosphatase activity and formation of the mineralized matrix as well as up-regulation of osteogenic markers in cells cultured on BMP-2 loaded oxidized GAGs multilayers. On the other hand, soluble released BMP-2 from native GAGs multilayers failed to trigger the targeted osteogenesis. In general, the molecular composition of multilayers had an effect on cells' differentiation. For instance, in the absence of signaling molecules; CS-based multilayers promoted osteogenesis while HA-based multilayers supported chondrogenesis.

Based on these findings; the selected type of GAG can be used to control the physiochemical characteristics of multilayers and to guide cell differentiation depending on the application. The *in situ* intrinsic cross-linking approach can avoid the necessity to use toxic chemical cross-linking agents. In addition to the ability of GAGs to bind growth factors due to their heparin binding domain, the intrinsic cross-linking offers an extra binding and control mechanism of growth factors release and delivery.

The oxidized GAGs multilayers can be further used for delivering more than one growth factor such as BMP-2 together with the vascular endothelial growth factor (VEGF) which promotes vascularization and ensure optimal results in terms of ostegenesis. In addition, multilayers of the 50:50 mixture of native and oxidized CS can be loaded with the growth and differentiation factor-5 (GDF-5) and be further used for cartilage regeneration applications, thanks to their efficient release profile, matrix-bound growth factor delivery and high water content. In addition, a surface coating with gradient property composing of two types of multilayers; oCS100/Col I loaded with BMP-2 from one side and oCS50/Col I loaded with GDF-5 from the opposite side, could be used for tendon/ ligament defect regeneration due to their complex gradient tissue structure that consists of multiple GFs and cell types. Moreover, further work for investigating the exact molecular mechanism behind controlling growth factor activity and delivery in intrinsically cross-linked multilayers will offer better understanding and new insights. For example, since the imine bond is partly hydrolyzed at acidic pH permitting uptake of BMP-2 during loading (pH 4) and these bonds are formed at neutral and basic pH; release could be studied at both acidic and neutral pH to see potential effect of imine bond formation on binding and release of BMP-2. Additionally, *In vivo* preclinical studies would offer a great

chance to the intrinsically cross-linked GAGs multilayers to explore their *in vivo* potential and future applicability.

In conclusion, the presented intrinsically cross-linked GAGs multilayers can be used as potential surface coatings for implants and tissue engineering scaffolds for effective delivery of physiological quantities of growth factors; for save, economic and effective medical materials to treat traumata and degenerative diseases of the skeletal system.

Acknowledgment

I would like to thank AGRIPOLY international graduate school for the scholarship and for funding this work and making this whole PhD possible.

Thanks to the Federal Ministry of Education and Research for granting me and M. Eng. Adrian Hautmann the "GoBio Initial" funding, for our "ActiveLayers" project, which gave us a great chance to explore and transfer our knowledge into application oriented methods and innovations.

Thanks to all the positive great people and friends who were helpful and supportive to me when I was down and helped me overcome hard times.

Moreover, there were always people behind the scenes who supported me on all aspects, my dear family. To my parents who were always encouraging, patient, positive, loving, believed in me and made my trip to Germany possible in the first place; I owe you a lot and I cannot do anything to pay you back what you offered and did for me.

Thanks to my beloved brothers, whom I lost one of them during the final stage of this PhD which was the hardest part of this journey and took me a lot of time to cope with that and heal to continue what I have started and reach the step of presenting this PhD thesis. It was always their dream to see this success and achievement I am presenting today. The little brother I lost was not only a brother to me but also my best friend. He was always positive, loving, kind and encouraging. His smile was always enlightening my way and pushing me forward to make his dream seeing me as a Dr. comes true.

Finally, I would like to thank myself for being strong, independent, drawing a smile on my face every day and keep myself motivated despite all the hard times, looking always at the full part of the glass and being always ambitious to learn new skills and accept new challenges.

Publication list with declaration of self-contribution to research articles

1. R. Anouz, A. Repanas, E. Schwarz, T. Groth, Novel Surface Coatings Using Oxidized Glycosaminoglycans as Delivery Systems of Bone Morphogenetic Protein 2 (BMP-2) for Bone Regeneration, *Macromolecular Bioscience,* **2018**.

My contribution was about 65%. I performed all experiments related to the synthesis, characterization and measurements of oxidized GAGs. I also did all cell experiments and BMP-2 release studies. I wrote the major parts of the manuscript and modified everything for the final submitted version with help of Prof. T Groth who revised the manuscript. The physical characterizations of multilayers were performed by Dr. A. Repanas and the related paragraphs were only initially written by him.

2. M. Zhao, R. Anouz, T. Groth, Effect of microenvironment on adhesion and differentiation of murine C3H10T1/2 cells cultured on multilayers containing collagen I and glycosaminoglycans, *Journal of Tissue Engineering,* **2020**.

My contribution was about 30%. I mainly contributed in writing and revision of the whole manuscript. I also contributed to the evaluation of results and answering the reviewers' comments.

3. R. Anouz, T. Selekere, A. Hautmann, C. Husteden, M. Menzel, C. Woelk, C. E. H. Schmelzer, T. Groth, Intrinsically cross-linked ECM-like multilayers for BMP-2 delivery and Bone regeneration, *Advanced Materials Interfaces,* **2023**.

My contribution was about 75%. I evaluated, presented and arranged all findings and wrote the whole manuscript with the help of Prof. T Groth who helped me planning the experiments and revised the manuscript. I performed all experiments except for the AFM which was done by M. Menzel under supervision of Dr. C. E. H. Schmelzer. Measurements for qRT-PCR were performed by C. Husteden from the group of Dr. C. Woelk. Quantifications of FA, actin filaments, BMP-2 fluorescence adsorption, Collagen fibers diameter and Young's modulus were done by A. Hautmann. T. Selekere performed the QCM, WCA, ALP assay and contributed to the immune-staining for adhesion and differentiation experiments.

Book Chapters:

1. R. Anouz, T. Groth, Biomimetic Surface Modifications of Biomaterials Using a Layer-by-layer Technique, In: H.S. Azevedo, JF. Mano, J. Borges (eds.), *Soft Matter for Biomedical Applications* **2021**, The Royal Society of Chemistry (RSC), Chapter 13, pp. 326 – 362.

My contribution was about 80%. I assembled and wrote all parts. Prof. Dr. T. Groth helped in planning and revising the manuscript.

Other publications that are not involved in this thesis:

Book Chapter:

1. R. Anouz, M. Zhao, F. Gong, T. Groth, Tailoring the Microenvironment of Cells towards Osteogenic Differentiation Using Multilayers of Glycosaminoglycans and Growth Factor Immobilization, In: S. Najman, V. Mitić, T. Groth, M. Barbeck, P. Chen, Y. Sun, B. Randjelović (eds.), *Bioceramics, Biomimetic and Other Compatible Materials Features for Medical Applications*, **2023**, Springer, Chapter 1, pp. 3 – 27.

My contribution was about 50%. I assembled and wrote all parts related to studies performed using C2C12 cells. Prof. Dr. T. Groth helped in planning and revising the manuscript.

Published Abstracts:

1. R. Anouz, T. Selekere, A. Hautmann, C. Husteden, C. Woelk, M. Menzel, C. Schmelzer, T. Groth, Intrinsically Cross-linked, Glycosaminoglycans Multilayers: a Tool to Control Cellular Behavior & BMP-2 Delivery for Bone Regeneration, *Tissue Engineering Part A* **2022**, *28*, Suppl. 1, pp.S-1-S-694 https://doi.org/10.1089/ten.tea.2022.29025.abstracts

<u>Oral presentations:</u>

1. R. Anouz, T. Selekere, A. Hautmann, C. Husteden, C. Wölk, M. Menzel, C. Schmelzer, T. Groth, Intrinsically Cross-linked, Glycosaminoglycans Multilayers: a Tool to Control Cellular Behavior & BMP-2 Delivery for Bone Regeneration, *6th World Congress of The Tissue Engineering and Regenerative Medicine International Society (TERMIS 2021)*, 15th – 19th November **2021**, Maastricht, The Netherlands. (Online).

2. R. Anouz, A. Hautmann, T. Groth, „ActiveLayers" The Multifunctional Therapeutic Membranes, *SCIDEA STAGE Pitch Competition*, 9th December **2021**, Halle, Germany. (Online).

3. R. Anouz, A. Repanas, E. Schwarz, T. Groth, Novel Surface Coatings as Biocompatible Reservoirs for Controlled Release of BMP-2 for Bone Regeneration, *The 8th Meeting of the International Federation for Artificial Organs (IFAO) and The 57th Annual Meeting of the Japanese Society for Artificial Organs (JSAO), 13th* – 15th November **2019**, Osaka, Japan.

4. R. Anouz, A. Repanas, E. Schwarz, T. Groth, Novel Surface Coatings as Biocompatible Reservoirs for Controlled Release of BMP-2 for Bone Regeneration, *AGRIPOLY Discussion Meeting, 1st* October **2019**, Halle, Germany.

5. R. Anouz, A. Repanas, E. Schwarz, T. Groth, Novel Surface Coatings as Biocompatible Reservoirs for Controlled Release of BMP-2 for Bone Regeneration, *Congress of The Tissue Engineering and Regenerative Medicine International Society- European Chapter Meeting (TERMIS-EU)*, 27th – 31st May **2019**, Rhodes, Greece.

6. R. Anouz, A. Repanas, E. Schwarz, T. Groth, Novel Surface Coatings as Biocompatible Reservoirs for Controlled Release of BMP-2 for Bone Regeneration, *Annual Meeting of The Controlled Release Society (CRS)-Germany Local Chapter*, 7th – 8th March **2019**, Leipzig, Germany.

7. R. Anouz, A. Repanas, E. Schwarz, T. Groth, Novel Surface Coatings as Biocompatible Reservoirs for Controlled Release of BMP-2 for Bone Regeneration, *45th Congress of the European Society for Artificial Organs (ESAO)*, 11th – 15th September **2018**, Madrid, Spain.

8. R. Anouz, A. Repanas, E. Schwarz, T. Groth, Novel Surface Coatings as Biocompatible Reservoirs for BMP-2 for Bone Regeneration, *Comprehensive Summer School on Tissue Engineering*, 18th – 23rd June, **2018** Trento, Italy.

<u>Posters:</u>

1. R. Anouz, A. Hautmann, T. Groth, "ActiveLayers" Development of multi-component films as a platform technology for applications in wound healing and surgery, *Congress of The Tissue Engineering and Regenerative Medicine International Society- European Chapter Meeting (TERMIS-EU)*, 28th June – 1st July **2022**, Krakow, Poland.

2. R. Anouz, T. Selekere, A. Hautmann, C. Husteden, C. Wölk, M. Menzel, C. Schmelzer, T. Groth, Intrinsically Cross-linked, Glycosaminoglycans Multilayers: a Tool to Control Cellular Behavior & BMP-2 Delivery for Bone Regeneration, *ESAO/TERMIS Winter School*, 24th – 26th February **2021**, Online.

3. R. Anouz, T. Selekere, A. Hautmann, C. Husteden, C. Wölk, M. Menzel, C. Schmelzer, T. Groth, Intrinsically Cross-linked, Chondroitin sulfate/Collagen I Multilayers: a Tool to Control Cellular Behavior & BMP 2 Delivery for Bone Regeneration, *AGRIPOLY Discussion Meeting*, 29th October **2020**, Halle, Germany.

4. R. Anouz, A. Repanas, E. Schwarz, T. Groth, Novel Surface Coatings as Biocompatible Reservoirs for Controlled Release of BMP-2 for Bone Regeneration, *ESAO Winter School,* 26th – 29th February **2020**, Lutherstadt-Wittenberg, Germany.

5. R. Anouz, A. Repanas, E. Schwarz, T. Groth, Novel Surface Coatings as Biocompatible Reservoirs for Controlled Release of BMP-2 for Bone Regeneration, *AGRIPOLY Discussion Meeting, 1st* October **2019**, Halle, Germany.

6. R. Anouz, A. Repanas, E. Schwarz, T. Groth, Novel Surface Coatings as Biocompatible Reservoirs for Controlled Release of BMP-2 for Bone Regeneration, *46th Congress of the European Society for Artificial Organs (ESAO)*, 3rd – 7th September **2019**, Hannover, Germany.

7. R. Anouz, A. Repanas, E. Schwarz, T. Groth, Novel Surface Coatings as Biocompatible Reservoirs for Controlled Release of BMP-2 for Bone Regeneration, *Pharma-Research-Day at Martin Luther University Halle-Wittenberg*, 26th June **2019**, Halle, Germany.

8. R. Anouz, A. Repanas, E. Schwarz, T. Groth, Studies on osteogenic differentiation of cells on multilayers loaded with BMP-2, *44th Congress of the European Society for Artificial Organs (ESAO)*, 6th – 9th September **2017**, Vienna, Austria.

9. R. Anouz, A. Repanas, E. Schwarz, T. Groth, Studies on osteogenic differentiation of cells on multilayers loaded with BMP-2, *Annual Meeting of the German Biomaterials Society (DGBM)*, 9th – 11th November **2017**, Würzburg, Germany.

10. R. Anouz, A. Repanas, E. Schwarz, T. Groth, Studies on osteogenic differentiation of cells on multilayers loaded with BMP-2, *bone-Tec International Bone-Tissue-Engineering Congress*, 12th – 14th October **2017**, Munich, Germany.

11. R. Anouz, T. Groth, Studies on osteogenic differentiation of cells on multilayers loaded with BMP-2, *Annual Meeting of The Controlled Release Society (CRS) – Germany Local Chapter*, 2nd – 3rd March **2017**, Marburg, Germany.

12. R. Anouz, T. Groth, Studies on osteogenic differentiation of cells on multilayers loaded with BMP-2, *BioNanoMed Congress*, 20th – 22nd March **2017**, Krems, Austria.

Curriculum vitae

Personal data

Name:	Reema Anouz
Date of birth:	01. January 1992 in Qabr Alset, Damas Suburb, Syria
Academic degree:	Dipl.-Pharm. (Diplom-Pharmacist)

Work Experience

11/2021 – 01/2023	Research associate/ Project manager of a "GoBio initial" BMBF funded project at Biomedical Materials Department, Institute of Pharmacy, Martin-Luther-University Halle-Wittenberg, Germany.
05/2017 – 09/2017	Research assistant at Biomedical Materials Department, Institute of Pharmacy, Martin-Luther-University Halle-Wittenberg, Germany.
09/2013 – 09/2015	Laboratory manager (Molecular Biology, Analytical Chemistry, Physical Pharmacy) at Arab International University (AIU), Damascus, Syria.

Education

10/2017 – 01/2023	PhD student in the group of Prof. Dr. rer. nat. habil. Thomas Groth, Institute of Pharmacy, Martin-Luther-University Halle-Wittenberg.
	Title of PhD thesis: "Intrinsic cross-linking of biomimetic glycosaminoglycan-based surface coatings for control of BMP-2 activity towards osteogenesis of cells".

11/2015 – 07/2017	Diploma student in the group of Prof. Dr. rer. nat. habil. Thomas Groth, Institute of Pharmacy, Martin-Luther-University Halle-Wittenberg.
	Title of diploma thesis: "Native and Cross-linked Multilayer Systems as Biocompatible Reservoirs for rhBMP-2 to Control Differentiation of Myoblasts to Osteoblasts".
10/2009 – 10/2013	Pharmacy Student at Arab International University (AIU), Damascus, Syria.

Awards / Grants

10/2021 – 01/2023	"Go-Bio *Initial*" project funding for life science research approaches with innovation potential, The Federal Ministry of Education and Research, Germany.
	Title of project: "ActiveLayers" Development of multi-component films as a platform technology for applications in wound healing and surgery.
11/2019	The Young Investigator Award (travel award), The International Federation for Artificial Organs (IFAO), Osaka, Japan.
09/2017	2nd Poster Award, The European Society for Artificial Organs (ESAO), Vienna, Austria.

Halle (Saale), 20.07.2023

Reema Anouz

Selbstständigkeitserklärung

Hiermit erkläre ich gemäß § 5 der Promotionsordnung der Naturwissenschaftlichen Fakultät I der Martin-Luther-Universität Halle-Wittenberg, dass ich die Ergebnisse der vorliegenden kumulativen Dissertationsarbeit

Intrinsic cross-linking of biomimetic glycosaminoglycan-based surface coatings for control of BMP-2 activity towards osteogenesis of cells

am Institut für Pharmazie in der Arbeitsgruppe Biomedizinische Materialien unter Anleitung von Prof. Dr. rer. nat. habil. Thomas Groth selbständig erarbeitet und die Dissertation ohne fremde Hilfe verfasst habe.

Weiterhin erkläre ich, dass ich keine anderen als die von mir angegebenen Quellen und Hilfsmittel zur Erstellung meiner Dissertation verwendet habe. Den benutzen Werken wörtlich oder inhaltlich entnommene Stellen sind als solche gekennzeichnet.

Ferner erkläre ich, dass ich mich mit der vorliegenden Dissertationsarbeit erstmals um die Erlangung eines Doktorgrades bewerbe.

Halle (Saale), 20.07.2023

Dipl.-Pharm. Reema Anouz